



DEGREE PROJECT IN TECHNOLOGY,
SECOND CYCLE, 30 CREDITS
STOCKHOLM, SWEDEN 2023

Spiking Neural Networks for Control

KTH Thesis Report

Max Schaufelberger

Author

Max Schaufelberger <maxscha@kth.se>
School of Engineering Sciences
KTH Royal Institute of Technology

Place for Project

Stockholm, Sweden
Ottignies-Louvain-la-Neuve, Belgium

Examiner

Prof. Elias Jarlebring
Department of Numerical Analysis
KTH Royal Institute of Technology
Stockholm, Sweden

Supervisor

Arvind Kumar
Division of Computational Science and Technology
KTH Royal Institute of Technology
Stockholm, Sweden

Supervisor

Frédéric Crevecoeur
Institute of Information and Communication Technologies, Electronics and Applied Mathematics
UCLouvain Catholic University of Louvain
Louvain-la-Neuve, Belgium

Abstract

The emergence of spiking networks as the third generation of neural networks has shown great success in solving various tasks. Here, networks of spiking neurons are used to control a linear system using biologically plausible methods. Spiking neurons are introduced, and different frameworks highlighted. The control concept consists of two efficient coding networks: one for generating the necessary input to drive the second network, simulating the dynamics. The precise network behaviour is explained using a geometric methods. Network parameters for the simulating network are learned using supervised and unsupervised learning rules. For the simulation, results from the spiking network are accurate for various system sizes. Acceptable results for control using two networks can be reached if either the learning or the input matrix of the problem is neglected. Control using learned matrices is limited by inaccuracies in the supervised learning of matrix parameters as well as problem-dependent tuning of hyper-parameters. Moreover, learning progress is hard to monitor without repeated testing by simulation.

The results of this thesis suggest that the methods are unable to capture a general black box problem of designing a controller but can be useful when additional information is available.

Keywords

Spiking networks, Control, Efficient Coding Networks, Learning

Abstract

Framväxten av spikande nätverk som den tredje generationen av neurala nätverk har visat sig vara mycket framgångsrik när det gäller att lösa olika uppgifter. Här används nätverk av spikande neuroner för att styra ett linjärt system med hjälp av biologiskt trovärdiga metoder. Spikande neuroner introduceras och olika ramverk belyses. Kontrollkonceptet består av två effektiva kodningsnätverk: ett för att generera den input som krävs för att driva det andra nätverket, som simulerar dynamiken. Det exakta nätverksbeteendet förklaras med hjälp av geometriska metoder. Nätverksparametrarna för det simulerande nätverket lärs in med hjälp av regler för övervakad och oövervakad inlärning. För simuleringen är resultaten från spiknätverket exakta för olika systemstorlekar. Acceptabla resultat för reglering med två nätverk kan uppnås om antingen inlärnings- eller indatamatrisen för problemet försummas. Styrning med hjälp av inlärda matriser begränsas av felaktigheter i den övervakade inlärningen av matrisparametrar samt problemberoende inställning av hyperparametrar. Dessutom är det svårt att övervaka inlärningsförfloppet utan upprepade tester genom simulering. Resultaten i denna avhandling tyder på att metoderna inte kan fånga ett allmänt black box-problem med att utforma en regulator men kan vara användbara när ytterligare information finns tillgänglig.

Nyckelord

Spikande nätverk, kontroll, Efficient Coding networks, lärande

Acknowledgements

I would like to express my sincere gratitude to my supervisors, Arvind Kumar and Elias Jarlebring, for their invaluable guidance, support, and encouragement throughout the research and writing of this thesis. Their expertise and constructive feedback have been instrumental in shaping the quality and direction of this work.

I am deeply appreciative of the time and effort they devoted to providing insightful suggestions and helping me navigate the challenges of this project.

In conclusion, I extend my sincere appreciation to Arvind Kumar and Elias Jarlebring for their unwavering support and mentorship. Their guidance has been instrumental in making this research endeavour a rewarding and successful experience.

Acronyms

AD	Automatic Differentiation
ML	Machine Learning
RL	Reinforcement Learning
BP	Back-Propagation
LSTM	Long Short-Term Memory
LTI	Linear Time Invariant
RNN	Recurrent Neural Network
NN	Neural Network
GD	Gradient Descent
EWC	Elastic Weight Consolidation
ANN	Artificial Neural Network
SNN	Spiking neural network
GPU	Graphics Processing Unit
BPTT	Backpropagation Through Time
RTRL	Real Time Recurrent Learning
SRDP	Spike Rate Dependent Plasticity
STDP	Spike Time Dependent Plasticity
LSM	Liquid State Machine
NEF	Neural Engineering Framework
SOP	Synaptic Operation
IF	Integrate and Fire
LIF	Leaky-integrate-and-fire
TTFS	Time to First Spike
SISO	Single Input Single Output
MIMO	Multiple Input Multiple Output
ODE	ordinary differential equation

LHS	Left Hand Side
RHS	Right Hand Side
HH	Hodgkin–Huxley
NLP	Natural Language Processing

Contents

1	Introduction	1
1.1	Background	2
1.2	Problem	2
1.3	Goal	3
1.4	Methodology	4
1.5	Outline	4
2	Theoretical Background	6
2.1	Related Work	6
2.2	Autoencoder	7
2.3	Neural Networks	8
2.3.1	Spiking Neural Network Choices	9
2.3.2	Spiking Neural Networks	17
3	Methods	22
3.1	Choice of Network Architecture	22
3.2	Approach	22
3.3	Simulation of Dynamic systems using SNNs	23
3.3.1	Balanced network simulation	23
3.3.2	Greedy Optimization of the Cost	24
3.3.3	Neuron Voltage	26
3.3.4	Regularization	27
3.4	Control of Dynamic Systems using SNNs	29
3.4.1	Balanced Networks as a Controller	29
3.4.2	Dynamics	30
3.4.3	The Instantaneous Decoding Weights	31
3.4.4	Extension with Direct Error Feedback	32

3.5 Learning of network parameters	32
3.5.1 Learning of Fast Connection Weights \mathbf{W}^f	33
3.5.2 Learning of Slow Connection Weights \mathbf{W}^s	35
4 Results	37
4.1 Results on the Simulation from section 3.3	37
4.1.1 Illustrative Example	37
4.1.2 Illustrative example in 2D: Geometric interpretation	39
4.1.3 Importance of Feed-Forward weights	41
4.1.4 Bigger Systems	41
4.1.5 Varying cost parameters μ, ν	43
4.2 Results on the Control	43
4.2.1 Acceptable Error	44
4.2.2 Implementation details	45
4.2.3 Network as the Controller	48
4.3 Results on the learning	52
4.3.1 Model problem	53
4.3.2 Only Learning of \mathbf{W}^f	54
4.3.3 Combined Learning	65
4.4 Results of the Learned Control Objective	76
4.4.1 Combining the Two Networks	76
4.4.2 Merging two Networks	78
4.4.3 Limitations	83
5 Conclusions	85
5.1 Future Work	87
5.2 Final Words	89
References	91

Chapter 1

Introduction

The human brain is a brilliant computing unit comprised of around 86 billion neurons[7]. Each of these neurons can have thousands of connections to other neurons. Between these connections, information travels through the network as electrical impulses that interact with the neuron's own electrical potential. With this network, the human brain is capable of performing vastly different and complex tasks. Machines and robots surpass humans in raw computing power by several orders of magnitude, yet many tasks are next to impossible to solve by machines and classical algorithms alone. Moreover, many machine implementations lack the speed, precision, or flexibility of their human counterparts.

Researchers have sought to address this by mimicking the brain's internal network structure to solve problems deemed unsuitable for classic algorithms. Artificial Neural Networks (ANNs) have shown a great success in previously hard-to-solve problems. However, the classical ANNs still struggle in the context of control. Where the highly abstract ANNs reach there limits, a more biologically plausible network type can overcome this obstacle. Spiking neural networks (SNNs) can provide a powerful framework to solve complex problems. Furthermore, with newer, more biologically inspired networks, we are able to solve a broader range of problems. The concept of SNNs will be described in detail in a later section. By Using SNNs, we set out to design such a network in order to control a linear system.

1.1 Background

The most common neural network architecture for ANNs is the feed-forward network. In these networks, information travels only in one direction and is not propagated by spikes but gradients of activation, usually set in the range $[0, 1]$ or $[-1, 1]$. Feed-Forward ANNs have made impressive progress in the fields of image recognition, autonomic driving, medical diagnosis[65] or Natural Language Processing (NLP) (using Transformers[82]). While this abstract representation brings advantages e.g in modelling and implementation, it also lacks some key features of the human brain. Due to the information travelling only towards the output, feed-forward networks cannot build a memory or easily process temporal data. Recurrent models exist, which allow for memory [30] and sequential data input but loose some of the advantages compared to the Feed-Forward networks due to their increased complexity.

A third generation[55] of network architectures has risen, aiming to be even more biologically plausible. Inspired by nature, they implement spiking behaviour and recurrence found in the human brain. This newer form of SNN is as powerful as the classic feed-forward but is better suited for temporal data encountered in control. While state-of-the-art Feed-Forward networks still outperform SNNs¹, in some cases, modern SNNs are on par[49] or more performant, with previous feed-forward implementations consuming more energy.

1.2 Problem

Conventional Feed-Forward neural networks are not designed to work with temporal data; they are static input-output machines. While this makes sense in the context of many tasks, it simultaneously limits the power of these networks. There are workarounds to handle temporal data, such as sampling previous values back into the network (used in time series forecasting [77, 81, 89]) or by quantizing the whole input if the entire time horizon is available, as with recorded audio data.

Instead of these workarounds, Recurrent Neural Networks (RNNs) are often proposed for such tasks. However, RNNs face challenges during training with back-propagation[9]. For RNNs and deep Feed-Forward networks gradients used in the

¹Most benchmarks are based on static information e.g. images, which are adapted to SNNs and therefore do not allow a perfectly fair comparison.

back-propagation algorithm can either explode or vanish. Different methods have been proposed to address this problem, such as batch normalization[39], using alternative activation functions (ReLU)[60], or gradient clipping[64], to name a few. Specifically for recurrent models, different architectures have been suggested, with the Long Short-Term Memory (LSTM) cell [32] being prominent and successful in various applications[51, 58, 69].

Yet, these recurrent designs are not a plausible representation of biological networks. RNNs still operate on a continuous range of values instead of discrete spikes. Utilizing this continuity, they are trained with the biologically implausible global learning rules, such as the Back-Propagation algorithm. Furthermore, SNNs come with the added benefit of consuming less power. Usually, deep ANNs are run on Graphics Processing Units (GPUs), especially for training, where energy consumption can exceed 400W for modern chips². In contrast, the brain is estimated to only consume about 20W [20] for its immense computing capacity. Accompanying SNNs with neuromorphic hardware can yield another boost in efficiency, with processors' energy consumption in the pJ per Synaptic Operation (SOP)[38], offering significant power savings.

1.3 Goal

The goal of this project is to create a SNN capable of controlling any given Linear Time Invariant (LTI) system. Furthermore, the Neural Network (NN) should be robust against failing neurons or connections. As an additional constraint, the objective is to achieve this goal using biologically tractable methods as much as possible. To mimic the brain's learning, we aim to employ local training rules that are biologically plausible.

Achieving optimality is an ideal, although it is often unclear if this is possible. Even in highly researched ANNs this is typically a challenging condition, as conventional NNs using Gradient Descent (GD) only guarantee a local minimum.

Furthermore, in nature, the brain does not offer separate between training and trial periods. The brain self-modulates its learning online, meaning that the network is expected to improve on itself as it works the task at hand.

Lastly, adjusting neural networks to a specific task usually requires manual tuning

²e.g. a NVidia RTX 4090

of hyperparameters. The goal here is to automate as much of the process as possible, allowing the network to find acceptable solutions given the task at hand, independent of the given control command or size of the system, without problem specific adjustments of hyper-parameters.

For the SNN itself, we aim to find a balance between the biological plausibility and performance. This means we seek key features of biologic networks such as irregular firing patterns, robustness to noise, and locality. Additionally, we seek optimal performance when the network controls a given system.

If successful, we would obtain a general purpose controller that allows us to control any given linear system simply by plugging in the given system and the desired reference trajectory.

1.4 Methodology

To achieve our set goal, we first investigate what kind of Spiking network architecture to use. There are many different ways to design a SNN each with its advantages and shortcomings. We aim to find an architecture that lies in between the most accurate biologic spiking model and yet allows some abstraction to apply it to our control problem.

Part of the goal is that the user does not have to interact with the neural network working underneath the control problem. Firstly, we set out to achieve our goal by implementing a SNN that allows us to simulate, not control, any given linear system with external inputs. With this network in place, another SNN that acts as the controller will be built and combined with the first. The controller would generate a control signal that is used as external input to the first, returning the new system state to the controller in the process. Afterwards, we equip the network dedicated to simulation with the ability to learn the given system at hand.

1.5 Outline

In the next chapter, related work, as well as background information on autoencoders and different neural networks, is provided. This is combined with a summary of the different spiking network design choices. Next, the derivations of the spiking

networks used for simulation and control are introduced in chapter 3. Alongside, the learning rules are presented. In chapter 4 results on the simulating network, the control, and the learning are presented. For the simulation, a visual interpretation of the network dynamics is provided. In terms of control, important implementation details are highlighted, and necessary conditions to enable control are explained. Afterwards, results of the learning include a parameter study on both the un- and supervised learning rule used in this approach, as well as the study of limitations for the learning. These steps are then combined to accomplish our set-out goal of control. We explore two different implementations and highlight their limitations. Lastly, we conclude in chapter 5 by summarizing our approach, its problems, and drawbacks. We furthermore express different points to improve the network's capabilities.

Chapter 2

Theoretical Background

In this chapter, we provide a detailed description of the background of the degree project is presented along with related work. The background covers the autoencoder, which describes the fundamental behaviour of the later chosen network. Additionally, we present a general overview of Spiking Neural Network (SNN) architectures and design choices.

2.1 Related Work

Spiking neural networks for control have found application in various contexts, including robotic movement, digit recognition[49], and object detection[71, 95].

In [13], spiking neurons are utilized to control target-reaching movements of a 4-DoF robotic arm using a plausible neuron model and learning rule. Their approach incorporates the DIRECT model from [18], which learns the a priori unknown robot kinematics by randomly repeating movement commands and learning the resulting translation of the end effector. Another approach for robotic arm control is presented in [23], utilizing the Neural Engineering Framework (NEF)[26]. Different regions of the brain are simulated to generate the trajectory and control signals. On the other hand, the authors of [53] used Reinforcement Learning (RL) in combination with a SNN and a variation of the Spike Time Dependent Plasticity (STDP) rule to control the cart-pole problem.

The authors in [10] summarized several approaches for robotic control of flying or driving robots and used layered spiking neurons with a local learning rule to train the network to reach the target while avoiding obstacles.

While each of these models incorporate some biological plausibility, they only take one or a few aspects into account in their model, be it the neuron model, the learning rule, encoding or network structure. Furthermore, these approaches are often targeted towards specific applications like robotic arms and may not address general control of dynamic systems.

Spiking neurons have also been explored for PID controllers. In [86] it is demonstrated that it is possible to construct a PID controller using three neurons, each representing P,I and D, respectively. However, no example using the network is provided, and the learning process relies on individual parameter tuning for each neuron. Moreover, the robustness of 3 neurons is not biologically plausible. In [72], a PID controller is designed using spiking neurons on neuromorphic hardware in order to control a 1-DoF UAE. However, details on how the network was trained on the neuromorphic hardware or how this approach can be scaled to larger systems remain unclear. Additionally, due to the prevalent background noise found in the brain, we strive for a noise robust solution which is not given in any of the above mentioned approaches.

In addition to the individually crafted models by authors, various public libraries and frameworks have been developed in order to facilitate SNN simulation. It is important to note that different libraries serve different purposes. While some act as hybrids for SNN with Machine Learning (ML) goals (e.g. `snnTorch`[27], `nengo` [8]), others are geared for fast and accurate neurologic simulations (e.g. `Brian`[73]). Each framework implements a different feature set such as GPU Support, Torch-like structure, convolution, learning rules, or support for neuromorphic hardware. For a summary, refer to [88].

2.2 Autoencoder

An autoencoder is a type of neural network designed to learn a representation of an input signal. It comprises an encoder and decoder function $z = f(x)$ & $\hat{x} = g(z)$. The encoder function maps from the input space, for example \mathbb{R}^n , to an encoded space \mathcal{Z} . Subsequently, the decoder reconstructs the data from \mathcal{Z} back to \mathbb{R}^n . The primary objective is to ensure that the decoded representation is as accurate as possible.

In the trivial case where \mathcal{Z} is equal to or larger than the input space, each possible input

can be encoded by its own value as

$$\begin{aligned} z &= f(x) = x \\ \hat{x} &= g(z) = z = x \end{aligned} \tag{2.1}$$

and the autoencoder essentially memorizes each input. However, in most cases, \mathcal{Z} is constrained, forcing the autoencoder to find the characteristic properties of the input. This is achieved by reducing the dimension of \mathcal{Z} or through regularization. The regularization term, denoted as $C(z)$, is added to the loss

$$\tilde{L} = L(x, \hat{x}) + C(z) \tag{2.2}$$

where L can be, for example, MSE. Regularization can enforce sparsity or other desired properties[29].

The functions f and g can be selected freely but play a crucial role in the performance. Frequently, they are combined in a neural network that is trained to adjust the network's parameters as well as function parameters. Additionally, the internal mechanism can also be freely chosen. Therefore, an autoencoder can also have a SNN at its core, where f and g serving as the encoder and decoder of spikes, respectively. This step is a pivotal aspect of the selected network architecture, essentially functioning as an autoencoder with spiking neurons. At each time step, a signal is encoded into a group of neurons, and the spiking dynamics are decoded to reconstruct the desired signal and each neuron projection different segments of the autoencoder's error.

2.3 Neural Networks

The topic of NNs is vast and has been extensively explored in numerous papers. In this section, we focus on design choices in neural networks and dedicated spiking models from the literature.

When designing a spiking neural network, various components must be selected to form the network. The following sections highlight the most crucial aspects and explain common choices. It is worth noting that SNNs are still under active research, many hybrids and combined methods exist, though they are not covered here.

2.3.1 Spiking Neural Network Choices

Copying nature to solve engineering problems is long-standing practise, and also extends to NNs. Numerous network architectures with varying levels of biological plausibility have been investigated and published, with little consent in design decisions. As a result different choices are made by different researches leading to various approaches that are similar yet different.

Biological realism can be incorporated at various points within the network, making it impractical to explicitly inspect each nuance. Apart from highly specific implementations illustrated in section 2.3.2, many SNNs can be categorized into different segments, showcasing certain designs found in the literature.

Neuron model

As outlined in more detail below, neuron models can vary in complexities and accuracy. By far, the most used model in the literature are Leaky-integrate-and-fire (LIF) and Integrate and Fire (IF) models.

Biological Neuron model

The first biologically accurate model of neuron spiking behaviour is the Hodgkin–Huxley (HH) model from 1952[34]. Since then the HH model has been extended in multiple ways to cover additional factors, such as different ion channels. The HH-model considers the neuron with its ion channels. The membrane acts as a capacitance and the travelling ions in each ion channel contribute a current to the overall membrane potential. These ion gates are voltage-dependent and are defined positive in direction out of the cell.

A particular ion channel for ion X can be modelled as

$$I_X = g_X \cdot (V - V_X) \tag{2.3}$$

These currents are summed for the different ion channels in question, most frequently for Sodium, Potassium and a leak current. In reality there is a plethora of different channels and channel properties¹. The V_X are the equilibrium potentials for each of

¹See channelpedia.epfl.ch for an extensive list

the channels and can be computed using the Nernst equation [45].

$$C \frac{dV}{dt} = g_{Na} \cdot (V - V_{Na}) + g_K \cdot (V - V_K) + g_L \cdot (V - V_L) \quad (2.4)$$

To model the voltage dependency of the ion channels, the conductances are described with gating variables, typically denoted as n , m and h for activation and inactivation of Sodium and Potassium channels. One gating variable is set between $[0, 1]$ and models the permeability of a gate. Multiple gates are employed to match experimental data and model behaviour for each ion channel.

Gates are modelled with order dynamics of the form

$$\frac{dn}{dt} = \alpha_n(1 - n) - \beta_n n \quad (2.5)$$

for the n gate. The other gates' dynamics are analogous. The functions α and β are voltage but not time dependent. The discussion of initial values as well as functions for α_p , β_p $p = (n, h, m)$ can be found in [33] or [45]. The gates' conductance for each ion channel have been derived from natural approximations as follows:

$$\begin{aligned} g_{Na} &= \bar{g}_{Na} n^4 \\ g_K &= \bar{g}_K m^3 h \end{aligned} \quad (2.6)$$

and give form to the final model

$$\begin{aligned} C \frac{dV}{dt} &= I(t) - \bar{g}_{Na} n^4 (V - V_{Na}) - \bar{g}_K m^3 h (V - V_K) - g_L (V - V_L) \\ \frac{dn}{dt} &= (1 - n) \alpha_n(V) - \beta_n n(V) \\ \frac{dm}{dt} &= (1 - m) \alpha_m(V) - \beta_m m(V) \\ \frac{dh}{dt} &= (1 - h) \alpha_h(V) - \beta_h h(V). \end{aligned} \quad (2.7)$$

We did not define a gate for the leak term as it is assumed constant.

IF and LIF

In contrast to the HH model in eq. (2.7), the simplest models of neurons are the IF and LIF models.

IF Neurons IF Neurons, as the name implies, integrate the incoming current over time:

$$\frac{dV(t)}{dt} = \frac{1}{C} I(t) \quad (2.8)$$

The membrane voltage is governed by the incoming current spikes of connected neurons and the membrane capacitance. The neuron potential does not change without a change of input current and thus presents itself as a perfect integrator of the input.

LIF Neurons In contrast, the LIF neuron contains a leak term on the Right Hand Side (RHS), bringing the voltage back to its resting potential over time. The model can be expressed as:

$$\tau \frac{dV(t)}{dt} = -(V(t) - E_r) + RI(t), \quad (2.9)$$

where $\tau = RC$ is the time constant composed of the membrane resistance R and the membrane capacitance C . In the absence of input $I(t)$, the voltage settles on the membrane potential E_r .

The input $I(t)$ encapsulates external inputs as well as a sum of Dirac functions indicating a firing neuron:

$$I(t) = \sum_k w_i \delta(t - t_i^k) \quad (2.10)$$

Every received spike k is multiplied by its respective synaptic strength from neuron i and added to the input current. When the membrane voltage exceeds the threshold potential \bar{V} , a spike is sent out by the neuron and the voltage sets back to its reset voltage V_{res} .

Izhikevich Neuron

While the above models deliver a useful and cheap model, they lack in accuracy. The Izhikevich model [40] of the neuron aims to be a blend of efficiency and accuracy. It is comprised of 2D ODEs with the membrane potential v defined as

$$\begin{aligned} \frac{dv}{dt} &= 0.04v^2 + 5v + 140 - u + I(t) \\ \frac{du}{dt} &= a(bv - u). \end{aligned} \quad (2.11)$$

With the chosen factors, the neuron experiences a spike when $u \geq 30\text{mV}$, in which case the neuron resets to

$$\begin{aligned} u &\leftarrow u + d \\ v &\leftarrow c. \end{aligned} \tag{2.12}$$

The parameters describe a as the scale of recovery, b as sensitivity, c as the reset potential of v , and d as the reset of variable u . Depending on these parameters, one can achieve different behaviours of the neuron, such as regular spiking, fast spiking, and low threshold spiking to name a few.

Encoding

The coding of information plays an important role in a SNN. Since the network works with discrete spikes, a methodology needs to be implemented to convert e.g continuous values into spikes. To let the network be susceptible to the outer world, a subset of neurons of the network are exposed to these external inputs.

Time to First Spike (TTFS) In this coding scheme, the information of an input is solely encoded in the time between the external input and the time neurons fire a spike. A simple visualization could be by implementing such that the stronger the input, the sooner the input neuron spikes after the input onset.

An extension of this idea is rank order coding, where the ordering of spikes encodes information[80].

Phase coding Phase coding is a slight variation of the TTFS code. Certain areas of the brain exhibit oscillations similar to a clock[41]. The premise of phase coding is that the oscillation of this clock can be used to convey information. Thus, a spike relative to the phase of a clock cycle entails information on the input signal.

Rate coding Rate coding transforms the intensity of a signal into a spiking pattern with a corresponding frequency. The intensity is often normalized to realistic spiking frequencies. Since the brain is noisy, the spike is not fired with the respective rate but rather with a Poisson process given a suitable rate λ . Using a Poisson point process comes with the drawback of comparatively high spiking rates to represent a value

accurately due to noise[22].

Population coding Population coding extends neuron encoding to multiple neurons. Instead of one neuron firing, a group of neurons is combined to encode information. This allows for redundancy and robustness. Inside this population, information can be embedded in different dynamics of this group. One way could be to consider the firing rate of the neurons as a group. Alternatively, pattern analysis can be performed to read out information in the distribution of spikes in the group.

Connectivity/Topology

The structure of neural networks is mainly distinguished between hierarchical and recurrent topologies. In hierarchical topologies, there are segments of neurons that follow a (often unidirectional) structure. Feed-forward NNs are a simple example of this architecture.

Recurrent networks allow for loops in the connectivity of neurons and therefore enable feedback and temporal patterns.

There can be hybrid implementations where different groups of neurons are connected in sequence.

Using RNNs offers a broader range of applications but has to deal with (as of this day) inferior or more complex learning paradigms.

Plasticity

The choice of plasticity determines how the network adapts its parameters during learning. In the literature, mostly two different approaches are used. The dominant of these is the adjustment of synaptic weights, similar to ANNs. It is noteworthy that most learning algorithms are based on this approach.

The alternative is to work on adjusting thresholds instead[5, 19]. One can adjust the frequency or likelihood of a neuron firing by lowering or increasing its threshold, making it harder or easier for a neuron to spike. Increasing the threshold after a spike was fired allows for the modelling of refractory periods seen in biological neurons.

Threshold adaptation can also be in conjunction with weight adaption policy. In [74], adaptive synapses are trained alongside connection weights.

Another form of plasticity concerns the retention of knowledge. In most ML applications, the learning is solely a part of the deployment of a NN. After the training period, the network parameters are fixed and further learning is frozen. This is in opposition to biological neural networks, where continuous learning is found not only due to the fact of neurons dying and getting replaced continuously but also due to the learning of new tasks.

ANNs struggle with adjusting to new tasks while retaining the same performance for previous tasks. Since the learning of the new task is allowed to adjust every weight, it completely ignores relevant weights for the previous task.

To combat this different ideas have been suggested. These include fixing parts of the weights, using Drop-Outs, or employing Elastic Weight Consolidation (EWC)[47]. In EWC, crucial weights are retained by augmenting the cost function with a penalization term on the parameters deviation from the previous task. The proportional factors are computed using the Fisher information matrix after the learning of one task is completed and focus crucial neurons with higher proportional factors.

A similar approach has been proposed with synaptic intelligence[92]. Here, a similar penalty term is introduced that computes the neurons individual importance. The difference is that this importance can be computed online. Each synapse tracks a scalar value describing the relative importance of decreasing the loss. This value is the base for the importance calculation that again penalizes deviations of parameter weights from the previous values.

However, as of now, this has only been implemented on ANNs with a Feed-forward architecture.

Learning Algorithms

Key to giving any NN the ability to solve a task is to learn/train the it. The adaptation of weights and biases is necessary to accomplish any functionality based on the underlying data[94]. There are a plethora of different learning techniques available; see [1, 75] for a review. The most fundamental distinction can be made between supervised, unsupervised, and reinforcement learning rules. Another distinction can be made by the biologic plausibility of a given learning rule. For example, for ANN the gradient based Backpropagation algorithm is biologically implausible in various ways, but most importantly in its non-locality, yet it has been immensely successful.

In this context, a loss function L is employed to calculate the derivative $\frac{\partial L}{\partial \theta_{ij}}$,

determining the contribution of each neuron's parameters θ_{ij} to the error. Subsequently, these parameters are adjusted iteratively until a minimum is reached. The computation of gradients is done efficiently using the backpropagation algorithm (reverse accumulation from Automatic Differentiation (AD)), in which the gradients are propagated from the output backward towards the input by making use of the chain rule and the fact that the NN has a layered structure. An in-depth explanation is given in, for example, [29] or [63].

If the chosen network is recurrent, using Back-Propagation (BP) to find gradients is more complex. To remedy this, adaptations of the classic BP algorithm have been proposed.

For recurrent networks, often the Backpropagation Through Time (BPTT) can be used. Its concept is based on using the conventional Backpropagation algorithm by "unrolling" the recurrent network into a feed-forward network in time. In addition to the original network inputs, additional inputs are designated in the feed-forward network that feed the internal network state to the next layer, representing the next time step.

With this structure in place, the gradients can now be computed either by propagating the error backward or by forward propagation of the activity gradient. The former is commonly known as the normal BPTT the latter is called Real Time Recurrent Learning (RTRL)[87]. While they allow the computation of the exact gradients, they can both suffer from issues like vanishing or exploding gradients [9, 64] resulting in getting trapped in local minima easily or divergence. This is due to the unrolling in time, which causes the network to become deep quickly. For each step of the input sequence fed into the network, an extra layer in the unrolled network is added.

Gradient-based methods require differentiability and therefore continuity, making them applicable only for ANNs. This means that they cannot be used for SNNs as spikes introduce discontinuities. Since spikes are discrete events the derivative is zero during no-spike periods and undefined during a spike.

While methods have been proposed to adapt backpropagation to spiking networks[49], they still lack a biologically plausible way to learn. The problem is that in biology, neurons do not have access to the global error from the loss function but only receive information from pre-synaptic neurons.

For spiking and recurrent networks, the BPTT algorithm can be combined with spiking networks, leading to the SpikeProp[12] algorithm. In SpikeProp, the optimization

is performed on the firing times, and the discontinuity is replaced by a linear function. Several variations have emerged with improved convergence[59], e.g by using different replacement functions [61, 79] or adaptive learning weights [70]. Alternatively, instead of optimizing the firing times and replacing the discontinuity in spike trains, SuperSpike[91] replaces the discontinuities in the membrane potential with an approximate continuous function.

(Anti-) Hebbian Learning and STDP

Tending towards more biologically plausible methods, STDP is the most prominent method. The Hebbian learning rule is one of the oldest learning principles for spiking networks with large experimental evidence in biology (see for example [28] for a summary). Its core idea can be encapsulated in the famous mnemonic "Neurons that fire together, wire together." Essentially, if the postsynaptic neuron repeatedly fires shortly after the presynaptic neuron, their connection strength is increased. Oppositely, if the postsynaptic neuron fires before the presynaptic, their connection strength is decreased.

This behaviour of potentiation and depression is illustrated in fig. 2.3.1 and build the bases for the STDP rule. It operates by increasing the synaptic weight of a synaptic connection when a presynaptic spike is followed by a postsynaptic spike, conversely, reducing the weight if the spikes occur independently, i.e. the postsynaptic neuron firing first. The longer the delay between firing activation, the smaller the increase.

Since then a plethora of variations have been proposed and demonstrated successfully[78, 85, 88]. In addition to the Hebbian rule, there is also the anti-Hebbian rule, which reverses the aforementioned behaviour. This implies that regular firing of pre- and postsynaptic neurons is discouraged and more irregular and distributed spiking is favoured. This can be understood as mirroring fig. 2.3.1 along the x-axis.

Several variations and extensions to STDP have been proposed, e.g. Spike Rate Dependent Plasticity (SRDP)[46] or reward modulated STDP[50].

These rules are rooted in biology and adhere to the constraints observed in nature. Many learning rules adapted from ANNs lack these properties e.g. locality.

Locality dictates that the basis of learning is restricted to having only the information of the direct pre- and postsynaptic neurons available. This already rules out most

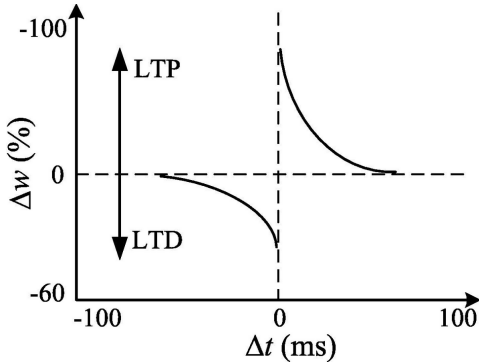


Figure 2.3.1: Graphical representation of STDP learning rule. Weight change depending on the time between pre- and postsynaptic activation. Negative time is the time between the postsynaptic neuron firing before the presynaptic. Graphic taken from [90].

backpropagation algorithms, as they derive the derivative with respect to a global cost function.

2.3.2 Spiking Neural Networks

Apart from the aforementioned segments of SNNs, various SNN archetypes have been studied in the literature. In the following sections, rate networks and Liquid State Machines (LSMs) will be presented. Note that the following sections do not represent a comprehensive review but rather a selective overview options. In addition to the SNN types mentioned below, other approaches exist, such as the NEF[26], SORN[48], or FORCE [62].

Rate Networks

Poisson or Rate networks are built around the idea that information is encoded in the firing rate of a neuron. The precise timing of a spike is essentially meaningless[17]. This contrasts with the approach chosen in this project. While states are also decoded using neuron firing rates, each fired spike is times exactly in order to minimize a cost function.

The encoding of a value in rate networks, e.g. four, is set by endowing the input neurons with a Poisson point process with a suitable encoding rate r_i [22].

One typically uses probabilistic stimuli because observations in the spiking of the human brain do are different in a trial-by-trial basis.

Input spikes traverse the recurrent network with weighted connections. The decoding is done by counting the spikes of output neurons over a certain time window. The time

window plays a crucial role in the decoding. If it is set smaller, spatio temporal patterns can be captured which can convey information about the input. Equally the sensitivity to noise becomes higher. If the time window is set too large, the firing patterns are lost due to exceedingly large averaging, although the impact of random spikes is reduced. Using this method is a comparatively simple way of encoding, as firing rates are used in favour of the individual spikes, which are modelled by random processes. Additionally, this approach is biologically not completely unsound. In nature, it has been shown that the firing rate does convey information about the stimuli's magnitude. [2].

The connection weights are subject to change over the learning/training period[4] and can be trained with different training algorithms, e.g. (anti-)Hebbian, STDP, gradient based or more involved training methods[21]. See [90] for an overview.

The challenge with a Poisson process generating spikes for its respective rate is that this process requires many spikes to accurately transmit a signal. For N neurons representing a given value, the error or variance scales with $\frac{1}{\sqrt{N}}$ [11]. In other words, to achieve accurate results, a substantial number of spikes must be fired. If the time between spikes follows an exponentially distributed pattern, and having a greater number of samples enhances the accuracy of estimating the rate parameter.

Theoretically, using a large number of spikes is unproblematic. Even with large spike counts, neuromorphic hardware is still highly energy efficient compared to deep neural networks when deployed[38].

However, there are more issues to this method. This approach has the limitation that responses are confined by the time window in which spikes are counted[6]. This implies that the rate decoding may be insufficiently swift to capture rapidly propagating information[31], necessitating the exploration of faster means to transmit information.

Despite the aforementioned challenges, rate-encoded SNNs have garnered interest in research. A significant hurdle in deploying SNNs is the lack of performant learning algorithms. Efforts have been made to train recurrent or convolutional ANNs using backpropagation and then convert the trained network afterwards to a SNN[66] using rate encoding[25][24].

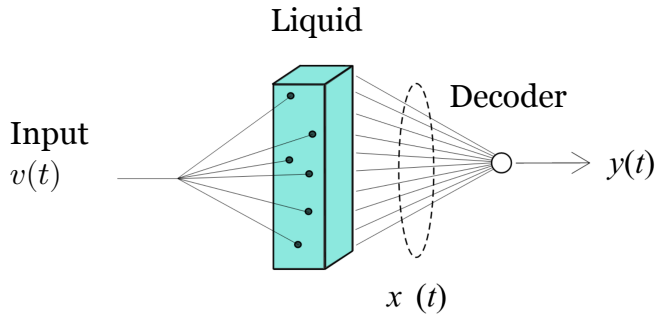


Figure 2.3.2: Abstract idea of Reservoir Computing. Adapted from [54]

Liquid state machines

One alternative method that has been proposed is the use of LSM or, more generally, Reservoir computing.

The term "Reservoir Computing" was introduced by Benjamin Schrauwen and describes a general group of recurrent network approaches[83].

The "reservoir" is a non-linear map from input to outputs that combines the input in various, even random ways. These operations include, but are not limited to, sums, differences, multiplications, division and exponentiation. Generally, the output $x(t)$ has higher dimension than the input $v(t)$, in order to allow for sufficient variety in the mapping. The output of the reservoir, which is usually treated as a black box, is fed into a linear decoder in order to retrieve the desired output signal.

The liquid can be made of any system that fulfils two properties.

- Non-linear nodes of computation
- Fading memory

Regarding these points, it is typically set for the system to be time-invariant[54]. A reservoir can be a mathematical abstract formulation or physical object, such as a literal bucket of water [76].

After the choice of "liquid" in the reservoir is fixed, its dynamics remain unaltered. Only the linear decoder is trained to produce the desired decoded output[42]. This is a considerable time-saving measure since training of recurrent networks is computationally expensive, whereas the linear decoder can be learned relatively inexpensively.

A reservoir computer is referred to as a LSM when a spiking neural network is chosen

as the reservoir. The aforementioned requirements are met by the recurrent structure, which retains information from the neurons and exhibits non-linear spiking behaviour. LSMs are capable of computing any dynamical system of any order of the form of

$$z^{(n)} = G(z, z^{(1)}, z^{(2)}, \dots, z^{(n-1)}) + u \quad (2.13)$$

given a sufficiently large liquid and a suitable feedback and decoder[57]. They have been applied in various domains, such as speech recognition[43][93] or object detection[71]. The systematic structure can be seen in fig. 2.3.3. The feedback $K(x, u)$ is a function of the dynamical system input $u(t)$ and the output $x(t)$. The result of $K(x, u)$ is fed back replaces the previous input $v(t)$ into the liquid. The decoder $h(x)$ is not linear but can be simplified to be in a cost-performance trade-off when using a sufficiently large Liquid.

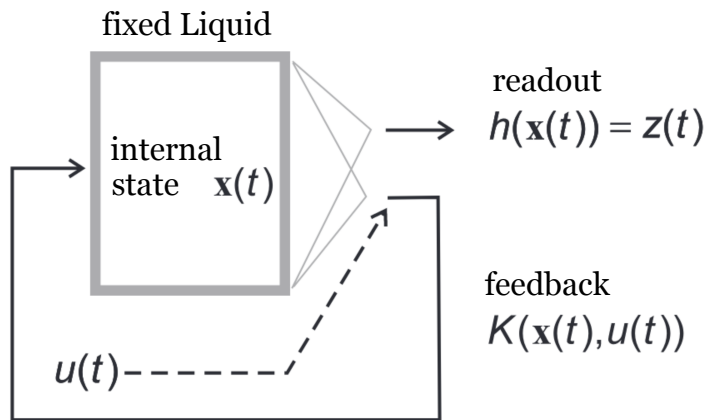


Figure 2.3.3: Adding suitable feedback allows LSMs to be universal approximator.
Adapted from [56]

Balanced Efficient Coding Networks

The concept of tightly balanced spiking networks was initially proposed by Boerlin et al.[11]. It uses predictive coding in combination with spikes to simulate arbitrary linear or non-linear systems[3]. The technical derivation will be described in section 3.3.1. The approach defines a cost function measuring the network's accuracy, along with regularization terms that moderate the spiking behaviour. Using a greedy optimization

algorithm, this cost function determines the voltage threshold and, consequently, the neurons' spiking behaviour.

For each neuron, voltage can be understood as a projection of the global system error to a local error. Each neuron tracks the system error only under its projection. When the error under this projection reaches a threshold, a spike is fired.

The firing of a neuron resets its voltage and corrects the system to reset the perceived projected error.

Balanced networks differ from the previous rate encoding in that excitation and inhibition are closely tracked. In rate-encoded networks, both inhibitory and excitatory spikes are received by a single neuron. A change of the variable is then governed by which type dominates. While this network utilizes rate coding as well, the key distinction to typical rate networks lies in the fact that each spike carries distinct information. In the matter of control, a combination with instantaneous decoding is utilized[44], giving even more influence to a single spike.

Each neuron projects some information about the state and the network. By projecting the system error in different directions, we assign each neuron to track one projection error, identified with a neuron's voltage. If a neuron's voltage reaches the threshold, the projected error exceeds the threshold, a spike is fired and counteracting the projected error.

The projection of the system error, therefore, has immense influence on an individual neuron's spiking behaviour but also the whole network.

On the other hand in rate networks, a population of neurons is given a value to represent and the population spiking rate encodes this value. An individual spike in this population does not have a direct relevance to the system and a discrete impact on its behaviour.

Chapter 3

Methods

3.1 Choice of Network Architecture

The field of SNNs is under ongoing research, resulting in various proposed network models and learning approaches, such as LSMs and REACH[23]. To follow the idea that every spike contains information, purely rate-based spiking networks are disregarded, as there is evidence that the precise spike timing is relevant in nature[17, 67]. On the other hand, the use of HH’s model is prohibitively complex. Additionally there are no learning rules available to solve such a high level problem.

The choice of Efficient coding networks allows us to maintain most of our biological plausibility requirements while enabling the use of high-level learning rules suited for our problem. Since the aim is to learn system dynamics, the SNN should mirror this by learning the dynamics instead of a decoder seen in LSMs. Moreover, the choice of Balanced networks enables us to potentially learn the decoder in addition to the dynamics as well. Lastly, with the proved properties towards noise and robustness it is optimally suited for our problem.

3.2 Approach

The construction of our SNN can be separated into several blocks. Firstly, a SNN is created for simulating a dynamic system with given external inputs.

As a second stage, we derive another SNN that acts as the controller, delivering the

relevant control signals to the first network.

With the controller in place, we focus on learning the dynamics of the first SNN from the ground up. Unfortunately, it was not possible to learn the dynamics of the controlling SNN. However, it is possible to avoid using a dedicated SNN to act as a controller. By replicating the key controlling behaviour of the control network, we are able to control the trained network directly.

3.3 Simulation of Dynamic systems using SNNs

In the following sections the simulation of dynamic systems using SNNs is derived and explained. This serves as a basic building block for our method to achieve our target set in section 1.3. We begin with the formal derivation of the network dynamics.

3.3.1 Balanced network simulation

This section follows the derivation found in [11] and [35]. The goal is to describe a dynamical system of the form

$$\dot{\mathbf{x}} = \mathbf{A}\mathbf{x} + \mathbf{c}(t) \quad (3.1)$$

with J state variables. The estimation is done by leaky integration of spike trains $\mathbf{o}(t)$ in

$$\dot{\hat{\mathbf{x}}} = -\lambda_d \hat{\mathbf{x}} + \boldsymbol{\Gamma} \mathbf{o}(t). \quad (3.2)$$

The Feed-Forward matrix $\boldsymbol{\Gamma}$ is a given matrix of size $\mathbb{R}^{J \times N}$, where N is the number of neurons and predetermined. $\mathbf{o}(t)$ is the spike train of all neurons, specifically

$$o_i(t) = \sum_k \delta(t - t_i^k) \quad (3.3)$$

for neuron i with spike times at times t_i^k .

From eq. (3.2), it becomes clear that each spike carries an important information for the state vector, as each spike in $\mathbf{o}(t)$ changes the approximation $\hat{\mathbf{x}}$ by some weights of $\boldsymbol{\Gamma}$. In addition to the estimate $\hat{\mathbf{x}}$ we define a spiking rate variable \mathbf{r} following the dynamics of

$$\dot{\mathbf{r}} = -\lambda_d \mathbf{r} + \mathbf{o}(t). \quad (3.4)$$

The rate variable is connected to the state vector in the decoding with

$$\hat{\mathbf{x}} = \boldsymbol{\Gamma} \mathbf{r}. \quad (3.5)$$

The spiking dynamics arise from the minimization of a cost function. A spike is fired if it minimizes the cost function that tracks the error between the true and estimated value over time

$$E(t) = \int_0^t \|\mathbf{x}(u) - \hat{\mathbf{x}}(u)\|_2^2 du. \quad (3.6)$$

3.3.2 Greedy Optimization of the Cost

The cost function eq. (3.6) is minimized using a greedy optimization, i.e., a spike is fired if it reduces the cost. For the derivation, we use the cost function in eq. (3.6) and add linear and quadratic cost for regularization, seen in eq. (3.24).

We express this as

$$E(t|i \text{ spike}) < E(t, i \overline{\text{spike}}) \quad (3.7)$$

If there is no spike fired, the rate and estimated state variable in eq. (3.2) and eq. (3.4) respectively behave as

$$\begin{aligned} \dot{\hat{\mathbf{x}}} &= -\lambda_d \hat{\mathbf{x}} \\ \dot{\mathbf{r}} &= -\lambda_d \mathbf{r} \end{aligned} \quad (3.8)$$

and therefore decay exponentially with $e^{-\lambda_d t}$.

If a spike is fired at time t^k , the inhomogeneous solution is found by variation of constants in eq. (3.4) to

$$\begin{aligned} r_i^h &= c_i(t) e^{-\lambda_d t} \\ c'_i(t) e^{-\lambda_d t} - c_i(t) \lambda_d e^{-\lambda_d t} &= -\lambda_d c_i(t) e^{-\lambda_d t} + \delta(t - t^k) \\ c'_i(t) &= \delta(t - t^k) e^{\lambda_d t} \\ c_i(t) &= e^{\lambda_d t^k} \mathbf{H}(t - t^k) \\ r_i &= e^{-\lambda_d t} + e^{-\lambda_d(t-t^k)} \mathbf{H}(t - t^k). \end{aligned} \quad (3.9)$$

The last equation is identical to the solution of eq. (3.8) with the addition of a decaying exponential added at time t^k . $\mathbf{H}(t)$ denotes the Heaviside step function. Analogously,

the estimate is updated at time t^k to

$$\mathbf{x} = \mathbf{x} + \boldsymbol{\Gamma}_i e^{-\lambda_d(t-t^k)} \mathbf{H}(t - t^k). \quad (3.10)$$

We look at the error a ϵ time in the future of t^k and check eq. (3.7)

$$\begin{aligned} & \int_0^{t^k+\epsilon} \left(\underbrace{\|\mathbf{x}(u) - \hat{\mathbf{x}}(u) - \boldsymbol{\Gamma}_i h(u - t^k)\|_2^2}_{\text{I}} + \underbrace{\nu \|\mathbf{r}(u) + \lambda_d \mathbf{e}_i h(u - t^k)\|_1}_{\text{II}} \right. \\ & \quad \left. + \underbrace{\mu \|\mathbf{r}(u) + \lambda_d \mathbf{e}_i h_d(u - t)\|_2^2}_{\text{III}} \right) du \\ & < \int_0^{t^k+\epsilon} (\|\mathbf{x}(u) - \hat{\mathbf{x}}(u)\|_2^2 + \nu \|\mathbf{r}(u)\|_1 + \mu \|\mathbf{r}(u)\|_2^2) du \end{aligned} \quad (3.11)$$

where we abbreviated $h(u) = e^{-\lambda_d(u)} \mathbf{H}(u)$. To treat each term individually, we start with I. Simplifying the norm, we obtain

$$\text{I} = \|\mathbf{x}(u) - \hat{\mathbf{x}}(u)\|_2^2 - 2h(u - t^k) \boldsymbol{\Gamma}_i^T (\mathbf{x}(u) - \hat{\mathbf{x}}(u)) + h^2(u - t^k) \boldsymbol{\Gamma}_i^T \boldsymbol{\Gamma}_i. \quad (3.12)$$

For II, the 1-norm and the rate ensure that the $r_i(u) > 0 \quad \forall i$. Thus, we can simplify $\|\mathbf{r}\|_1 = \sum_k r_k$ resulting in

$$\text{II} = \nu (\|\mathbf{r}\|_1 + h(u - t^k)). \quad (3.13)$$

Similarly to I, III can be simplified by $\|\mathbf{r}\|_2^2 = \mathbf{r}^T \mathbf{r}$, giving

$$\text{III} = \mu \|\mathbf{r}\|_2^2 + \mu h^2(u - t^k) + 2\mathbf{r} \cdot \mathbf{e}_i h(u - t^k). \quad (3.14)$$

After cancellation, the remaining terms are grouped grouped by time dependency to yield

$$\begin{aligned} & \int_0^{t^k+\epsilon} h(u - t^k) \boldsymbol{\Gamma}_i^T (\mathbf{x}(u) - \hat{\mathbf{x}}(u)) - \mu r_i(u) du \\ & > \frac{1}{2} \int_0^{t^k+\epsilon} h^2(u - t^k) \boldsymbol{\Gamma}_i^T \boldsymbol{\Gamma}_i + \nu h(u - t^k) + \mu h^2(u - t^k) du \end{aligned} \quad (3.15)$$

Using the fact that the Heaviside function in eq. (3.9) and subsequently in $h(u)$ allow us to change the borders of integration to $\int_{t^k}^{t^k+\epsilon}$. Lastly, we simplify $h(t) = 1$ if $t \approx \epsilon$, and have

$$\boldsymbol{\Gamma}_i^T (\mathbf{x} - \hat{\mathbf{x}}) - \mu r_i > \frac{\|\boldsymbol{\Gamma}\|^2 + \nu + \mu}{2} \quad (3.16)$$

We note the Left Hand Side (LHS) as the voltage

$$V_i(t) = \mathbf{\Gamma}^T(\mathbf{x}(t) - \hat{\mathbf{x}}(t)) - \mu r_i(t) \quad i = 1 \dots N. \quad (3.17)$$

and the constant RHS as the voltage threshold T_i

$$V_i > T_i = \frac{\|\mathbf{\Gamma}_i\|^2 + \nu + \mu}{2}. \quad (3.18)$$

The dynamic variable \mathbf{x} is tracked by firing spikes in when the defined "voltage" of a neuron surpasses its threshold.

For negligible quadratic cost μ , the voltage can be understood as a measure of the error projected on $\mathbf{\Gamma}_i$.

3.3.3 Neuron Voltage

As mentioned above, a neuron spikes if it meets the condition eq. (3.18). But so far, it is unclear how neuron voltage evolves over time. Denote \mathbf{L} the left pseudo-inverse of $\mathbf{\Gamma}$

$$\mathbf{L} = (\mathbf{\Gamma}\mathbf{\Gamma}^T)^{-1}\mathbf{\Gamma} \quad (3.19)$$

such that $\mathbf{L}\mathbf{\Gamma}^T = \mathbf{I}$.

Next, taking the derivative of eq. (3.17) yielding

$$\dot{\mathbf{V}}(t) = \mathbf{\Gamma}^T(\dot{\mathbf{x}}(t) - \dot{\hat{\mathbf{x}}}(t)) - \mu \dot{\mathbf{r}}(t). \quad (3.20)$$

Now using the pseudo-inverse to rewrite the voltage equation eq. (3.17) as

$$\begin{aligned} \mathbf{V}(t) &= \mathbf{\Gamma}^T(\hat{\mathbf{x}}(t) - \mathbf{x}(t)) - \mu \mathbf{r}(t) \\ \mathbf{L}\mathbf{V}(t) &= (\mathbf{x}(t) - \hat{\mathbf{x}}(t)) - \mu \mathbf{L}\mathbf{r}(t) \\ \mathbf{x}(t) &= \mathbf{L}\mathbf{V}(t) + \hat{\mathbf{x}}(t) + \mu \mathbf{L}\mathbf{r}(t) \end{aligned} \quad (3.21)$$

Now the derivative terms in eq. (3.20) are replaced with their respective equations eq. (3.1), eq. (3.2) and eq. (3.4). Lastly, we substitute eq. (3.21) into eq. (3.20) and

obtain

$$\begin{aligned}\dot{\mathbf{V}} = & \mathbf{\Gamma}^T \mathbf{A} \mathbf{L} \mathbf{V} \\ & + (\mathbf{\Gamma}^T \mathbf{A} \mathbf{\Gamma} + \mu \mathbf{\Gamma}^T \mathbf{A} \mathbf{L} + \lambda_d \mathbf{\Gamma}^T \mathbf{\Gamma} + \mu \lambda_d) \mathbf{r} \\ & + (\mathbf{\Gamma}^T \mathbf{\Gamma} + \mu \mathbf{I}) \mathbf{o} + \mathbf{\Gamma}^T \mathbf{c}.\end{aligned}\quad (3.22)$$

The last argument is to consider the network behaviour for larger networks. We increase the number of neurons $N \rightarrow \infty$ and require that the network output as well as the firing rates remain constant.

When looking at the decoding at eq. (3.5) we therefore need to scale $\mathbf{\Gamma}$ by $\frac{1}{N}$. To make sure that the threshold in eq. (3.18) will not get dominated by cost terms μ & ν , they should also scale with $\frac{1}{N^2}$. As the threshold decreases with $\frac{1}{N^2}$ so does the Voltage itself. With this in mind, all terms that scale with $\frac{1}{N^2}$ are neglected. As a substitute for the neglected voltage term, a generic leak term is added, making these LIFs neurons. The dynamics are therefore

$$\begin{aligned}\dot{\mathbf{V}} = & -\lambda_V \mathbf{V} + \mathbf{W}^s \mathbf{r} + \mathbf{W}^f \mathbf{o} + \mathbf{\Gamma}^T \mathbf{c} + \sigma_V \boldsymbol{\eta}(t) \\ \mathbf{W}^s = & \mathbf{\Gamma}^T (\mathbf{A} + \lambda_d \mathbf{I}) \mathbf{\Gamma} \\ \mathbf{W}^f = & -(\mathbf{\Gamma}^T \mathbf{\Gamma} + \mu \mathbf{I})\end{aligned}\quad (3.23)$$

Lastly, to complete the derivation, a noise term $\boldsymbol{\eta}$ with scaling factor σ_V was added to simulate the inherent noise found in the brain.

3.3.4 Regularization

Two regularization terms were added to influence spiking behaviour.

$$E(t) = \int_0^t (\|\mathbf{x}(u) - \hat{\mathbf{x}}(u)\|_2^2 + \nu \|\mathbf{r}(u)\|_1 + \mu \|\mathbf{r}(u)\|_2^2) du \quad (3.24)$$

The parameter ν controls the amount of spiking by penalizing the total number of spikes as

$$\|\mathbf{r}(t)\|_1 = \sum_i |r_i(t)| = \sum_i r_i(t). \quad (3.25)$$

The firing rate is directly related to the number of spikes, and therefore the cost is reduced by fewer spikes.

The second term solves different issues at the same time. One problem concerns networks that have decoding kernels with the same direction but opposite sign. To show this, we imagine a network of only two neurons. A network of two neurons is sufficient to simulate a scalar ordinary differential equation (ODE) i.e $\mathbf{A} \in \mathbb{R}$. We further assume that the feed-forward weights Γ have the form

$$\Gamma = \begin{bmatrix} -1 \\ 1 \end{bmatrix} \quad (3.26)$$

Ignoring the cost terms in eq. (3.18), the threshold is set at

$$V_i > \frac{\|\Gamma_i\|^2}{2} \quad (3.27)$$

after which that a spike is fired, and the voltage of neuron i resets to

$$V_i = V_i + \mathbf{W}_{ii}^s = V_i + \|\Gamma_i\|_2^2 \quad \text{with } \mathbf{W}^f = \begin{bmatrix} -1 & 1 \\ 1 & -1 \end{bmatrix} \quad (3.28)$$

ideally setting the Voltage to $-T_i$. This can be seen when looking at the threshold as

$$T_i = \frac{\|\Gamma_i\|^2}{2} = \frac{-\text{diag}(\mathbf{W}^f)}{2}. \quad (3.29)$$

The repolarization of the spiking neuron acts as a depolarization or pushing the voltage towards its threshold for neurons with opposing signs. The problem now is that for neurons with the same kernel magnitude, the depolarization is large enough to push this neuron over the threshold. The subsequent spike repolarizes the neuron but in turn excites the first neuron over its threshold. This back and forth pattern of "ping-ponging" repeats indefinitely.

For the given example above, the threshold is set to 0.5 for both neurons. The neurons' voltages of are identical up to the sign, as they are tracking the error for the same variable. When one neurons reaches the threshold of 0.5 the second neuron's voltage is close to -0.5 considering noise (in a perfect system minus the value of the spiking neuron). After the spike is fired, the first neuron is reset to -0.5 , stemming from

\mathbf{W}_{00}^f ,

$$\begin{aligned}\mathbf{V} &= \mathbf{V} + \mathbf{W}^f \mathbf{o} = \mathbf{V} + \mathbf{W}^f \begin{bmatrix} 1 \\ 0 \end{bmatrix} = \mathbf{V} + \mathbf{W}_{*0}^f \\ \mathbf{V} &= \begin{bmatrix} 0.5 \\ -0.5 \end{bmatrix} + \begin{bmatrix} -1 \\ 1 \end{bmatrix} = \begin{bmatrix} -0.5 \\ 0.5 \end{bmatrix}\end{aligned}\tag{3.30}$$

whereas the second neuron gets pushed up to 0.5, causing a spike. This, in turn, reverts the changes of eq. (3.30), resulting in a loop. This problem is caused by the greedy optimization, looking only at the immediate future to decrease the cost.

To fix this, the threshold is slightly increased, disallowing a spike to reach the opposing neuron's threshold. As seen above in eq. (3.18), this can be done by either raising the linear or quadratic cost.

The second issue fixed by adding quadratic cost is when there are neurons with similar kernel direction but non-normalized. In a perfect noise-free scenario, the neuron with the smaller threshold will always fire first. The neurons reset after the spike will reset the neurons with similar direction, inhibiting the second neuron from ever firing. The linear cost does not make a difference since it is penalizing the global number of spikes but does not discern where the neurons are firing. By penalizing the rate in the 2-norm, it forces the network to spread the firing among the whole network.

3.4 Control of Dynamic Systems using SNNs

3.4.1 Balanced Networks as a Controller

We now make the step to use the balanced network approach from above as a controller mechanism.

The idea was adopted from [37] and is illustrated in fig. 3.4.1. With the given reference signal, the produced network spikes are decoded into a control signal, which is then further fed into the dynamical system.

The system itself is simulated using a common numerical method, i.e. explicit Euler. Yet the goal is to capture the entire problem using SNNs. The control signal \mathbf{u} is generated using the an independent SNN which is, in turn, the command \mathbf{c} for a separate SNN simulating the states with feedback to the controlling SNN.

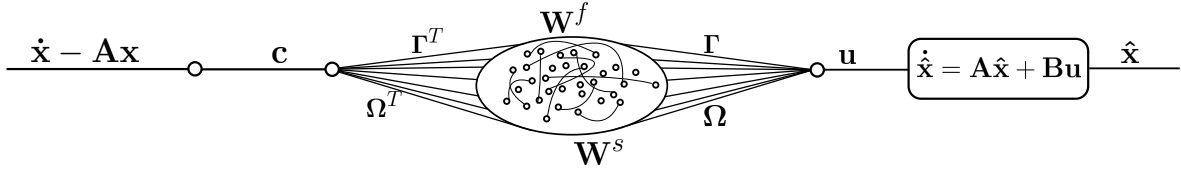


Figure 3.4.1: Schematic to illustrate the use of balanced networks as controllers.

3.4.2 Dynamics

The derivation of this method is similar to the one in section 3.3. Names and variables are reused if not stated here.

The system in question has the form

$$\dot{\hat{x}} = A\hat{x} + Bu. \quad (3.31)$$

The basic definitions of the SNN remain the same with rate r as well as decoding weights Γ . Additionally, [37] defines instantaneous decoding weights Ω with the same shape as $\Gamma \in \mathbb{R}^{J \times N}$. It is important to note that J does not represent the number of state variables but the number of inputs. The decoding is the same as in eq. (3.5) with the added Ω giving.

$$u(t) = \Gamma r + \Omega o. \quad (3.32)$$

The derivation of the network dynamics in [35] is similar to [11] and the derivation presented above. Differences arise in the computation of the cost function as the spike changes the system to

$$\begin{aligned} u &= u + h(t - t^k)\Gamma_k + \Omega_k \\ r &= r + h(t - t^k)e_k \\ \hat{x} &= \hat{x} + h(t - t^k) \int_0^{t-t^k} e^{(\mathbf{A} + \lambda_d \mathbf{I})\zeta} d\zeta \mathbf{B}\Gamma_k + e^{A(t-t^k)} \mathbf{B}\Omega_k \end{aligned} \quad (3.33)$$

where Γ_k and Ω_k correspond to the k -th column of Γ , Ω and h the same as defined above. Results are similar for the rate and control signal whereas the state update is obtained by formally integrating the system. The rest of the derivations are analogous

and completely derived in [37]. The results summarize to eqs. (3.34) to (3.39).

$$\mathbf{V} = \boldsymbol{\Omega}^T \mathbf{B}^T (\mathbf{x} - \hat{\mathbf{x}}) - \mu \mathbf{r} \quad (3.34)$$

$$\dot{\mathbf{V}} = -\lambda_V \mathbf{V} + \boldsymbol{\Omega}^T \mathbf{B}^T \mathbf{c}(t) + \mathbf{W}^f \mathbf{o} + \mathbf{W}^s \mathbf{r} \quad (3.35)$$

$$\mathbf{c} = \dot{\mathbf{x}} - \mathbf{A} \mathbf{x} \quad (3.36)$$

$$\mathbf{W}^f = -(\boldsymbol{\Omega}^T \mathbf{B}^T \mathbf{B} \boldsymbol{\Omega} + \mu \mathbf{I}) \quad (3.37)$$

$$\mathbf{W}^s = -\boldsymbol{\Omega}^T \mathbf{B}^T \mathbf{B} \boldsymbol{\Gamma} \quad (3.38)$$

$$T_i = \frac{\boldsymbol{\Omega}_i^T \mathbf{B}^T \mathbf{B} \boldsymbol{\Omega}_i + \nu + \mu}{2} \quad (3.39)$$

Note that the notation differs in the original paper and the reference signal is denoted by $\hat{\mathbf{x}}$ instead of \mathbf{x} here and $\boldsymbol{\Omega}_i$ again refers to the i -th column of $\boldsymbol{\Omega}$.

3.4.3 The Instantaneous Decoding Weights

The presence of instantaneous decoding is necessary; otherwise no spiking can occur. In eq. (3.33), the control signal is integrated with the matrix exponential. The problem is that the integral

$$\lim_{t \rightarrow 0} \int_0^t e^{(\mathbf{A} + \lambda_d \mathbf{I})\zeta} d\zeta = 0 \quad (3.40)$$

for our small ϵ time horizon.

This is true for any matrix exponential $e^{\Lambda\zeta}$ seen by Taylor expansion

$$\begin{aligned} \lim_{t \rightarrow 0} \int_0^t e^{\Lambda\zeta} d\zeta &= \lim_{t \rightarrow 0} \int_0^t \sum_{k=0}^{\infty} \frac{(\Lambda\zeta)^k}{k!} d\zeta \\ &= \lim_{t \rightarrow 0} \sum_{k=1}^{\infty} t \frac{(\Lambda t)^{k-1}}{k!} = 0. \end{aligned} \quad (3.41)$$

This means that the rate decoding vanishes in the derivation of eqs. (3.34) to (3.39). Therefore, the firing threshold condition becomes

$$-\mu \mathbf{r}_i > \frac{\nu + \mu}{2} \quad (3.42)$$

if $\boldsymbol{\Omega}$ is ignored, which is an insatiable condition since \mathbf{r} is always non-negative.

3.4.4 Extension with Direct Error Feedback

The same group of [37] later published a new but very similar approach in [36] which is based on the same idea. However the approach in [36] makes the error a direct part of the voltage dynamics. The difference arises from the an new derivation avoiding the pseudo-inverse \mathbf{L} .

Instead, during the analogous step of eq. (3.20), they set $\hat{\mathbf{x}}$ and \mathbf{x} to follow the same dynamics, namely

$$\dot{\mathbf{x}} = \mathbf{Ax} + \mathbf{c}(t) \quad (3.43)$$

for the reference signal and

$$\dot{\hat{\mathbf{x}}} = \mathbf{A}\hat{\mathbf{x}} + \mathbf{Bu} \quad (3.44)$$

for the system.

In total, this adjustment changes the dynamics of eq. (3.35) to

$$\dot{\mathbf{V}} = -\lambda_V \mathbf{V} + \boldsymbol{\Omega}^T \mathbf{B}^T \mathbf{A} \mathbf{e}(t) + \boldsymbol{\Omega}^T \mathbf{B}^T \mathbf{c}(t) + \mathbf{W}^f \mathbf{o} + \mathbf{W}^s \mathbf{r}. \quad (3.45)$$

Due to the assumption of eq. (3.43), the derivation changes in two aspects. Firstly, the construction of the pseudo-inverse can be avoided, making the consideration of the limit is rendered obsolete. Instead of eliminating the \mathbf{x} , it is kept directly in the voltage equation and with the substitution of eq. (3.43). Without considering the limit, the definition of \mathbf{W}^s changes to

$$\mathbf{W}^s = -\boldsymbol{\Omega}^T \mathbf{B}^T \mathbf{B} \boldsymbol{\Gamma} + \mu \mathbf{I}. \quad (3.46)$$

As done previously, a white noise process η is added to complete the dynamics.

3.5 Learning of network parameters

All the methods described above work on the optimally ideal weights for the dynamics. However in nature often new skills or dynamics are learned and not optimally tuned for the problem at hand. In the following chapter the optimally of derived is explained and local learning rules for the weights are introduced. Specifically, the learning rules presented in [14–16].

3.5.1 Learning of Fast Connection Weights \mathbf{W}^f

Before deriving the learning rule, we are first going to establish the idea that the minimization of the loss is equal to minimizing the fluctuations of the membrane potential.

This assumption is based on the fact that the voltage is the projected error of the tracked signal to the reference. Therefore, good tracking should cancel out

$$\mathbf{V} = \boldsymbol{\Gamma}(\mathbf{x} - \hat{\mathbf{x}}) \approx \mathbf{0} \quad (3.47)$$

neglecting the regularization terms.

Therefore, the average membrane voltage

$$L = \int_0^T \frac{1}{2} \mathbf{V}(t)^2 dt \quad (3.48)$$

over time serves as a good and simple measure of tracking performance.

Since the voltage is bound by the threshold, the computation of the average can be reduced to averaging of the spikes.

Learning with L_1 Costs As such, the minimal variation is given if the voltage threshold and its respective reset are centred around zero. Voltage resets, given by \mathbf{W}_i^f for spiking neuron i , need to be strengthened if its reset undershoots the negative threshold value T_i and vice versa. A spiking reset that hyperpolarized the neuron over the negative threshold will be weakened.

Mathematically, this averaging over spikes condition is formulated as the loss at time t , using the fact we can express the voltage post-spike \mathbf{V}^{post} as

$$\mathbf{V}^{\text{post}} = \mathbf{V}^{\text{pre}} + \mathbf{W}^f \mathbf{e}_i \quad (3.49)$$

for neuron i firing a spike.

Taking the derivative of the loss function in eq. (3.53) with respect to Ω yields

$$\frac{\partial L_t}{\partial \mathbf{W}^f} \propto (2\mathbf{V}^{\text{pre}}(t) + \mathbf{W}^f \mathbf{e}_i) \mathbf{e}_i^T \quad (3.50)$$

Rewriting the equation above and adding a tuning parameter gives the learning rule

$$\Delta \mathbf{W}_{ij}^f = -\frac{\partial L_t}{\partial \mathbf{W}_{ij}^f} \propto -(\mathbf{V}_i^{\text{pre}}(t) + \beta \mathbf{W}_{ij}^f). \quad (3.51)$$

It is important to note that this learning rule only becomes active during the firing of a spike. This means that if no spike is fired, no learning takes place. To introduce spiking and learning, smoothed noise is often used to induce firing of all neurons.

The role of β is to regulate the amount of spiking by artificially increasing the magnitude of the recurrent weights. Therefore, with increased magnitude, neurons are overly hyperpolarized after a spike, making it harder to spike again soon, similar to how the linear costs above reduce spiking activity.

Choosing $\beta \approx \frac{1}{2}$ will lead to low linear costs at the risk of degrading into ping-pong patterns described previously. It is important to note that this learning rule is entirely local and can be categorized as a Hebbian learning rule, as the presynaptic voltage is multiplied by the postsynaptic reset, given by the column in \mathbf{W}^f .

Learning with L_2 costs

The previous derivation only incorporated $L1$ costs using the β parameter, but did not implement any $L2$ regularization as in the derivation in section 3.3. With $L2$ costs, the optimal matrix is given by the addition of the quadratic cost term to the diagonal as in eq. (3.23). Since the cost term is added to the matrix \mathbf{W}^f and the voltage definition in eq. (3.17), the voltage no longer explicitly tracks the projected error. To reuse the argument about minimizing Voltage fluctuations as a performance measure, we, therefore add the terms again to cancel out the terms from the previous definition. Specifically, we want to work with true projection error \mathbf{V}_{ex} and therefore compute the loss in eq. (3.53) using

$$\begin{aligned} \mathbf{V}_{\text{ex}} &= \mathbf{V} + \mu \mathbf{r} \\ \mathbf{W}_{\text{ex}}^f &= \mathbf{W}^f + \mu \mathbf{I}. \end{aligned} \quad (3.52)$$

We then formulate the same argument on the loss

$$\begin{aligned} L_t &= \left\| \frac{1}{2} (\mathbf{V}_{\text{ex}}^{\text{pre}}(t) + \mathbf{V}_{\text{ex}}^{\text{post}}(t)) \right\|^2 \\ &= \left\| \mathbf{V}^{\text{pre}}(t) + \mu \mathbf{r}(t) + \frac{1}{2} (\mathbf{W}^f + \mu \mathbf{I}) \mathbf{e}_i \right\|^2 \end{aligned} \quad (3.53)$$

and take the derivative with respect to \mathbf{W}^f , resulting in the learning rule of the form

$$\Delta \mathbf{W}_{ij}^f = -\frac{\partial L_t}{\partial \mathbf{W}_{ij}^f} \propto -\beta (\mathbf{V}_i^{\text{pre}}(t) + \mu \mathbf{r}_i(t)) - \mathbf{W}_{ij}^f - \mu \delta_{ij} \quad (3.54)$$

when a spike is fired.

3.5.2 Learning of Slow Connection Weights \mathbf{W}^s

The recurrent weights \mathbf{W}^s are called slow because they are in conjunction with the filtered spike train $\mathbf{r}(t)$ in eq. (3.22) in contrast to \mathbf{W}^f , which resets the neuron voltage after a spike.

For learning \mathbf{W}^s an adaptive learning approach from [15] is used.

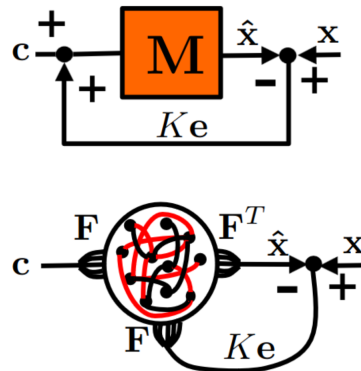


Figure 3.5.1: Schematic of error feedback in the learning of \mathbf{M} resp. \mathbf{W}^s . Taken from [15].

For this, we consider a "learner" dynamic system of the form

$$\dot{\hat{\mathbf{x}}} = \mathbf{M}\hat{\mathbf{x}} + \mathbf{c}(t) \quad (3.55)$$

where the matrix \mathbf{M} changes to allow $\hat{\mathbf{x}}$ to follow the same dynamics of \mathbf{x} given by

$$\dot{\mathbf{x}} = \mathbf{A}\mathbf{x} + \mathbf{c}(t). \quad (3.56)$$

Over time, \mathbf{M} should converge to \mathbf{A} . To facilitate this, the error $\mathbf{e} = \mathbf{x} - \hat{\mathbf{x}}$ is fed back into the learner system $\dot{\hat{\mathbf{x}}} = \mathbf{M}\hat{\mathbf{x}} + \mathbf{c}(t) + K\mathbf{e}$ to direct \mathbf{M} .

The adjustment of \mathbf{M} in the modified dynamics

$$\dot{\hat{\mathbf{x}}} = (\mathbf{M} + K\mathbf{I})\hat{\mathbf{x}} + \mathbf{c}(t) + K\mathbf{x} \quad (3.57)$$

is then calculated by using minimizing the loss

$$L = \frac{1}{2} \mathbf{e}^T \mathbf{e} \quad (3.58)$$

with respect to the matrix parameters M_{ij} and changing their value according to

$$\dot{M}_{ij} = -\frac{\partial L}{\partial M_{ij}} = \left(\frac{\partial \hat{\mathbf{x}}}{\partial M_{ij}} \right)^T \mathbf{e}. \quad (3.59)$$

The derivative in $\frac{\partial \hat{\mathbf{x}}}{\partial M_{ij}}$ is computed under the assumption that K is much larger than the eigenvalues of \mathbf{M} and $\mathbf{c} = \text{const}$. As a simplification we choose $\mathbf{c} = \mathbf{0}$. and formerly integrate eq. (3.56) to obtain $\mathbf{x} = e^{\mathbf{A}t} \mathbf{x}_0$. We plug this in eq. (3.57), solve again and obtain

$$\hat{\mathbf{x}} = (\mathbf{A} + K\mathbf{I} - \mathbf{M})^{-1} K e^{\mathbf{A}t} \mathbf{x}_0 + e^{(\mathbf{M}-K\mathbf{I})t} \hat{\mathbf{x}}_0 \approx e^{(\mathbf{M}-K\mathbf{I})t} \hat{\mathbf{x}}_0. \quad (3.60)$$

The first term is neglected due to the assumption and the inverse approximation

$$(K\mathbf{I} + \mathbf{A} - \mathbf{M})^{-1} = K^{-1}\mathbf{I} - K^{-2}(\mathbf{A} - \mathbf{M})^{-1} + \mathcal{O}(\|\mathbf{A} - \mathbf{M}\|^2). \quad (3.61)$$

From this approximation, the desired derivative of eq. (3.59) is given by

$$\frac{\partial L}{\partial \mathbf{M}} \propto \hat{\mathbf{x}}^T \mathbf{e} \quad (3.62)$$

To convert this learning rule for the system \mathbf{A} into a learning rule for \mathbf{W}^s , the change of \mathbf{W}^s is identified by a change in the underlying dynamical system $\Gamma^T \mathbf{M} \Gamma$. The corresponding learning rule becomes

$$\dot{\mathbf{W}}^s \propto \Gamma \dot{\mathbf{M}} \Gamma. \quad (3.63)$$

Another interpretation of the formulation is in a form of feedback alignment. As the error is feed back into the network via Γ (fig. 3.5.1), the matrix \mathbf{M} (and in extension \mathbf{W}^s) self-aligns to the error along Γ^T . This has been demonstrated in [52] and has shown comparable performance to BP.

Chapter 4

Results

In the following chapter we present the results from implementing the in chapter 3 introduced methods in the same order. We start by giving an interpretation of the networks behaviour in simulation with a subsequent parameter study.

Afterwards, the control approach is discussed and both derivations are briefly compared. To that important implementation details are explained to facilitate acceptable performance. It is also illustrated that the network as described acts more as an open loop controller. Control is displayed with both a dynamic system as well as a network as the underlying system to control.

As a next step, the results on the learning are presented and a parameters study is conducted for selected parameters and corresponding values. Also different sequences for learning are considered.

Lastly all of the previous steps are combined in an attempt to control a system.

4.1 Results on the Simulation from section 3.3

4.1.1 Illustrative Example

The results from simulating the network with a given input $c(t)$ can be seen in fig. 4.1.1. The external input follows a linear increase until 0.15s, after which it remains constant. In this scalar example, the ODE

$$\dot{x} = -10x + c(t) \quad (4.1)$$

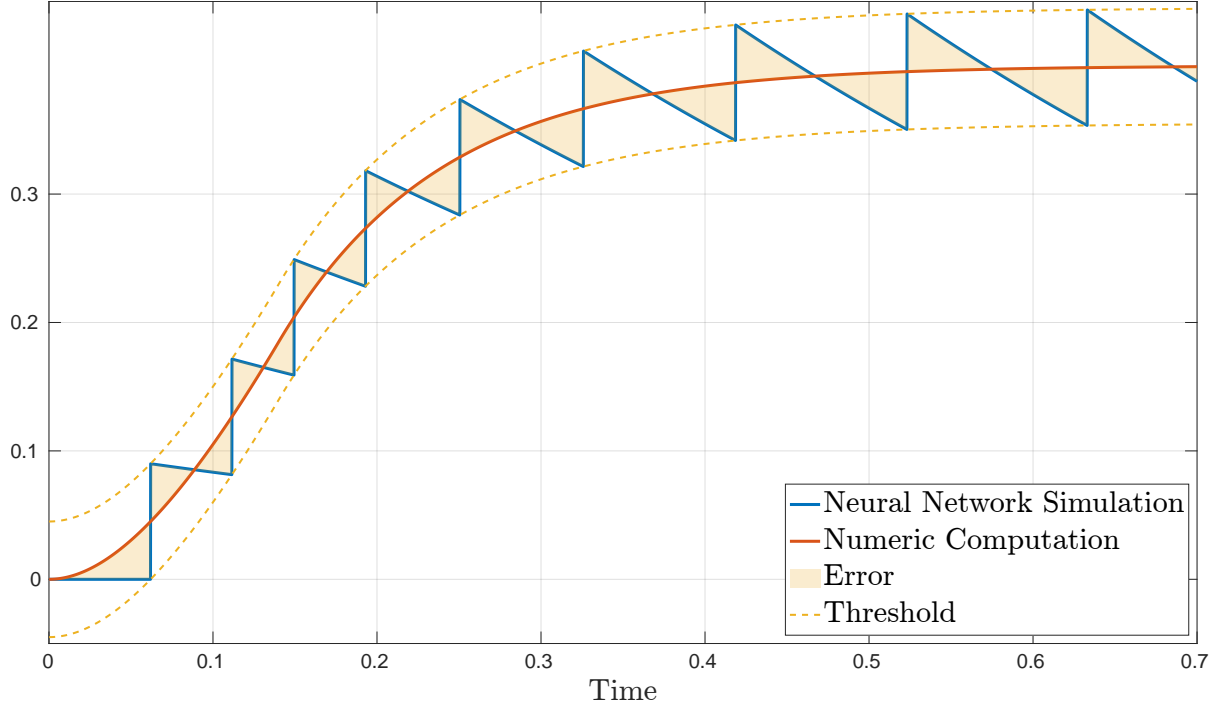


Figure 4.1.1: Baseline example

is simulated with 2 neurons. One neuron corrects the network simulation of the system up and down, respectively. As shown before, this correction happens immediately after each spike by adding weights of the relevant decoding vector to the trajectory. Since this example is following a scalar variable with two neurons, the decoding matrix $\Gamma \in \mathbb{R}^{1 \times 2}$ is set to $[0.09, -0.09]$ for this example. This can be seen in fig. 4.1.1, where the neural network simulation jumps up after each spike by 0.09 is added.

For reference, a conventional numerical solution is given which lies directly between the two neurons' thresholds, visualized with dotted lines.

Already for this example, different parameters can be tuned to get different results.

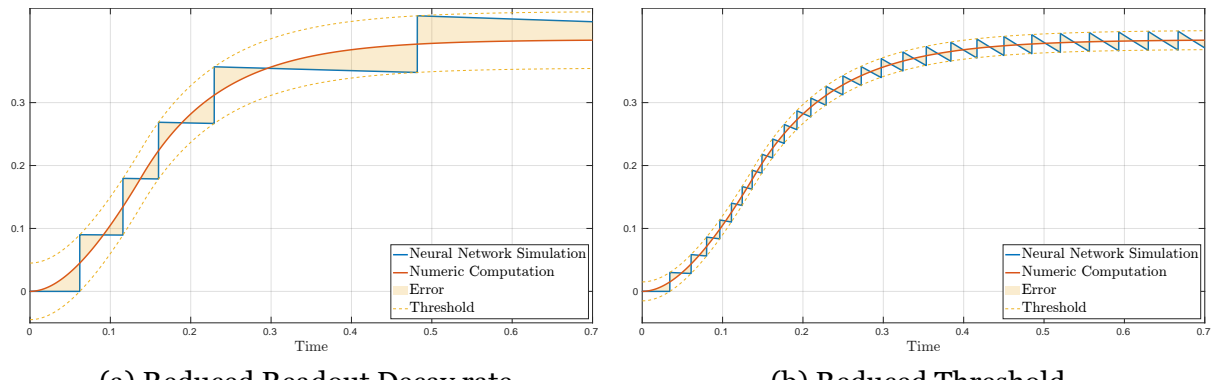


Figure 4.1.2: Variation of Readout Decay and Decoder for a simple 1D system.

In fig. 4.1.2a, the readout decay is reduced compared to fig. 4.1.1, which reduces how

fast the output tends to zero. This also elevates the importance of a single spike, as it has longer lasting effects on the output, seen by the system showing fewer spikes than before.

Alternatively, if the decoding weights can be scaled to let each spike make a smaller change in the output, seen in fig. 4.1.2b. Since the threshold is closely tied to the Decoding weights this also reduces the spike threshold and therefore yields more accurate results.

4.1.2 Illustrative example in 2D: Geometric interpretation

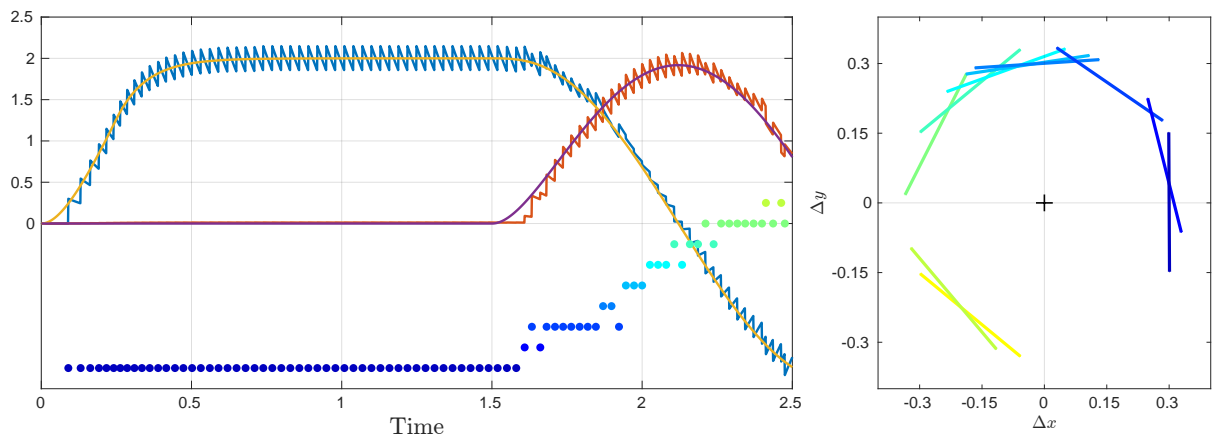


Figure 4.1.3: Simple 2D example with numerical solution and spike response. Curves for x in yellow/blue. Curves for y in purple/red. The network's output closely tracks the perfect numerical solution. For the network, each decoding vector was chosen from a normal distribution and normalized to $\|\Gamma_i\|_2 = 0.3$. Beneath a raster plot for each spiking neuron. On the left, the threshold for each neuron's projected error.

In two dimensions, the network also allows for a geometric interpretation. For this, we let the network simulate a simple leaky integration of inputs as in eq. (4.1) but in two dimensions. In fig. 4.1.3, we can see that at different times different neurons are activated. The corresponding fires according to the phase plot on the right in fig. 4.1.3. In detail, this can be seen in fig. 4.1.4. Here a simulation is run with just 4 neurons, covering the two axes. The lines in the bottom right panel show the thresholds of each neuron in the direction of its projected error. As the input c is fed into the net, the error rises while the network remains dormant. This can be seen in the zoom-in section of fig. 4.1.4 in the bottom left. This error is also shown as an orange arrow of originating from the origin in the bottom right panel. The Voltage, and thus the error, rise until the threshold is reached. After a spike is fired, indicated by the spike plot underneath on the left and the crossing of the threshold in dark blue, the network output is shifted by

adding Γ_i to it. This can also be observed, as the error in the bottom left panel moves closer to the origin. With the continuous input c , next the threshold of the neuron in green is reached, causing a spike to be fired resetting the error again and adding a jump in negative y direction to the network output. The spike moves the error orthogonal to the threshold line closer to the origin. In networks with more neurons, this jump can reduce or increase the errors of other neurons and even bring them to fire. From the perspective of the neuron with the turquoise limit, a spike of the dark blue neuron directly increases its perceived error. If no regularization in terms of μ or ν is used, a spike from one side of the threshold would move the signal exactly to the opposite neuron threshold.

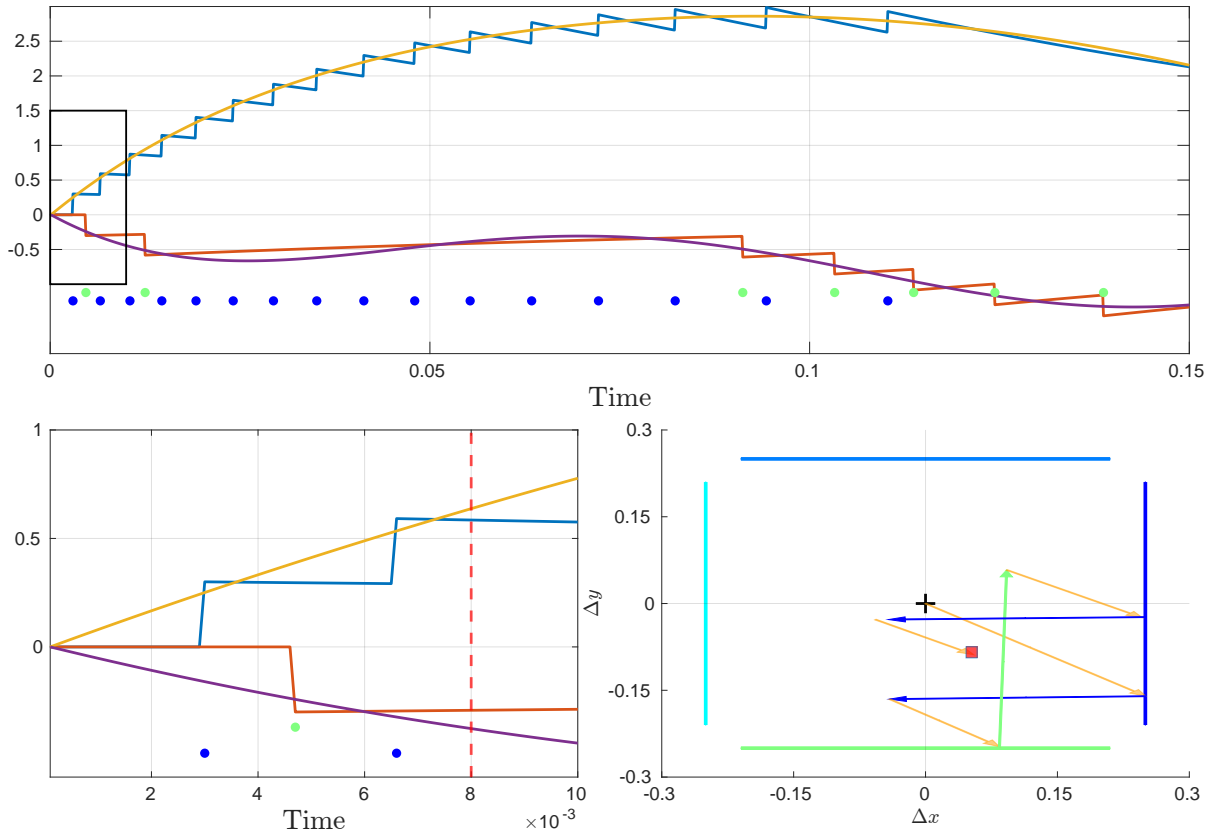


Figure 4.1.4: Simple 2D example with numerical solution and spike response. Curves for x in yellow/blue. Curves for y in purple/red. The network's output closely tracks the perfect numerical solution. For the network each decoding vector was chosen from a normal distribution and normalized to $\|\Gamma_i\|_2 = 0.3$. Beneath a raster plot for each spiking neuron. On the left the threshold for each neuron's projected error. The quadratic cost $\mu = 0.3$.

4.1.3 Importance of Feed-Forward weights

So far, we have not given much attention to Feed-Forward weights. Yet, they play a crucial role in the performance of our network, as seen in fig. 4.1.5. Here we simulate again a simple leaky integration as in eq. (4.1) however this time in 2D. With the output, in each test we also plot the bounding box of neuron thresholds for the projected error. The bounding box of the error is the normal to each of the decoding weights. In eq. (3.2), the network output gets the i th column Γ added when the i th neuron spikes. From the minimization of the cost, we know that the spike of neuron i reduces the error in the direction by Γ_i . If we know imagine the origin of the fig. 4.1.5 l to always be on top of the true trajectory of $[x, y]^T$, the network's error is just the deviation from the origin.

As can be seen in the fig. 4.1.5, the more uniform the decoding weights are distributed, the better the network accuracy. In fig. 4.1.5a, it is possible to see the spiking neurons engage after another as the input is alternating. This can also be observed in fig. 4.1.5b, although higher irregularity in the spiking can be observed compared to fig. 4.1.5a. This is because in the second quadrant of the projected error plot, more neurons are more densely packed. Meanwhile, in the third and the fourth quadrant, approximately only three neurons cover the bottom limit (if their lines are extended). This cone comprised of the dark blue and yellow neuron engages in rapid alternating firing in order to keep follow the trajectory.

In the last example, a particularly bad choice of Feed-Forward weights is displayed. Here, the box is not fully enclosed by neurons, resulting in the network being completely blind to errors in these directions.

4.1.4 Bigger Systems

Until now, the systems we considered at were only in 1D or 2D. However, our network can also simulate more complex higher-dimensional systems. In the example in fig. 4.1.6, we simulated a linear n-mass spring system with the dynamics

$$m_i \ddot{x}_i = K \cdot \begin{bmatrix} 1 & -2 & 1 \end{bmatrix} \cdot \begin{bmatrix} x_{i-1} \\ x_i \\ x_{i+1} \end{bmatrix} + c_i(t). \quad (4.2)$$

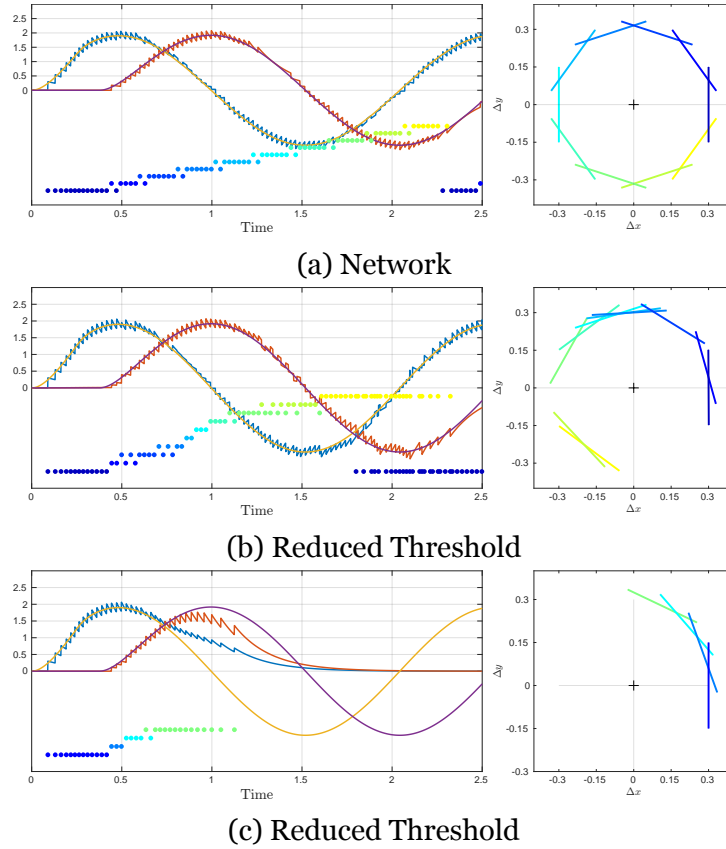


Figure 4.1.5: Network output after leaky integration of oscillating input with different decoding vectors.

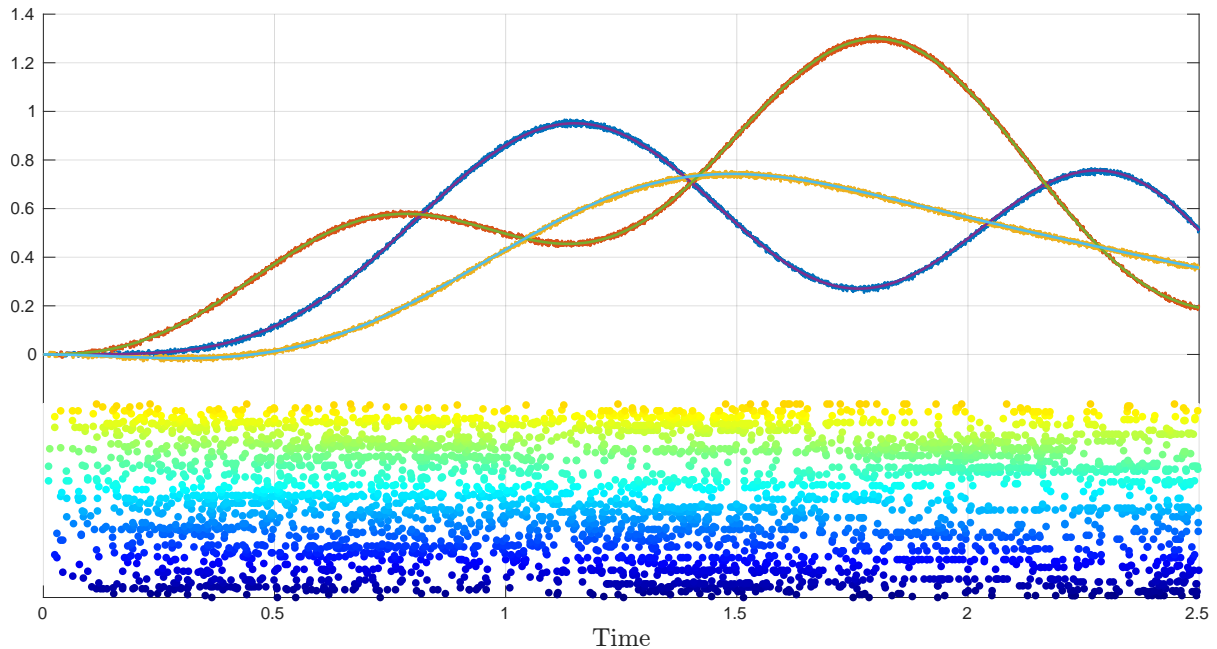


Figure 4.1.6: Trajectory of dynamic mass spring system with 100 masses and 2 thousand neurons. Only the first 3 trajectories are plotted and the spikes for the first 200 neurons.

The external forces were each offset sinusoidal waves with varying frequency and amplitude for the first 3 masses and random forces for the rest. As can be seen from the figure, the network perfectly overlays the numerical solution even when tasked to simulate 200 DoFs and 2 thousand neurons. The accuracy remains high throughout all simulated states and is not concentrated to only few states.

4.1.5 Varying cost parameters μ, ν

After demonstrating the theoretical and geometric interpretation of regularization, we quickly show their effects on the whole network simulation. In fig. 4.1.7, the same simulation as in section 4.1.3 with different μ and ν is run. Comparing each the bottom two plots with the reference shows the influence of the regularizations. Without any regularization, accuracy is good with frequent spiking. A small segment of the simulation shows first signs of ping-ponging behaviour, seen either in the spike histogram or the raster plot of spikes. Here, ping-ponging can be seen between 2s–2.5s with two neurons firing ($3 \leftrightarrow 11$ or $4 \leftrightarrow 11$) repeatedly.

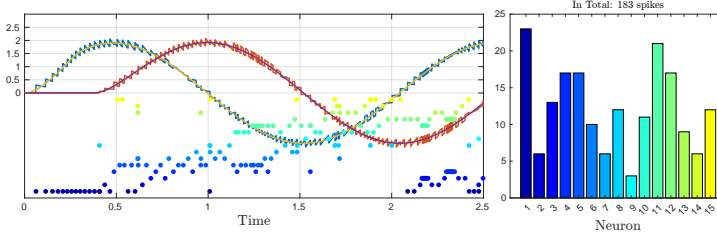
Adding L1 costs μ successfully removes the ping-pong behaviour visible in the spike plot while also cutting the total amount of spikes in half, yielding a net reduction in spikes without noticeable loss of accuracy. However, spiking remains imbalanced with one neuron firing almost three times the average number of spikes.

In contrast to fig. 4.1.7b, in fig. 4.1.7c shows the same network with μ regularization instead. As before, ping-ponging can be avoided, but also spike firing is more evenly distributed compared to fig. 4.1.7b, while also saving 50% of spikes compared to fig. 4.1.7a and no perceivable loss of accuracy. However, both μ and ν need to be adjusted when larger networks are to be used. When increasing network size, the relative importance of a fixed regularization weight increases as well. Setting too large costs can lead to insufficient or a total lack of spiking, increasing the error.

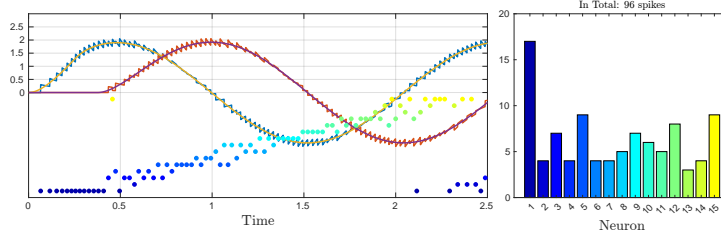
4.2 Results on the Control

For the evaluation of the results for the control problem derived in section 3.4, we first note a few important implementation details in order to obtain useful results.

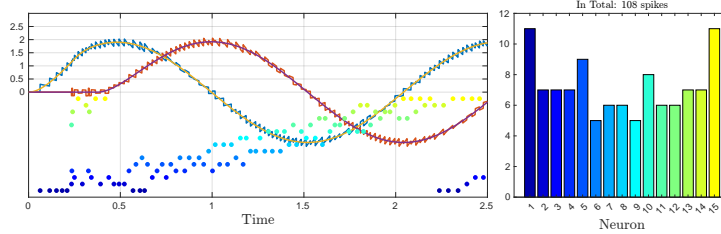
Afterwards, we compare the performance of the two different derivations from sections 3.4.2 and 3.4.4 and briefly discuss the necessary condition for the control schemes to function. With the chosen network architecture, robustness against neuron



(a) Network simulation without any regularization. Left: Histogram of spike distribution per neuron.



(b) Network simulation with pure linear costs ν . Left: Histogram of spike distribution per neuron.



(c) Network simulation with pure linear costs μ . Left: Histogram of spike distribution per neuron.

Figure 4.1.7: Output of networks after leaky integration of oscillating input. The networks were run with 15 neurons each and identical parameters set except regularization. Feed-Forward weights were chosen uniformly around the unit circle and normalized to $\|\Gamma_i\| = 0.3$.

failure and noise has already been tested and verified by previous authors. To avoid repetition, specific testing into these topics is omitted.

4.2.1 Acceptable Error

Due to the network's discrete nature of spikes, any error below the threshold cannot be eliminated. This threshold is fixed by the fact that a spike of neuron i produces a constant change in the signal given by the decoding Γ_i . Accuracy levels commonly observed with classic control schemes and numerical methods are unattainable due to this restriction. On the other hand, error is also bound from above by the threshold. While it is theoretically possible to achieve arbitrarily small errors by scaling Γ_i , the error is bound by the spiking threshold $\frac{\|\Gamma_i\| + \mu}{2}$ and is only considered in the directions projected by Γ .

4.2.2 Implementation details

Before any simulation can be run it is important that certain detail in the implementation are set in the correct order for the results to make sense.

Multiple Spikes per Time Step

Although this also applies for the simulation step in section 4.1, its affects are much more pronounced in the control setting.

Single Spike

As the outlined dynamics suggest, the simulation step includes a check if a threshold has been reached.

A simple implementation in MatLab pseudo code is seen in Listing 4.1.

```
1
2 for t_step = 1:N_step
3     V = update_Voltages(V,dt,Ws,Wf,c,...);
4     [value, index] = max(V-Threshold);
5     spikes(index,t_step) = 1;
6     V = V + Wf(:,k);
7     ...
8 end
```

Listing 4.1: Single spike implementation

While this works for a variety of problems, it does not give results for any given system and reference trajectory.

Especially problems with an abrupt change underperform since the network is only allowed to correct the error by one spike each time step. However, by jumps and rapid changes, this is not sufficient to compensate errors, and the networks struggles for many iterations to recover, ruining the overall accuracy in the process.

Parallel Spikes

The direct way to fix this is to find all neurons that have reached their thresholds. Since networks have numerous neurons, letting every neuron spike increases the networks ability to correct errors. A potential implementation is seen in Listing 4.2.

1

```
2 for t_step = 1:N_step
3     V = update_Voltages(V,dt,Ws,Wf,c,...);
4     spiking_neurons = V>Threshold; % procudes a list
5     spikes(spiking_neurons,t_step) = 1;
6     V = V + Wf(:,spiking_neurons);
7     ...
8 end
```

Listing 4.2: Letting every neuron spike in parallel

The problem with this implementation is that the error gets tracked by multiple neurons simultaneously and also in both positive and negative directions. To illustrate this, we consider a simple example where we have a single control variable u and $2N$ neurons, where N neurons track positive and negative error, respectively.

Disregarding noise, the threshold is reached by N neurons synchronously. As long as the total error is larger than the compensation of N neurons in the first place, this works just fine. However, this is not permanent, and at some point, all N neurons firing overly depolarize the opposite side neurons to the extent that they all fire in the next iteration regardless of the real system error.

The root cause is that a single spike influences the whole network. In this extreme case, 1 spike resets all other $N - 1$ neurons that were spiking as well and, therefore, does not provide any performance boost compared to the previous approach.

The network with this implementation behaves normally while a rapid change is underway but will evolve into N neurons spiking in alternating cadence, respectively. To remedy this, it is necessary that one dimension of the error is only projected onto two neurons. While this can be achieved by carefully selecting the decoder it is not a generic approach. Moreover this reverses the idea of multiple neurons tracking the error for robustness.

Therefore, we need to let a single neuron spike multiple times.

Multiple Spikes

The correct way to handle this problem is to allow more than one spike per time step but compute each spike's change in the network separately. This way, we can achieve the necessary performance without the problems of the previous approach. An implementation of such a regime is seen in Listing 4.3

```
1
2 for t_step = 1:N_step
```

```

3 V = update_Voltages(V,dt,Ws,Wf,c,...);
4 [value, index] = max(V-Threshold);
5 while value > 0
6     spikes(index,t_step) = 1;
7     V = V + Wf(:,k);
8     ...
9     [value, index] = max(V-Threshold);
10 end
11 end

```

Listing 4.3: Letting each neuron spike as many times as necessary while computing each spike's influence sequentially.

In order to retain biological plausibility, it is necessary to limit the number of spikes fired in one time step. While this is not a problem in most cases when hyperparameters are properly tuned, it can be an issue for certain sudden jumps or rapid transitions.

Slow Connectivity Term

In their derivation, authors consider network in the limit for $N \rightarrow \infty$ neurons. Specifically, the derivation arrives at

$$\begin{aligned}
 \dot{\mathbf{V}}(t) &= \boldsymbol{\Omega}^T \mathbf{B}^T (\dot{\hat{\mathbf{x}}}(t) - \dot{\mathbf{x}}(t)) - \mu \lambda_d \dot{\mathbf{r}}(t) \\
 &= \boldsymbol{\Omega}^T \mathbf{B}^T \mathbf{A} \mathbf{L} \mathbf{V}(t) \\
 &\quad + \left(\mu \lambda_d \boldsymbol{\Omega}^T \mathbf{B}^T \mathbf{A} \mathbf{L} + \mu \lambda_d^2 \mathbf{I} - \frac{1}{\lambda_d} \boldsymbol{\Omega}^T \mathbf{B}^T \mathbf{B} \boldsymbol{\Gamma} \right) \mathbf{r}(t) \\
 &\quad - (\boldsymbol{\Omega}^T \mathbf{B}^T \mathbf{B} \boldsymbol{\Omega} + \mu \lambda_d^2 \mathbf{I}) \mathbf{o}(t) \\
 &\quad + \boldsymbol{\Omega}^T \mathbf{B}^T (-\mathbf{A} \hat{\mathbf{x}}(t) + \dot{\hat{\mathbf{x}}}(t))
 \end{aligned} \tag{4.3}$$

where

$$\mathbf{L} = (\mathbf{B} \boldsymbol{\Omega} \boldsymbol{\Omega}^T \mathbf{B}^T)^{-1} \mathbf{B} \boldsymbol{\Omega}$$

is the pseudo-inverse of $(\mathbf{B} \boldsymbol{\Omega})^T$. Our focus is now set on the terms in front of the rate \mathbf{r} . As [37] and the original derivation in [11] argue, the term $\mu \lambda_d^2$ vanishes in the limit and can therefore be neglected, yielding the above result for \mathbf{W}^s above in eq. (3.38). However in the testing it was noticed that this derivation only produces acceptable results for a small range of values for λ_d , explicitly $\lambda_d \leq 20$. For higher values, the

performance deteriorates rapidly if not a large number of neurons are considered. After testing the relative importance of terms it was noted that the term $\mu\lambda_d^2$ does improve the performance with a smaller number of neurons significantly compared to the other terms and was therefore added in the results from now on. Furthermore, the authors' examples clearly indicate their use of the extra term as well in the calculation of \mathbf{W}^s . This, in addition to our testing, confirms the permanent addition of $\mu\lambda_d^2$.

4.2.3 Network as the Controller

Now we start to compare both methods against each other. Except for an introductory example we will mostly outline observed differences. Both methods require receiving the desired state trajectory as input. To test their usability, different size problems as well as configurations of \mathbf{B} and \mathbf{C} have been tested.

For testing purposes, we set the test system \mathbf{A} to

$$\mathbf{A} = \begin{bmatrix} 0 & 1 \\ -1 & 10 \end{bmatrix}. \quad (4.4)$$

Additionally, for the $N = 50$ neurons, we choose their instantaneous decoding weights Ω randomly and normalize them to 0.01 without any rate decoding Γ .

Single Input Single Output (SISO) Systems

Both methods performed identically well with SISO systems. Error levels are limited by the scaling of Γ with single spike deviations from the target.

To influence the control behaviour, different parameters can be tuned. Increasing costs μ and ν will lead to an increased settling time. Increasing the number of neurons or the number of allowed spikes per neuron will improve the error, especially the immediate increase seen in the top panel of fig. 4.2.1. Lastly, the scale of the rate encoding Γ can be tuned to lower the rise time. However, this can lead to overshoot, seen in the bottom panel of fig. 4.2.1. In general, the rate encoding Γ introduced with the control is mainly responsible for reducing the amount of spiking in the network. As can be seen in fig. 4.2.1 the absence of Γ is only noticeable in the slower settling time. With purely instantaneous encoding, the control signal has to be constructed for each time-step from zero only with spikes. This extensive firing causes quadratic costs $\mu\|\mathbf{r}\|_2^2$ to

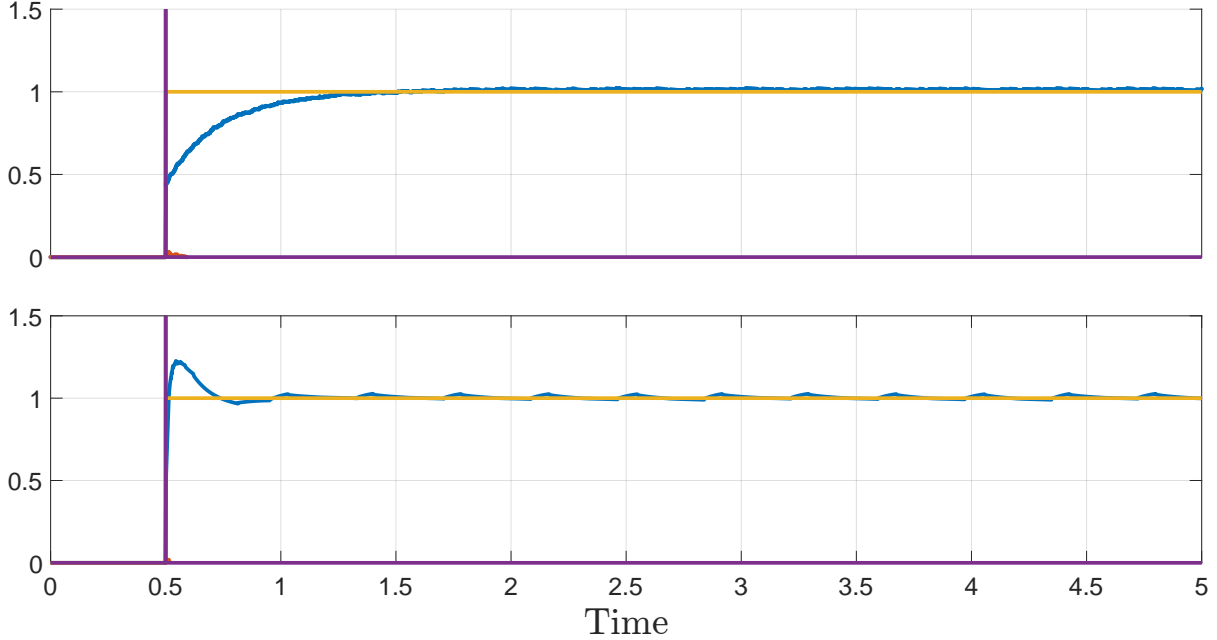


Figure 4.2.1: Step response for simple 2D system. Both runs are identical except for $\Gamma = 0$ (top) and $\Gamma = 100 \cdot \Omega$. Both approaches performed identically.

rise and slow down spiking of repeatedly firing neurons. Thanks to a large number of neurons for this problem and low quadratic costs $\mu = 1 \cdot 10^{-6}$ this is not a problem in the shown example. On the other side, the addition of Γ brings additional momentum, given by the slower-changing rates r , that, in case of sudden changes, first needs to be counteracted, seen by the overshoot in fig. 4.2.1.

In the presence of noise, the control scheme with the direct error performed slightly better. This was expected as the explicit error term in the voltage equation benefits the compensation of noise in the network.

Suboptimal B, C and Multiple Input Multiple Output (MIMO)

Difficulties arise when more complex problems are considered.

In order for the control schemes to work, the necessary condition $\mathbf{B}^T \mathbf{C}^T \neq 0$ has to hold[35]. However, the condition has to be understood as $\text{rank}(\mathbf{B}^T \mathbf{C}^T) = \text{rank } \mathbf{B}$. Otherwise, certain state variables cannot be controlled. These "invisible states" are neglected by the network. This limitation is shared between both methods. The reason behind that is that the matrix $\mathbf{B}^T \mathbf{C}^T$ blinds the Voltage on projecting the error properly in eq. (3.34) and eq. (3.45).

If $\mathbf{B}^T \mathbf{C}^T$ exhibits rank deficiency, certain neurons do not receive the input \mathbf{c} . They are, therefore, only affected indirectly in eq. (3.35) by the spiking of other neurons and not

by the target trajectory. This results in either the output trajectory not being tracked in the first place, or if the output is tracked, the internal states are moving freely.

To ensure the rank condition, this restricts the possibilities of \mathbf{B} and \mathbf{C} . If $\mathbf{B} \in \mathbb{R}^{n \times J}$ and $\mathbf{C} \in \mathbb{R}^{m \times n}$ we need to enforce that $m \geq J$. In order for $\mathbf{B}^T \mathbf{C}^T$ to have full rank J , it is necessary that \mathbf{C}^T has at least rank J due to

$$\text{rank}(\mathbf{B}^T \mathbf{C}^T) \leq \min(\text{rank}(\mathbf{B}^T), \text{rank}(\mathbf{C}^T)) = \min(J, m) \quad (4.5)$$

Equivalence of $\hat{\mathbf{x}}$ and \mathbf{x}

For the direct error method to work, it is crucial that the external input \mathbf{c} is accurately calculated from the reference by

$$\dot{\hat{\mathbf{x}}} = \mathbf{A}\hat{\mathbf{x}} + \mathbf{c}. \quad (4.6)$$

This represents an open-loop controller without any feedback from the system itself. Even though the network output is directly part of the equation, the error term is present due to the definition of the voltage. In previous derivations, this term was neglected after considering the limit of $N \rightarrow \infty$.

Now, as both $\hat{\mathbf{x}}$ and \mathbf{x} follow the same dynamics, it appears natural that they can be interchanged to allow for true feedback. Use the actual network output in order to compensate for any errors when determining the network input \mathbf{c} . However, in practice, plugging this in eq. (3.45) can pose problems for the network, even if \mathbf{C} and \mathbf{B} are chosen ideally.

While they both follow the same dynamics, their values may be different. Yet even with tiny differences, \mathbf{c} can ruin the control completely.

After careful investigation, the problem stems from the aforementioned supposed equivalence for \mathbf{c} .

To illustrate the problem we consider a 1D example.

$$\hat{\mathbf{x}} \neq \mathbf{x}$$

The reason for control failure when using the network output instead of the reference was found to lie in the error term of eq. (3.45) in [36]. To illustrate this, it is useful to consider their basic example of a scalar system

$$\dot{x} = -10x + u \quad (4.7)$$

but only two neurons with weights

$$\begin{aligned}\Omega &= k \cdot [-1, 1] \quad k > 0 \\ \Gamma &= [0, 0]\end{aligned}\tag{4.8}$$

and no additional cost terms.

This configuration allows for a straightforward allocation of functions to individual neurons. In the provided illustration, Neuron 2's voltage tracks the error whenever the network output \hat{x} lags behind the reference value x . It becomes active if the deviation surpasses

$$V_2 = 1c(x - \hat{x}) < \frac{k^2}{2}\tag{4.9}$$

prompting a corrective response to increase the network output. We now consider the error term with $e(t) = x - \hat{x}$. At the start of the control, both spikes and rates are zero. Voltage dynamics are reduced to

$$\begin{aligned}\dot{\mathbf{V}} &= \Omega \mathbf{B}^T \mathbf{A} e(t) + \Omega^T \mathbf{B}^T \mathbf{c} \\ \dot{\mathbf{V}} &= -10k \cdot \begin{bmatrix} -1 \\ 1 \end{bmatrix} e(t) + \Omega^T \mathbf{B}^T \mathbf{c}.\end{aligned}\tag{4.10}$$

Now, the scenario where the network is falling short of the reference value is considered, leading us to deduce that $e(t) > 0$. Consequently, we can conclude that the error term is conflicting with the intended definition of our voltage by inadvertently increasing the voltage of Neuron 1 in the wrong direction while it is Neuron 2 that should increase its voltage.

Due to the minus sign obtained from $\mathbf{A} = -10$, the respective projections of the error by Ω get flipped leading to an exponential increase in voltage. If \mathbf{c} is calculated from the reference trajectory and its derivative, this error is compensated for. However, by the erroneous substitution this is no longer the case and the error increases while \mathbf{c} does not compensate.

The problem is that the reference \mathbf{x} changes on scales that the network cannot resolve. These small changes are amplified by the multiplication of \mathbf{A} in eq. (3.37), allowing to balance the error term. The network state $\hat{\mathbf{x}}$ is not accurate enough to resolve this, e.g. when the simulation is starting and all neuron activity is zero. One way to resolve this issue is to artificially set the error to zero if $\|\mathbf{A}\| \ll \|x\|$. This is possible since in most problems the error term only contributes a negligible amount to the total voltage

change. The biggest contribution is from c after which the error is small enough to be ignored directly.

In the error-free formulation, the aforementioned issues are less significant. Since there is no direct error in the network, the network state \hat{x} can be substituted instead of the reference. However, this substitution breaks down as soon as jumps or discontinuities are present.

Conclusion

Due to conditions imposed by the control network, it is most feasibly used in problems without output C . Since it is required to supply the full state trajectory, the obstacles arising from $C \neq I$ with respect to the previously mentioned rank of $B^T C^T$ limit the network's applicability.

Nonetheless, if the conditions are met, control performance is within the margin of a single spike away from the target. In ideal conditions, both networks perform indistinguishably well. Only in the presence of considerable noise the error term slightly improve performance.

4.3 Results on the learning

To provide a comprehensive examination of results, the rigorous testing required to demonstrate them is infeasible. Therefore we restrict our testing to a select model problem and only demonstrate a selection of interesting results. Meanwhile testing has been conducted with more and different settings than presented here which will be mentioned occasionally for the purpose of completeness.

For our result evaluations, we use a simple test scenario to assess the learning performance for W^f and combined learning separately. Slow learning alone is skipped, as in [15] it is expected to be applied in conjunction to the fast learning. Furthermore, while testing, it has been observed that the reliability and performance lack behind when only the slow weights W^s are trained.

For the combined training, we set out to find the determining source of error in overall performance. To access we look into different metrics to determine the progress of learning and highlight key parameters for the success of learning the given system, e.g hyper-parameters or learning input sequences.

Lastly, we describe the limits of this methods found in different configurations where the learning breaks down.

4.3.1 Model problem

As the first problem, we consider a simple 2D example given by a damped oscillator of the form

$$\dot{\mathbf{x}} = \begin{bmatrix} 0 & 1 \\ -1 & -10 \end{bmatrix} \mathbf{x} + \mathbf{c}(t). \quad (4.11)$$

Since we are only concerned with the learning, we neglect the control at this point. We give a predefined input $\mathbf{c}(t)$ set as a single square impulse. With this trajectory we can observe the systems response to a sudden jump as well as the evolution of the system in the absence of external input. This allows us to see the system's performance in both scenarios of the control problem later on.

Testing

To measure the learning performance, we consider different metrics in order to get a complete picture.

Due to the analytical solution, we are in the fortunate position to compare the learning values to the optimal values. Yet, different measures of performance can be evaluated. The most important and meaningful measure to consider is the network error after learning in a simulation.

As a reference, we plot the optimal solution of our example here. As can be seen from fig. 4.3.1, the network perfectly follows simulates the system's behaviour. However, other measurements could also be obtained to assess the networks learning. Alternatively, one can consider the convergence of the matrix parameters to their optimal values. Therefore, we measure the maximum relative deviation from the optimal value as

$$\Delta^{\text{rel}} \mathbf{W}_{ij} = \left| 1 - \frac{\mathbf{W}_{ij}^{\text{learned}}}{\mathbf{W}_{ij}^{\text{ex}}} \right| \quad (4.12)$$

for each parameter. From there, we can measure the maximum relative deviation or compute the sum of deviations to assess the parameter convergence.

Alternatively, since we are working with matrices, we can look at the convergence of eigenvalues.

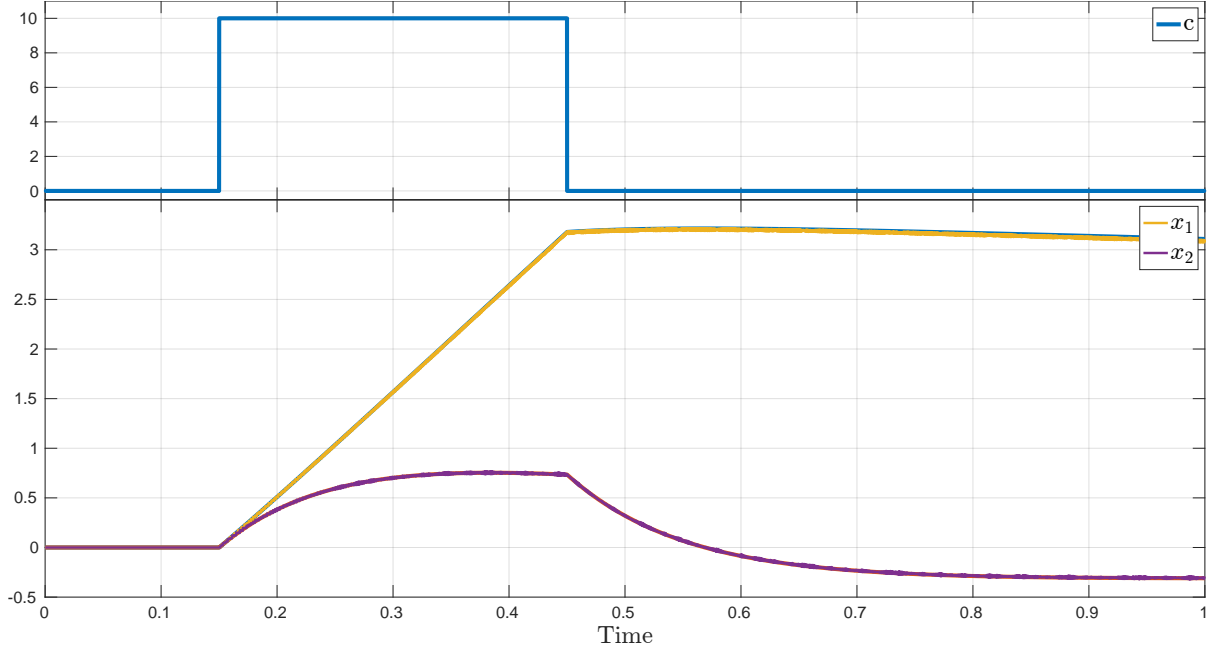


Figure 4.3.1: Simulation of our example with the given external input c . The network simulation perfectly overlaps with the analytical solution. Maximum error in this example is < 0.04 .

Knowing the optimal values to

$$\begin{aligned} \mathbf{W}^f &= -(\boldsymbol{\Gamma}^T \boldsymbol{\Gamma} + \mu \mathbf{I}) \\ \mathbf{W}^s &= \boldsymbol{\Gamma}^T (\mathbf{A} + \lambda_d \mathbf{I}) \boldsymbol{\Gamma} \end{aligned} \quad (4.13)$$

the eigenvalues can be computed.

For \mathbf{W}^f we only need to look at the eigenvalues of $\boldsymbol{\Gamma}^T \boldsymbol{\Gamma}$ and shift them by μ . $\boldsymbol{\Gamma}^T \boldsymbol{\Gamma}$ itself only has J non-zero eigenvalues $\text{rank}(\boldsymbol{\Gamma}^T \boldsymbol{\Gamma}) = J$ since $\text{rank}(\boldsymbol{\Gamma}) = J$.

For \mathbf{W}^s , only J eigenvalues are non-zero since again the $\text{rank}(\boldsymbol{\Gamma}) = J$.

Thus, we assess the learning progress by measuring the distance of the learned eigenvalues compared to the true eigenvalues.

4.3.2 Only Learning of \mathbf{W}^f

To evaluate the learning performance individually, we first consider each learning algorithm separately. Later, we use both to assess the overall performance.

This also allows us to see the effects of changing learning parameters individually. To isolate the learning of the fast weights, we set the learning rate for the slow weights to zero and initialize \mathbf{W}^s to the optimal values from the analytic solution given in

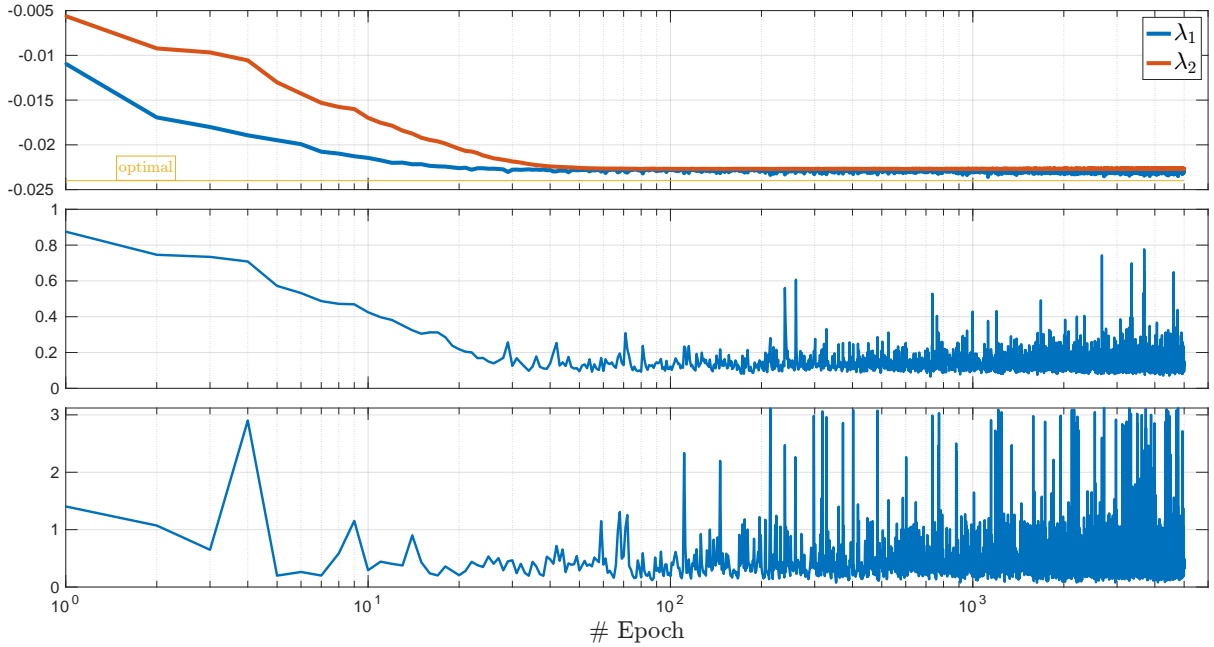


Figure 4.3.2: Learning of W^f matrix and the end of the epoch. The top panel shows the movement of the two non-zero eigenvalues of W^f . The middle panel shows the largest relative deviation of W^f calculated from eq. (4.12). The bottom panel shows the maximal error during simulation between the learned and the optimal matrix.

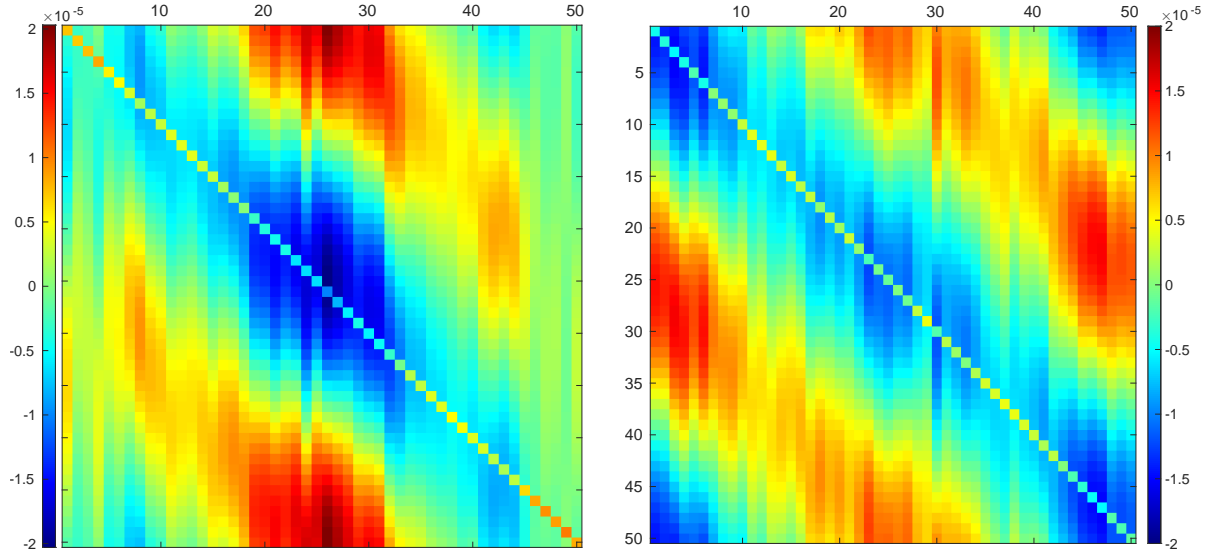
section 3.3. This provides optimal conditions for the learning algorithm.

We start first by looking at the convergence over learning before examining errors in order to see whether any of the aforementioned measurements indeed give a meaningful insight into the network's performance.

The learning performance of W^f is seen in fig. 4.3.2. As can be seen, the two non-zero eigenvalues of the matrix converge close to the optimal values, which are reached after ≈ 130 epochs and keep hovering around. We also see that the largest relative deviation is following the same trend in the beginning, but instead of settling down at ≈ 130 , it starts jumping around. Although the plot prints the absolute relative deviation, the jumps are only in positive direction.

Before the jumps begin, the learning algorithm manages to get the largest deviation to less than 9.5% away from the optimal value. Using this set of learned parameters, the maximum absolute error during that simulation was 0.1187, which corresponds to a relative error of $< 4\%$.

The overall best performance according to our measures was reached in epoch 724, but because of the rapid fluctuations it can be assumed that the parameter set was found randomly. Interestingly, did this not also give the best error results but an relative error



(a) \mathbf{W}^f matrix after 724 epochs of learning.
Displayed are the parameter differences
 $\mathbf{W}^f - \mathbf{W}_{\text{exact}}^f$

(b) \mathbf{W}^f matrix after 1640 epochs of learning.

Figure 4.3.3: Matrix' learning progress for the best error performance (a) and best relative deviation (b). Learned was with different smoothed Gaussian noise for each epoch for 10^5 timesteps.

of more than 10%. The best overall performance was in epoch 1630 with a relative error of $< 3\%$. The largest relative deviation of the matrix in that epoch was $\approx 12\%$ from the optimal value.

Visualizing the matrices' differences from the optimal weights of both of these epochs in fig. 4.3.3, it is apparent to see that the columns $i = [1, \dots, 15] \cup [42, \dots, 50]$ are learned slightly more accurately. These correspond to the reset of voltages of neurons i . The reason this is important is that for our test example, these neurons are by far the most active. Thus by learning these neurons accurately while other weights are further apart from the optimal value gives better results for our example but worse results when looking at the largest deviation.

A possible reason for this behaviour is that the weights are too much dependent on the input of the learning input sequence that is used for learning in the current epoch. This will be investigated in a later section.

However, this also means that neither the eigenvalues nor the largest relative deviation give reliable ways to measure our performance without looking at the simulation error. Also, other measures like the sum of all deviations do not give a good account of the learning progress. Moreover, all these measures rely on the information given by the optimal weights, which in general is not available information. From this plot,

it becomes clear that it is hard to predict the network performance without actually testing it. While the eigenvalues or the largest relative deviation might indicate a good set of parameters, the error can still make the whole simulation unusable, as the error climbs as high as the original simulation in fig. 4.3.1. Therefore, it is either necessary to find a better measure or avoid the oscillating effect by adjusting the learning parameters. Latter will be tested in the next section.

Lastly, it is interesting to note that for all tests in which the results were not completely unusable the biggest error was after the stimulus c was absent. Furthermore, the error crept up over time and the maximum error was often found towards the end of the simulation. This hints that the network's accuracy is deteriorating mostly when it is evolving on its own.

Parameter analyses

Parameter: β

The prime parameter for the learning of W^f is the parameter β . With the same learning and simulation setup as above, we test different values of β . Empirically, we know that values outside the range of $(0.50, 0.54)$ do not perform well enough to compare or do not converge outright. For the learning, the identical input sequences were used.

To illustrate the influence of β , we run the simulation with a value close to 0.50, close to the upper limit and an the best empirically found value. In fig. 4.3.4, it becomes visible that with larger β the rapid oscillations are reduced. However with $\beta = 0.54$ in the orange line the error is prohibitively high. The eigenvalues are not shown as they all follow a very similar convergence path as seen in fig. 4.3.2.

The best performance was found empirically at $\beta = 0.522$ with comparatively good error measures while having few rapid jumps.

It is interesting to see that for different β , sudden changes in the error seem to happen after the same training epochs, indicating that the input sequence for this epoch influenced the learning enormously. This can be seen the easiest between epoch 7–180 where spikes can be observed for each β . This indicates that the parameter changes learned in that epoch are too dominant for the whole network, and the learning rate must be adjusted.

Unfortunately, none of our previously discussed measures is able to detect these

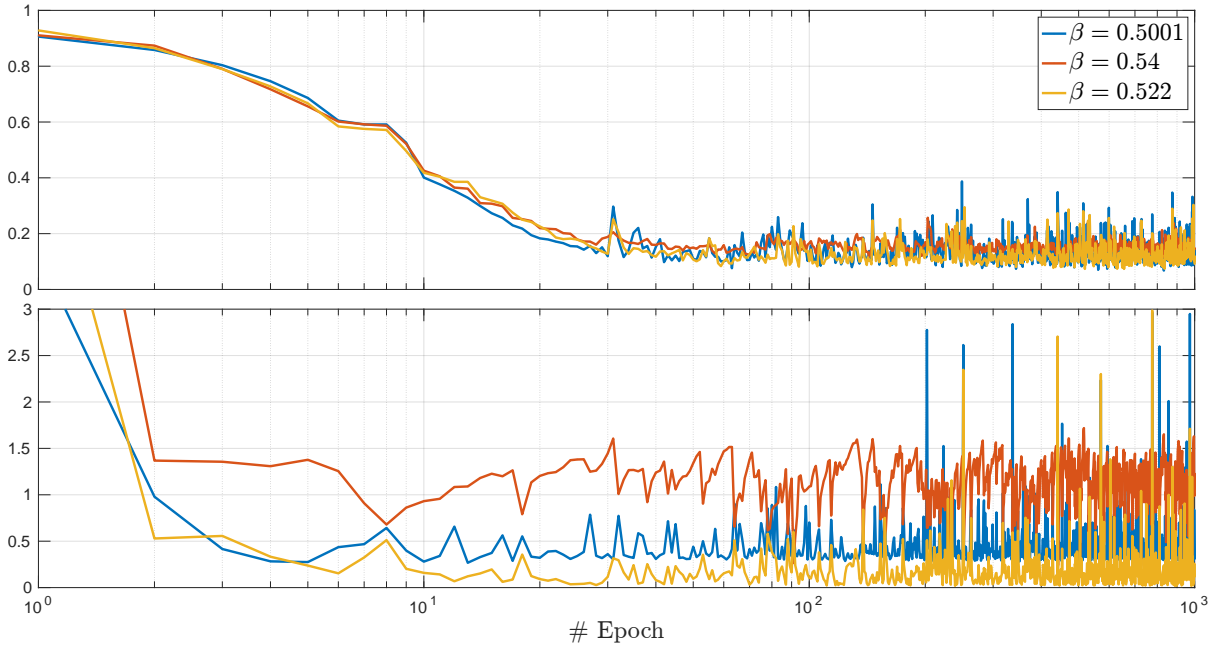


Figure 4.3.4: Learning of the example eq. (4.11) with different β . The top panel shows the relative deviation, and bottom panel shows the absolute error.

anomalies, leaving us again with no other option than explicit testing of the network in simulation. To mitigate this either the input sequences need to be modified or the learning rate adjusted. Latter will be the topic of the next section.

Learning rate

Adjusting the learning rate for \mathbf{W}^f is an easy way to dampen the oscillations seen in the previous plots, though coming with an increased computational cost. For comparison, we ran the learning algorithm with different learning rates to compare cost to performance in fig. 4.3.5. As expected, reducing the learning rate reduces the oscillations. While the oscillations still occur with the lower learning rate, its magnitude is greatly reduced. With the smallest tested learning rate $\alpha_f = 0.0001$, the noticeable oscillations occur after ≈ 2500 epochs. The downside is that just to reach useable results with a relative error of less than 10% learning must continue for more than 1000 epochs. In addition, this is for a small system while we can expect even longer learning times for bigger systems.

On the other hand, the largest learning rate exhibits the largest error as well as enormous error variability. The learning rate for fig. 4.3.4 was double of the one used in fig. 4.3.5. However, it is apparent that already in the first epoch the error reduces significantly.

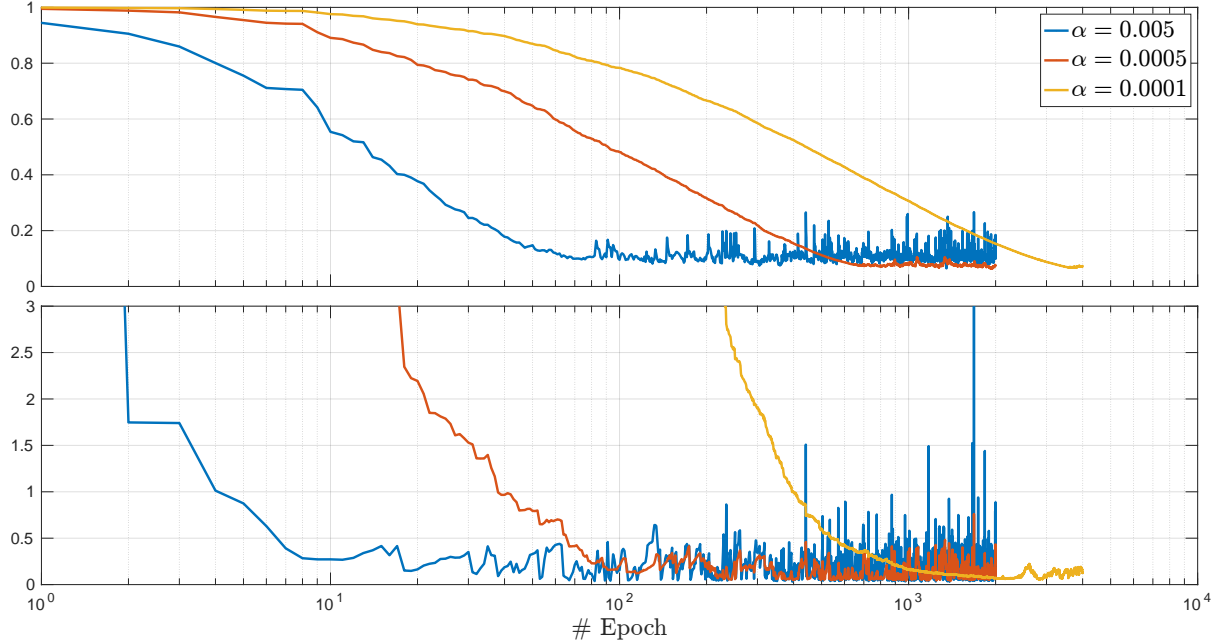


Figure 4.3.5: Learning of example eq. (4.11) with different learning rates α^f . Top panel shows the relative deviation and bottom panel the absolute error.

To combine the benefits of both approaches in ??, we see gradually lowered the learning rate after each epoch. We start with the previously used learning rate $\alpha_0^f = 0.005$ and gradually lower it to $\alpha_M^f = 0.0001$ over the course of 1000 epochs.

For the reduction, a value $p \in [0, 1]$ was chosen beforehand and the learning rate for the next epoch m calculated as

$$\alpha_m^f = ((1 - p)^m + 0.02) \cdot \alpha_0^f, \quad (4.14)$$

essentially allowing for an exponential decay of the learning rate with a backstop to avoid too small learning rates.

In fig. 4.3.6 learning results for different p are displayed. As can be seen, all variations perform more reliably than the any approach before as well as reaching comparable performance with fewer epochs. Furthermore, the fast drop rate of $p = 0.09$ appears to give the more consistent results. The improvement of performance is not reflected when looking at the largest deviation, though with the reduced oscillations thanks to the parameter tuning, the eigenvalues allow for a more accurate description of the learning status. While convergence to the true values does not occur, the convergence to a value itself can be seen as the completion of learning. This can be seen in fig. 4.3.6 where learning could be halted when the eigenvalues have converged. However, the convergence depends on the initial learning rate as well as the parameter p and

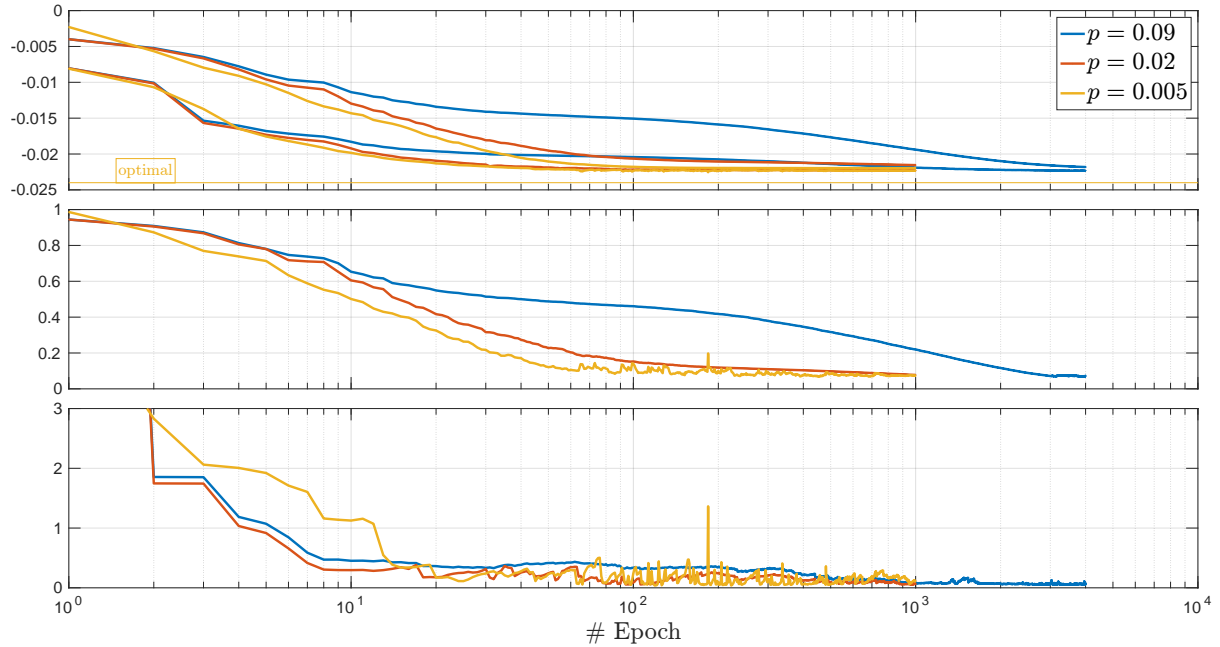


Figure 4.3.6: Learning of example eq. (4.11) with different learning rate drops p starting from $\alpha_0^f = 0.005$. Top panel shows the learning rate for each epoch. Middle panel the relative deviation and bottom panel the absolute error.

therefore requires hand-tuning to avoid unnecessary long training times or premature stopping. This can be seen again in fig. 4.3.6, in which for $p = 0.09$, the network is performing adequately much before the eigenvalues or the largest deviations would suggest good results can be obtained. Only after ≈ 4000 epochs, the largest deviation appears to level, whereas the second non-zero eigenvalue still does not appear to have converged yet. The reason the largest deviations do not show appropriate results can be explained when looking at the parameters itself.

For the above example with $p = 0.09$, the weights of \mathbf{W}^f are shown at different times of the learning phase in fig. 4.3.7 rows 1 & 2. The desired outcome after learning is that every parameter is close to zero. With fig. 4.3.7, it becomes apparent that certain columns of \mathbf{W}^f become trained early. The late stages of training exhibit emerging diagonal lines caused by the optimal value of these matrix parameters being close to zero and therefore making the relative deviation more visible for errors while the whole matrix is converging to the optimum.

The reason behind the surprisingly low error in the early learning stages lies in the choice of our input sequence c . The choice of c in fig. 4.3.1 only causes the neurons with quickly learned weights to spike and therefore giving a lower error than expected. The spiking neurons and therefore the error do not yield a complete representation of the training state.

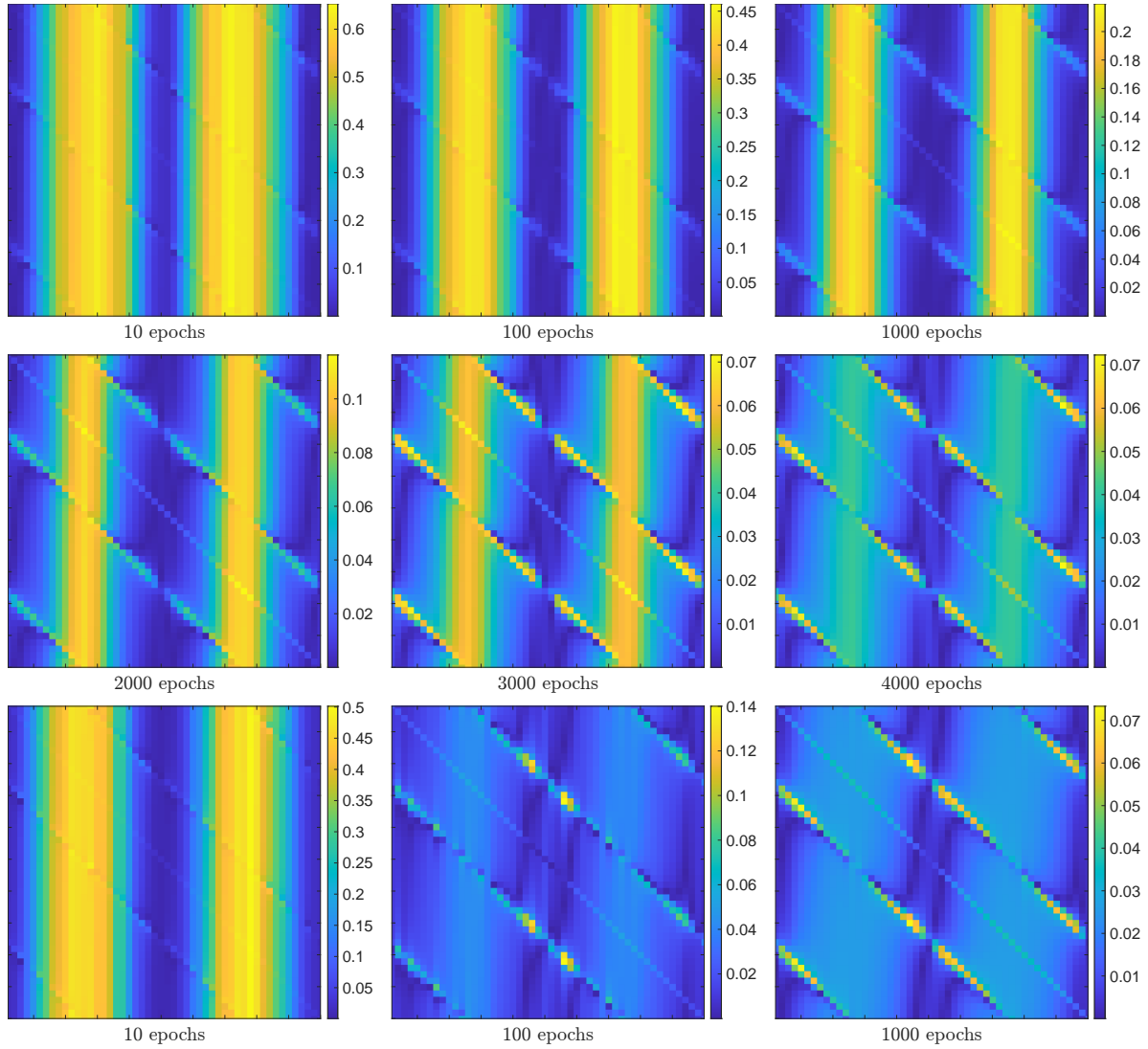


Figure 4.3.7: Relative deviation for matrix weights at different times of learning. Note the different colour scale. The top 2 rows display the learning of \mathbf{W}^f with $p = 0.09$. The bottom row for $p = 0.005$. The same input sequences have been used for training.

If we instead use a more complex external input sequence $\mathbf{c}(t)$ that ideally forces all neurons to spike, we obtain a different picture seen in fig. 4.3.8. Note that this evaluation is on the same data used for fig. 4.3.6. However, with fig. 4.3.8, the error follows both the eigenvalues and the largest relative deviation. It also becomes apparent that the lack of convergence seen in fig. 4.3.7 contributes two orders of magnitude to the error compared to the previous case. Moreover, judging by the error plots, the choice of $p = 0.005$ vastly outperforms the previous pick of $p = 0.09$. With the lower drop rate p , imbalances that dominate the complete learning like in fig. 4.3.7 can be corrected faster as the learning rate has not dropped significantly yet, seen by the row 3 of fig. 4.3.7.

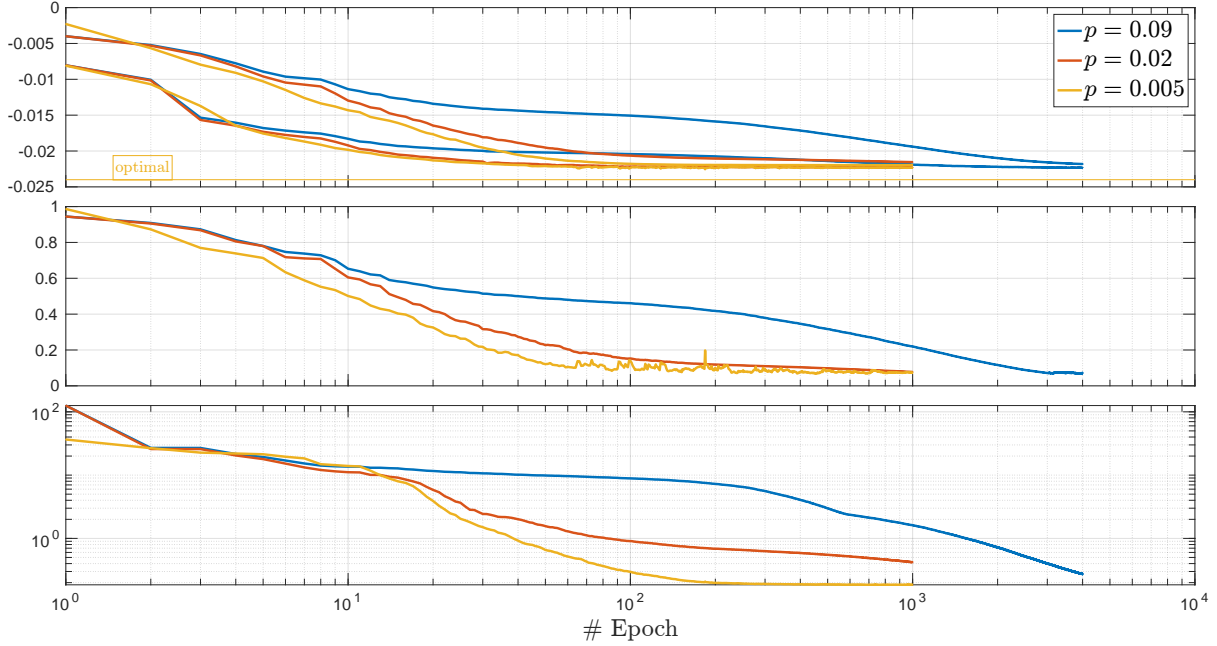


Figure 4.3.8: Evaluation of training progress using an oscillating input $\mathbf{c}(t) = [c_1(t), c'_1(t)]^T$ with $c_1(t) = (1 - e^{-4t}) \sin(3\pi t)$ with different drop rates p . The top panel shows the non-zero eigenvalues. The middle panel the largest relative deviation and the bottom panel the maximum error during simulation in log-log scale.

Lastly, the choice of learning input sequences can be questioned to avoid the imbalances in early-stage learning. So far, for all previous examples, input sequences were smoothed Gaussian white noise. The role of the input sequence will be considered when both matrices are trained.

All in all, good approximations of \mathbf{W}^f can be learned with the given learning rule; however, the hyper-parameters p, α^f , as well as the learning period are sensitive to the problem at hand and therefore require manual tuning. Moreover, the shown learning results were obtained under ideal learning conditions.

Learning networks with more neurons or random initialization of \mathbf{W}^f complicates the learning phase. However, good learning results can still be achieved, albeit with an increase in learning time.

When assessing the state of training, it is crucial to choose appropriate test sequences to reflect different sources of error. This means forcing all neurons to spike as well as cutting external input such that the network evolves by itself. Former examines whether matrix weights have been learned for all neurons, while the latter highlights small errors over time that do not become apparent when external input is dominating. The small errors incurred from suboptimal resets accumulate over time if no external

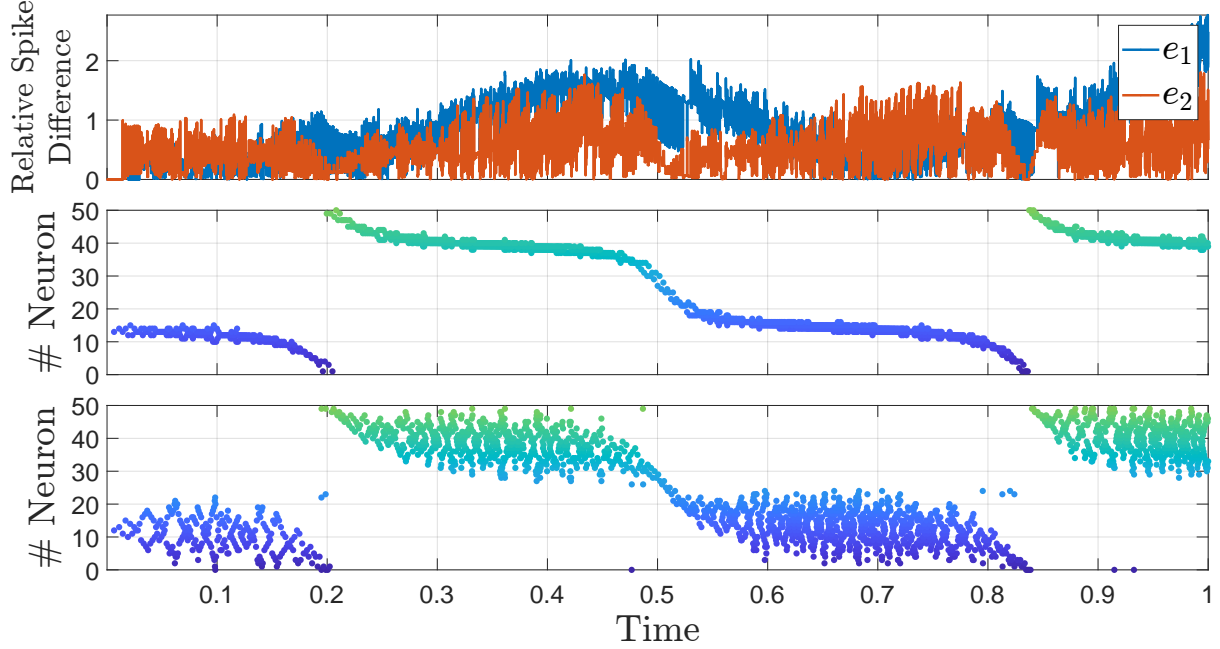


Figure 4.3.9: Top panel: Relative Spike Difference between the network with L_2 costs added to \mathbf{W}^f after learning and no addition. Error is given in multiples of decoder norm $\|\Gamma_i\|_2$. Middle panel: Raster spiking plot of $N = 50$ neurons after simulation without the L_2 costs added afterwards. Bottom panel: Raster plot with costs added. Both matrices were trained for 1000 epochs with identical settings and received a scaled sin wave as external stimulus c . For these simulations, noise terms during training and simulation have been disabled.

input is present, even though Γ and \mathbf{W}^s are chosen optimally. Therefore a combination of both presented sequences should be used.

Lastly, our measures to assess the network's learning progress rely on the knowledge of the optimal matrices or the repeated expensive computation of eigenvalues. Without online measures, frequent testing is a necessity to avoid extensive learning periods.

Spiking behaviour

So far, we have not touched on the spiking behaviour. For the previous examples, the learning rule of eq. (3.51) was used. Said learning rule does not incorporate L_2 costs to encourage distributed spiking. When looking at raster plot in the middle panel of fig. 4.3.9 this disadvantage becomes apparent. Spiking is shared among 4 neurons at most. This is biologically implausible. When using the adapted learning rule of eq. (3.52) other problems arise.

As noted in the supplementary of [16], this particular learning rule does not learn the optimal weights but the optimal structure. As such it is therefore only a qualitative

learning of the \mathbf{W}^f . The scaling factor is not known a priori. The different scale of \mathbf{W}^f is detrimental to the networks convergence. In tests, no parameter set was found that mitigated this.

It is therefore mandatory to allow the Feed-Forward Γ weights to adjust, i.e. they are learned as well. With Feed-Forwards also scaling over the course of training allows the different scales to balance out.

To verify this, learning of Γ was adopted from [16] which allowed the network to converge.

After convergence was achieved, the hyper-parameter scaling factors for \mathbf{W}^f and Γ were tuned.

Goal of the tuning was to empirically find a parameter set of scaling factors s.t. the scale of Γ remains unchanged throughout learning and transfer this to the learning with fixed Γ . However this again led to unusably erroneous results or failure in convergence outright.

For comparison, the error plots in [16] are not calculated using the learned decoder Γ (denoted by \mathbf{F}) but the mathematically optimal decoder

$$\mathbf{F}^T = \min_{\mathbf{F}^T} \|\hat{\mathbf{x}} - \mathbf{x}\| = \min_{\mathbf{F}^T} \|\hat{\mathbf{x}} - \mathbf{F}^T \mathbf{r}\| \quad (4.15)$$

using conventional methods of regression. While the learned decoding weights do converge, they lag behind the presented precision by orders of magnitude.

All the above testing was conducted only on the original example with $A = -\lambda_d \mathbf{I} \rightarrow \mathbf{W}^s = \mathbf{0}$. With custom \mathbf{A} , convergence was not achieved with any parameter set or configuration.

This lack of convergence, the sensitive hand-tuning of the scaling parameters for \mathbf{W}^f and Γ even without the training of \mathbf{W}^s , led to the rejection of the the adoption of the improved learning rule in eq. (3.52).

Instead, to reestablish a more plausible spiking behaviour, we artificially introduce the diagonal term from the analytic solution for \mathbf{W}^f . Since the first learning rule approaches $\mathbf{W}^f = \Gamma^T \Gamma$ the addition is the most convenient way to reach our target ideal matrix $\mathbf{W}^f = \Gamma^T \Gamma + \mu \mathbf{I}$. The change in spiking behaviour can be seen in fig. 4.3.9 bottom panel.

In comparison to the ideal network, both simulations performed well with an absolute error less than 0.1 compared to the optimum. The dynamics between both networks also differ only marginally. In the top panel of fig. 4.3.9, the differences in networks

dynamics are displayed by the relative difference of spikes. For each spike of neuron i , the output signal shifts by Γ_i as it is added to the spike train. From the top panel of fig. 4.3.9 it can be seen that the differences between both simulations were never more than three spikes different from each other.

4.3.3 Combined Learning

In this chapter, we consider the combined learning performance of slow weights \mathbf{W}^f and slow weights \mathbf{W}^s . We skip the investigation of \mathbf{W}^s alone, as the authors of the slow learning rule [15] emphasize learning both matrices simultaneously. Indeed, slow weights struggle to converge without learning of \mathbf{W}^f .

For the investigation of the training of \mathbf{W}^s , we apply the previously mentioned improvements of \mathbf{W}^f too. We start by looking again at our simple system before investigating parameter and input dependencies.

To begin, we revisit the results for eq. (4.11) for reference. We adjust our external input sequence $\mathbf{c}(t)$ to excite each neuron to spike so we have a better picture of the whole learning progress of all neurons. Yet we keep a segment in which no input is given, such that we can see the network's own evolution over time.

In fig. 4.3.10, the ideal results are displayed again with the given external $\mathbf{c}(t)$ input. To investigate the learning, we will again look at the the measures defined in the previous section. Moreover, we will measure which matrix is more detrimental to the overall performance and therefore should be learned more accurately. Additionally, we will conduct a parameter analyses to identify ideal settings. Lastly, we will investigate how the training sequences influence the learning behaviour. So far, all learning was done with smoothed Gaussian noise. But, very little attention went into our choice of learning input.

Starting, we first compare the trajectories of the ideal against the learned weights to see where potential discrepancies arise. In fig. 4.3.11, we can observe the network's response for learned and ideal weights after training are identical. Moreover, the error is significantly better than the training of just \mathbf{W}^f . While the error is generally acceptable, it becomes clear that the error sources change when the external input $\mathbf{c}(t)$ is absent and the network evolves by its own. While in the beginning, the network is driven by the external input, neurons fire frequently. Therefore, resets after spikes are given by \mathbf{W}^f , playing a heightened role. Slight errors can cause a delay or pre-firing of a spike compared to the ideal weights. This can be seen in fig. 4.3.11 just before 0.1s,

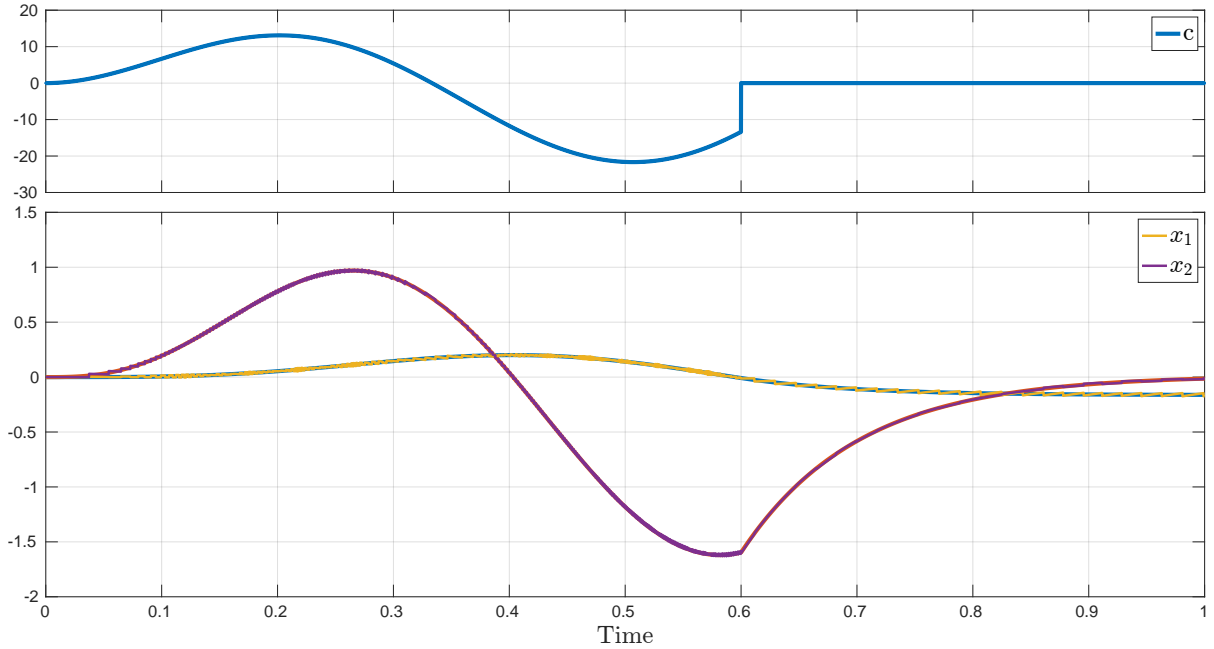


Figure 4.3.10: Exemplary results for our network with ideal weights. In the top panel, the external input $c(t) = [0, c]^T$. The bottom panel shows the calculated system response using numerical methods and the network's response. The network superimposes the numerical results exactly.

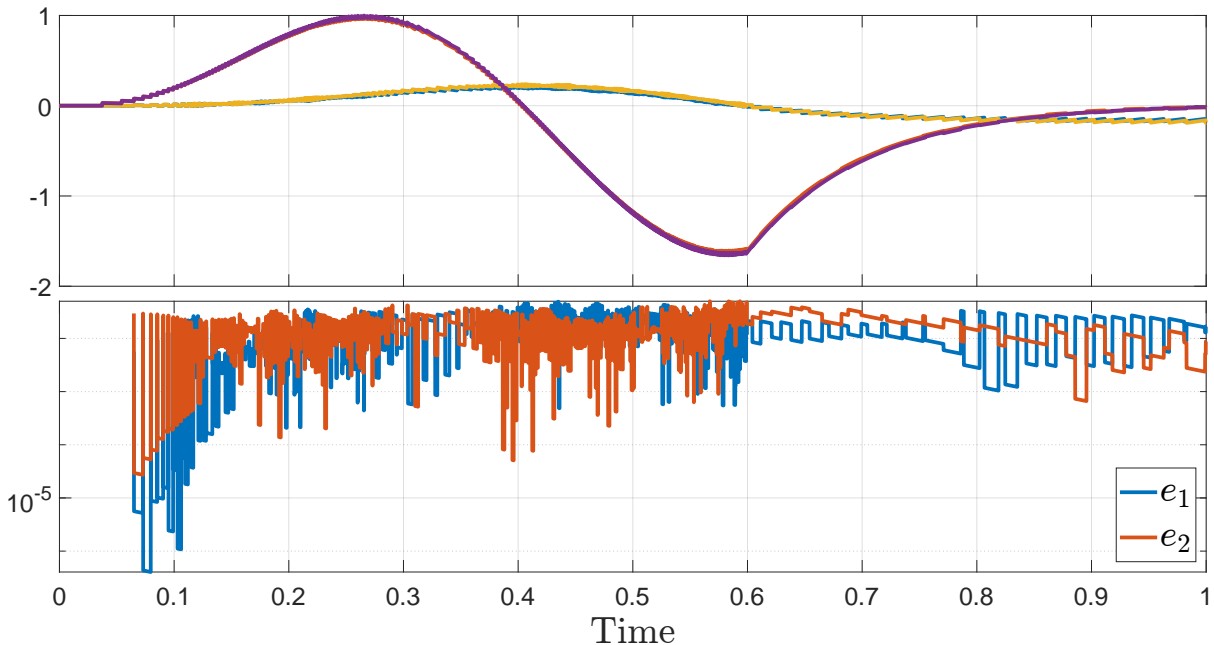


Figure 4.3.11: Computed error between ideal and learned weights. The bottom panel shows the error over time between x_1 and x_2 . Matrices were trained for 4000 epochs.

where the error jumps up after the learned network fired spikes the ideal network. The error jumps back down after the ideal network catches up. However, later this discrepancy becomes too large, and the error appears somewhat chaotic.

With the absence of the external input, the error becomes fine-grained again since the repeated spiking of caused by external input disappears. Now the weights \mathbf{W}^s play an important role. Errors in the slow connections can add up slowly and cause wrong neurons to fire.

Parameter Analysis

The following subsections are dedicated to investigating the parameters concerning the learning of \mathbf{W}^s and the learning of the network in general. This includes the error weight K , the slow learning rate α^s , the learning input sequences to train the network.

Learning rate

In fig. 4.3.12, it appears that much larger learning rates can be applied to \mathbf{W}^s than expected. While all tested learning rates α^s reach the same level of error, the larger α^s the faster this level is reached. Furthermore, it becomes clear that the learning of \mathbf{W}^s is related to the accuracy of \mathbf{W}^f . Only when deviations in the parameters of \mathbf{W}^f are small, the learning of \mathbf{W}^s can reach errors less than 0.1, corresponding to a relative error of $\approx 10\%$. It is also clear that the learning rate of \mathbf{W}^s does not affect the behaviour of \mathbf{W}^f and, therefore, can be learned with the same or larger learning rates. This contrasts with [15] where it is recommended to learn \mathbf{W}^s with a smaller learning rate compared to \mathbf{W}^f to ensure resets of neurons are learned quickly, such that learning of \mathbf{W}^s can converge.

For future evaluations, we select $\alpha^s = 0.01$ as it marginally improves performance in the error and shows less variability in the rel. deviations. This choice comes at the cost of training for 100 more epochs before reaching slightly better performance.

To combat the unsteady behaviour in the first panel we again attempt to reduce the learning rate over time. To do this we again set our learning rate according to eq. (4.14) and test different p . In fig. 4.3.13, we observe the effect of different values for p . As expected was the error in the bottom panel of fig. 4.3.13 not reduced by this addition. Moreover, under a linear scale, the largest rel. deviations are not noticeable and will

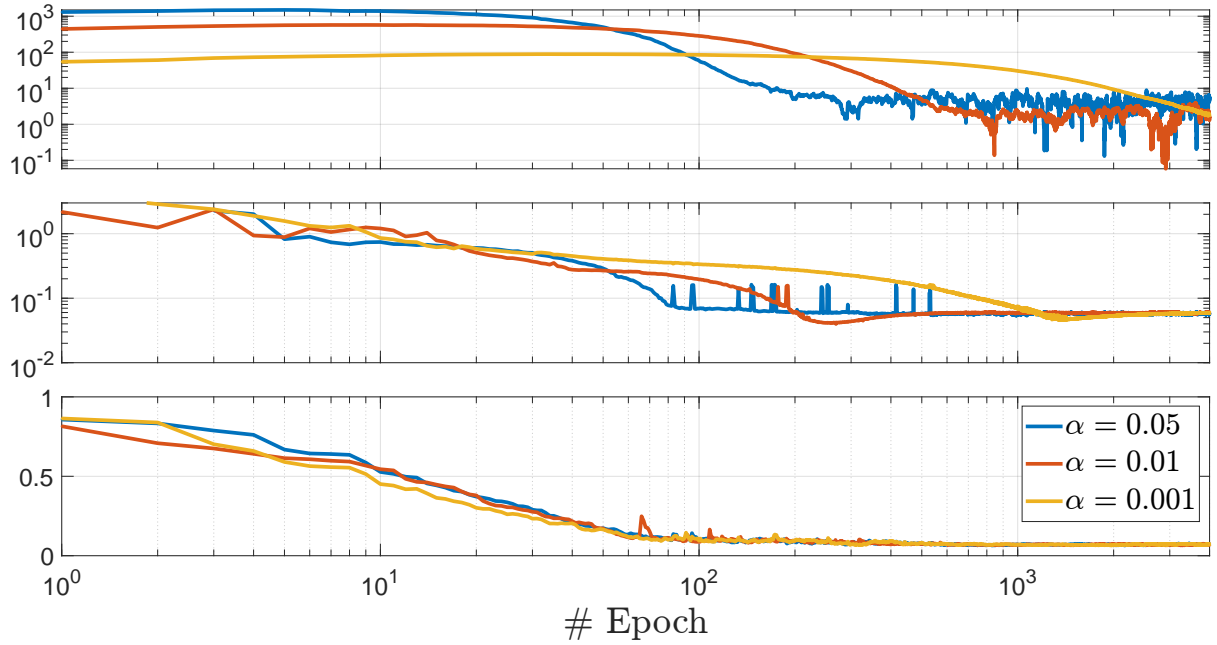


Figure 4.3.12: Top panel showing the largest rel. deviation after each epoch for different learning rates α^s . Middle panel shows the maximum error during simulation with the learned \mathbf{W}^f and \mathbf{W}^s in log scale. Bottom panel shows largest rel. deviation for \mathbf{W}^f .

therefore be omitted for future tests. Lastly, we have not examined the eigenvalues of \mathbf{W}^s yet. Fortunately, the non-zero eigenvalues do allow for a coarse estimate of the learning progress. In all test including fig. 4.3.12 the eigenvalues converged to the optimal values and usable results could be obtained after both eigenvalues converged.

Error Gain

The parameter K describes the influence of the error during training. With increasing K , the importance of the error and, therefore, the teacher grows.

As can be seen in fig. 4.3.14, the parameter K only slightly impacts the network's learning. Also in contrast to the derivation in which K is assumed to be large, the smaller the error gain K , the better the network performs. Furthermore, in this example, values $K > 100$ did not give acceptable results. For $K > 500$, convergence did not occur in the 4000 epochs of learning.

In the middle panel of fig. 4.3.14 tested values above 50 ($K = 100, 200, 500, 1000$ not all shown) present a bend in the error after ≈ 1050 epochs, and the error starts increasing again. With larger K , the bend is more pronounced and occurs after fewer epochs.

The bend is likely caused by the error gain having too much influence over the network

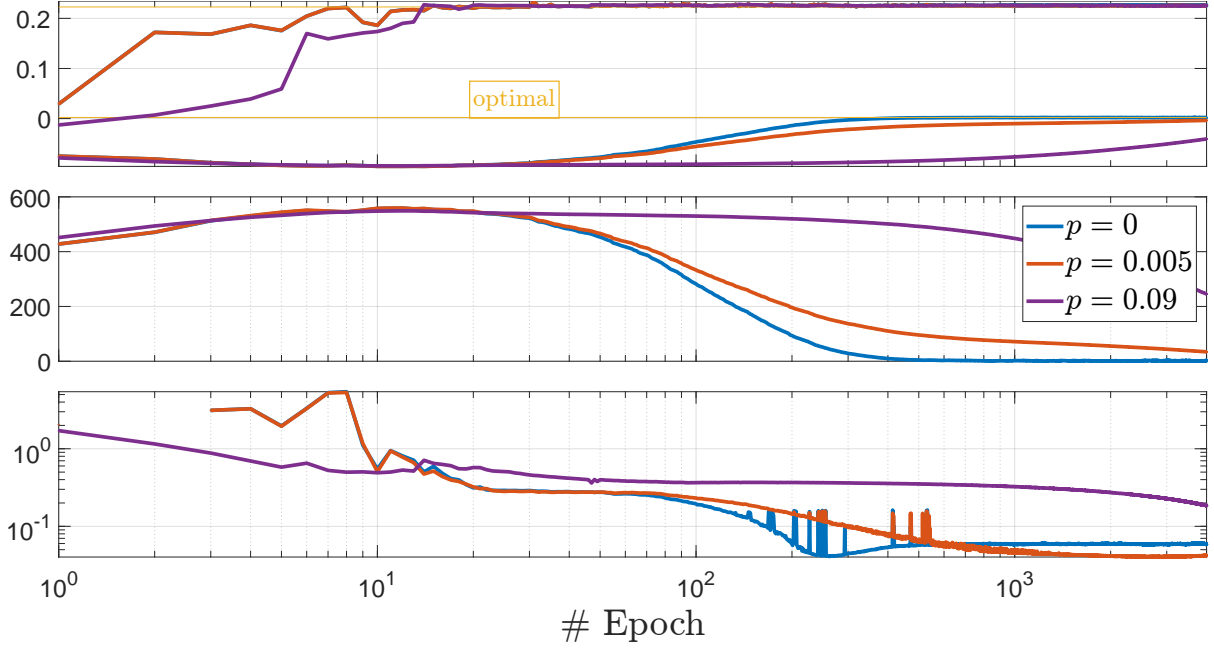


Figure 4.3.13: Top panel showing the two non-zero eigenvalues of \mathbf{W}^s after each epoch for different drop rates p and starting learning rate of $\alpha^s = 0.1$. Middle panel shows largest rel. deviation for \mathbf{W}^s . Bottom panel shows the maximum error during simulation with the learned \mathbf{W}^f and \mathbf{W}^s .

dynamics, overly correcting errors in matrix parameters to the point where the network error is now bound by these parameter values.

On the other hand, values $0.5 < K < 5$ all performed almost identical to $K = 1$ shown in the plot.

In the last panel of fig. 4.3.14, we chose $K = 10$ to test the main source of error. For this we ran the simulation with \mathbf{W}^f learned using the optimal \mathbf{W}^s and vice versa. The results are seen in the bottom panel of fig. 4.3.14. Without a good approximation of \mathbf{W}^f , the error is more than 2 orders of magnitude worse than the opposite configuration. However, this normalizes after around 30 epochs after which the the error in \mathbf{W}^s dominates. Only after more than 1000 epochs \mathbf{W}^s is accurate enough such that the small errors in \mathbf{W}^f from learning become relevant once more. However, after more than 1000 epochs the error less than 0.04 or $\approx 3\%$ relative error.

Input Learning Sequences

So far, we have not touched on the training input. As often seen in the literature of this network architecture (e.g. [3, 15, 16, 84]), training is performed using smoothed Gaussian noise. However, little detail is given on the specifics. Moreover, as speculated

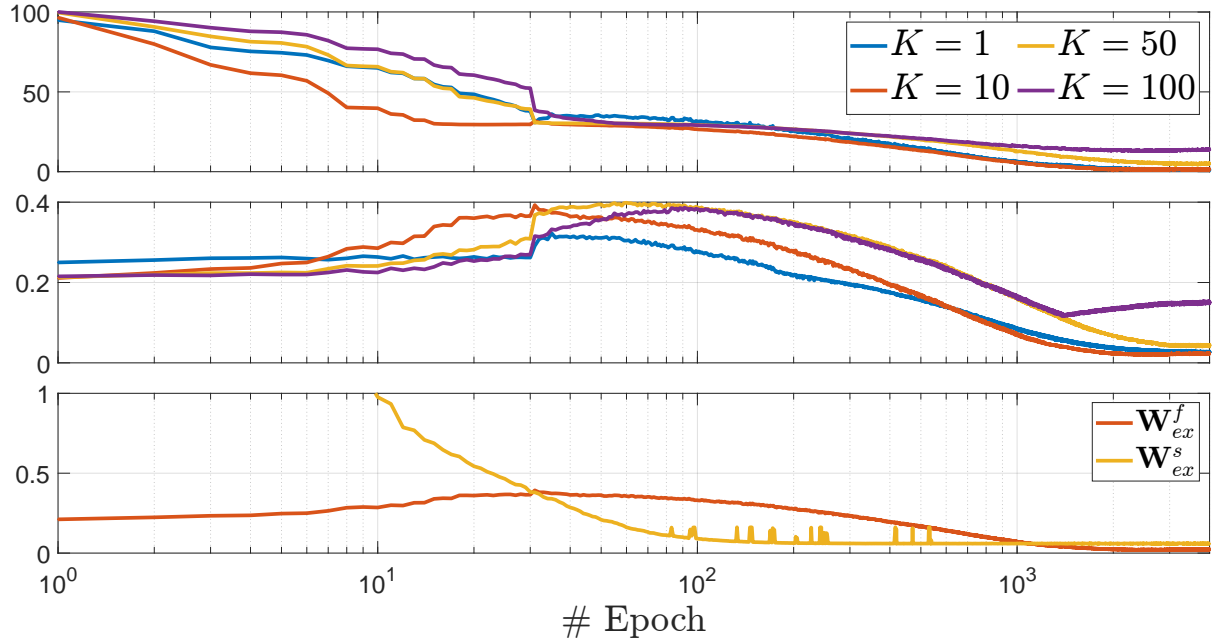


Figure 4.3.14: Top panel shows the rel. deviation for each K . Middle panel shows the maximum error during simulation after each epoch using both \mathbf{W}^f and \mathbf{W}^s from training using different K . Bottom panel shows the error for $K = 10$ while using either the optimal \mathbf{W}^f or \mathbf{W}^s respectively.

above, the choice of input sequence could potentially affect the learning outcome. Therefore, in the next section, we will investigate different patterns of input and potential influence on the results.

With the right training sequence, it may be possible to find ways to make our network even more accurate.

Firstly, we note the current setup of our learning. So far we have used white noise smoothed by a Gaussian kernel. Already, the number of tunable parameters is large when considering different kernels to get smoother or more variable input sequences. However there are also completely different functions that can be tested. For now, we compare the currently used Gaussian noise again pure sine waves and individually stimulating each neuron for training.

Gaussian Noise and Smoothing

The current setup of learning is based on a sequence \mathbf{v} of white noise that is generated for each epoch. One sequence is 100000 timesteps long and each gets convoluted by an exponential kernel to obtain \mathbf{c} . Different standard deviations σ for smoothing are visualized in fig. 4.3.15. In all runs, the standard deviation was chosen $\sigma = 6$ to allow for rapid movement of \mathbf{c} allowing for great variety which drives the error and subsequently

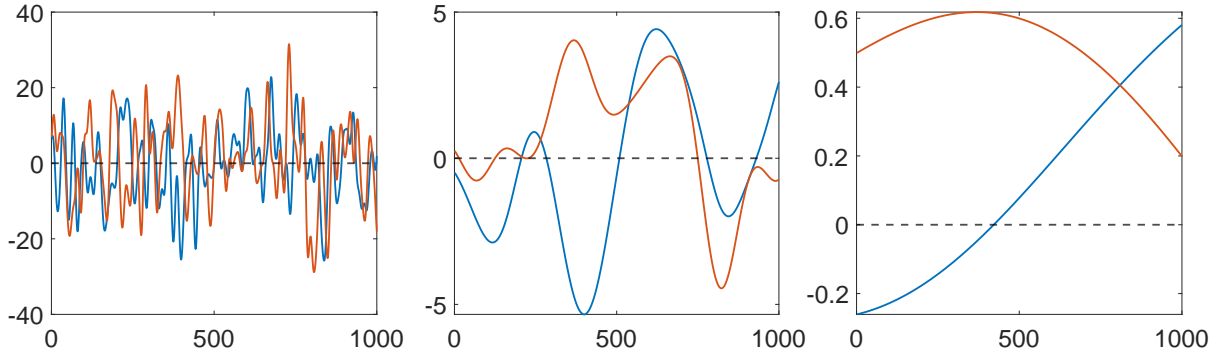


Figure 4.3.15: Illustration of smoothing with σ changing in the kernel. F.l.t.r $\sigma = \{6, 60, 600\}$. Plots show only the first 10% of a learning epoch for visibility.

the learning of \mathbf{W}^s .

This can be seen in fig. 4.3.16. For $\sigma = 6$, a tiny smoothing window, the networks shows the best results with an maximum absolute error of 0.03 which is within one spike difference from the ideal with the given scaling of Γ . The second best option is for $\sigma = 60$ with double the error of $\sigma = 6$. Also, in the convergence of both \mathbf{W}^f and \mathbf{W}^s the least amount of smoothing appears to yield the best results. Though this is heavily depending on the signal that the network is being tested with. Moreover, the difference between the errors is reduced when tested with alternative input signals c . With oscillating input similar to what was used in testing the network or larger amplitude input is used, the difference in error between the trials with higher smoothing are almost completely removed.

Alternative Learning Inputs

The importance of sudden movement and, therefore, the necessity for tiny smoothing becomes apparent when comparatively smooth input sequences are tested. To illustrate this, the network is trained with the previous white noise with $\sigma = 60$ and compared to similar magnitude sine and square waves.

To introduce some variability in the sine wave, for each epoch, the phase for each input is varied.

The square wave is explicitly structured to enforce firing of 2 specific neurons at a time. As illustrated before, each neuron i projects the error along Γ_i direction and fires when the threshold is reached. To target neuron i directly, we project the square wave on each dimension c_j of the input by multiplying it with Γ_{ij} . Using this approach, neuron i fires the earliest and will be trained. During the off cycle of the square wave the same happens with the neuron geometrically opposing i .

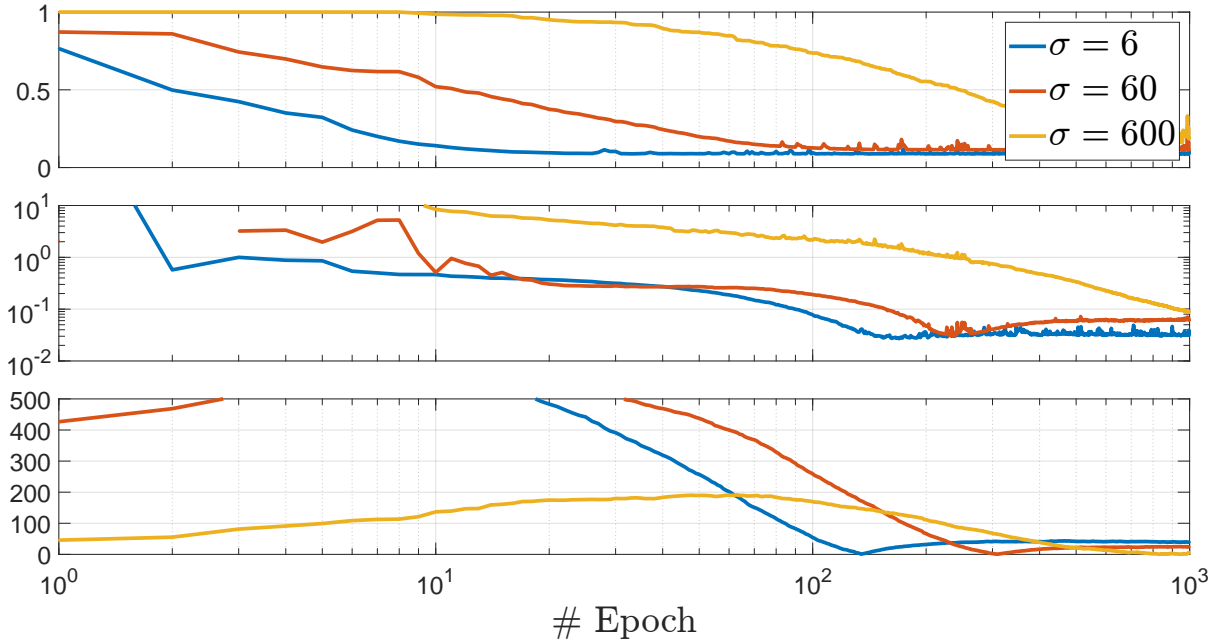


Figure 4.3.16: Learning results for different smoothing grades of c . Smoothing is governed by the std. dev. σ of the exponential kernel. Top and bottom panel show the largest rel. dev. of \mathbf{W}^f and \mathbf{W}^s respectively. Middle panel shows the absolute error. Trained was for 1000 epochs.

To verify this, we can look at the spiking behaviour during training. In fig. 4.3.17, we can see the cumulative spiking of each neuron during training for the Gaussian noise, sine and square wave. The square wave clearly shows our desired pattern in which for each epoch a new pair of neurons is trained, illustrated by the diagonal edges. From this it can also be seen that the test used 50 neurons. At the mark of 50 epochs, a rotation is completed indicated by the first diagonal line ending there. Furthermore, after 25 epochs each pair of neurons has been trained once, indicated by the two diagonal lines starting from the top left corner entering the section of geometrically opposing neurons.

Surprisingly, the spiking behaviour with the sine wave and the Gaussian noise exhibit an aggregation of spikes only on certain neurons. From the colour grading it becomes apparent that certain neurons spike more often during training than others. This is caused by the lack of regularization and subsequent distribution to spikes in our learning scheme due to aforementioned problems. Solely from judging fig. 4.3.17, it would be natural to guess that the learning using square waves would perform the best thanks to the even distribution of spikes and therefore even learning. However, this would be wrong as can be seen in fig. 4.3.18. While the trajectory for x_2 follows the main numerically calculated solution in blue, x_1 does not follow the expected trajectory

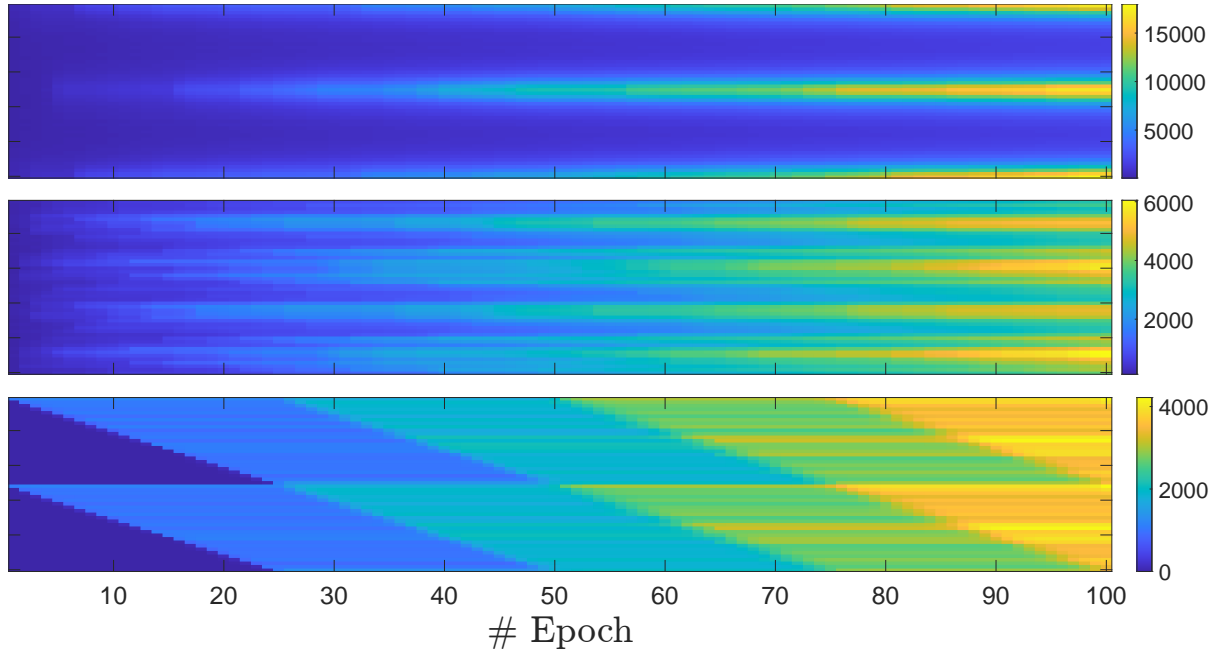


Figure 4.3.17: Cumulative spikes for each neuron over training. Top: Gaussian noise, Middle: Sine wave, Bottom: Square wave. Only a segment of the entire training process is shown. Note the different colour scales.

at all. This misbehaviour is caused by the input sequences overshooting the scale of the parameters of \mathbf{W}^s . Similarly this occurred as well when using heavily smoothed noise. The sine and square wave created, similar to the heavily smoothed, stretches of repetitive stimulus that appears to cause the corresponding weights for spiking neurons to be oversaturated. Lowering the input amplitude did improve performance at the cost of longer training times. With the reduced input, the convergence of \mathbf{W}^f is slowed down by the reduced number of spikes necessary. Furthermore, \mathbf{W}^s learning rule is directly depending on the error and the rate, therefore depending on the state vector \mathbf{x} that is once more dependent on the input \mathbf{c} .

Random Initialization of Matrices

As we have done in the section section 4.3.2, results so far have only considered optimal conditions for learning. In light of more challenging conditions, especially the initialization of \mathbf{W}^f and \mathbf{W}^s to zero is a significant aid toward the learning and network performance.

To test the influence of initial weights in both matrices we initialize the matrices with random numbers scaled to the appropriate range of \mathbf{W}^f and \mathbf{W}^s respectively.

For the first test both matrices were initialized to random numbers of the same scale as

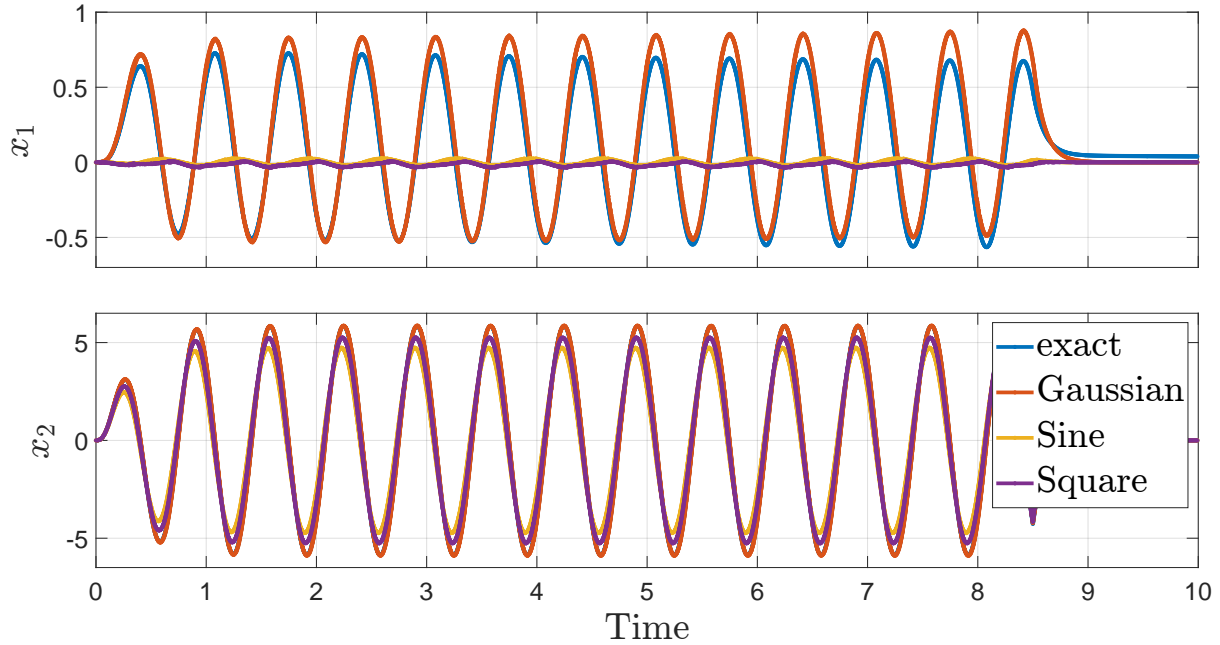


Figure 4.3.18: Network responses for each training sequence type with an oscillating input c .

their optimal values. Results showed that from 1000 epochs of training 920 networks did not converge at all while in the remaining 80 epochs, results were unusable. It was observed that while training, the matrix eigenvalues diverged further from their optimal values. This was also observed when measuring the largest rel. deviation.

When initializing with random values 50% of the scale convergence was obtained during all of training. However, the relative error was more than 100%, rendering results useless.

If only either \mathbf{W}^f or \mathbf{W}^s is initialized randomly it becomes apparent that the \mathbf{W}^s is the reason for the aforementioned problems. When initializing \mathbf{W}^s to zero, acceptable results were obtained with \mathbf{W}^f initialized to the previously impossible 100% noise scale. However, this was only achieved after at least doubling the training time.

On the contrary, the initialization of \mathbf{W}^s with just 5% scale to noise prohibited any convergence during training. The hypothesis, that potentially flipped signs in \mathbf{W}^s being the reason for the lack of convergence was rejected, as there was no change when each \mathbf{W}_{ij}^s was given the same sign of the respective analytical value.

Thus, \mathbf{W}^s has massive influence on \mathbf{W}^f . This can also be seen when attempting to run a simulation with learned \mathbf{W}^s and analytical \mathbf{W}^f as the network fails to converge. Yet when simulating the opposite configuration results can be obtained, although of subpar quality to the completely learned configuration.

This shows that \mathbf{W}^s influences \mathbf{W}^f to adapt to the (wrong) structure of itself. Hence it

is advisable to only allow noise to impact \mathbf{W}^f . While this notion deviates from biologic plausibility since noise is inherent to any system and connectivities between neurons are not nullified when learning commences, this is a manageable restriction for the sake of usable results.

Limitations

Limitations in the learning of \mathbf{W}^s arise when the eigenvalues of \mathbf{A} have positive real parts. For purely imaginary eigenvalues, results depend on the magnitude of the imaginary part. For increasing imaginary parts, the matrices converge to the correct structure but not the correct magnitude. This can be combatted by tuning of hyper-parameters, though it depends on the \mathbf{A} , making it infeasible for wide range use. Without tuning, the error remains high and results unusable.

The second big limitation comes with the choice of Γ . During testing, the choice of Γ impacted network accuracy. With randomly chosen Γ on S^n , the network error was too large to be useful. This was especially the case when working with higher-dimensional systems ($J \geq 4$). The necessary accuracy for \mathbf{W}^f to yield a functioning network was not learned anymore. Without sufficiently approximated \mathbf{W}^f , training was incapable of producing acceptable network results.

Instead, Γ was chosen as equidistant points on S^n to have uniform error projection and retain accurate results.

Apart from the choice of Γ , higher order problems pose a problem for the networks learning. Due to small inaccuracies in training, errors add up in the integration of higher order problems. Especially \mathbf{W}^s is the main factor in network error.

However, this becomes significant only when no or little external input $\mathbf{c}(t)$ is applied. If $\mathbf{c}(t)$ is zero for large parts of the simulation time, errors in \mathbf{W}^s compound to the point where the network produces unusably erroneous results. If $\mathbf{c}(t)$ is non-zero, errors in \mathbf{W}^s become less significant compared to \mathbf{c} and the network output acceptable. This is because the most tests of our networks the relative importance of $\Gamma^T \mathbf{c}$ in the Voltage computation was an order of magnitude higher compared to $\mathbf{W}^s \mathbf{r}$.

It is unclear what causes \mathbf{W}^s to fail to reach the same accuracy compared to lower dimensional problems. No parameter set or amount of learning yielded the same level of precision seen in the results above. It is therefore necessary that the problem exhibits continuing external input.

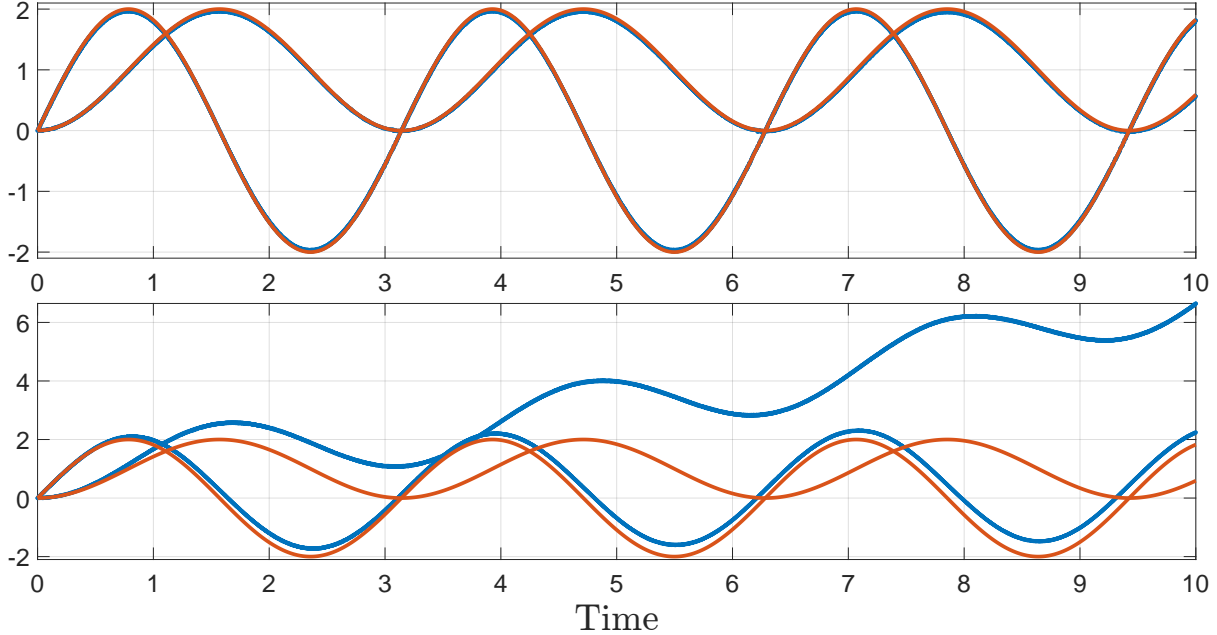


Figure 4.4.1: Control of our model problem with the controlling and simulating network in series. Latter produces $c = Bu$, fed to the former. Both networks used 50 neurons and analytically computed parameters. Top: Analytically computed matrices. Bottom: Trained matrices from section 4.3. In blue, the networks' output to the target (red).

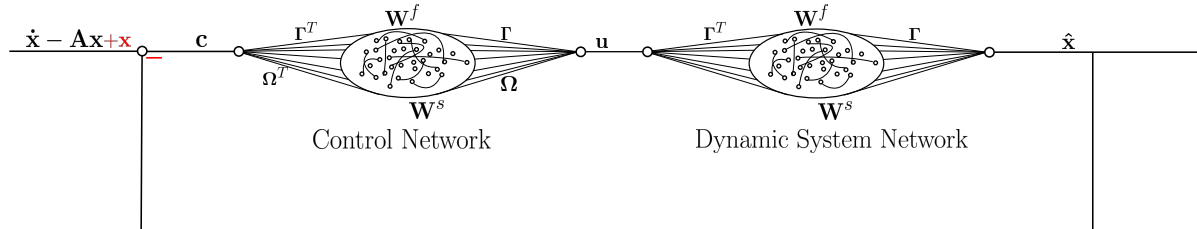
4.4 Results of the Learned Control Objective

4.4.1 Combining the Two Networks

As is, with suitable B and C , it is now possible to combine this network with the previous simulating network for control. Given our model problem, $B = [0, 1]^T$ and $C = I$, the performance is comparable to control of the dynamic system directly. This can be seen successfully applied in fig. 4.4.1. However, these results only apply to the analytically computed matrices W^s and W^f . When learned matrices are used, control quickly deteriorates independent of which derivation of control is implemented.

The error introduced to the system by the learned matrices is too much for the open controller to handle. Thus, a way to mitigate this by using an additional feedback line around the network. To add feedback, we add the error between target and network output to the input c of the control net. In the computation of c , we add the reference target x and subtract the network output to construct the error signal. The computation of c changes to

$$c = \dot{x} - Ax + x - \hat{x}. \quad (4.16)$$



(a) Add an extra loop to introduce feedback into the control network.

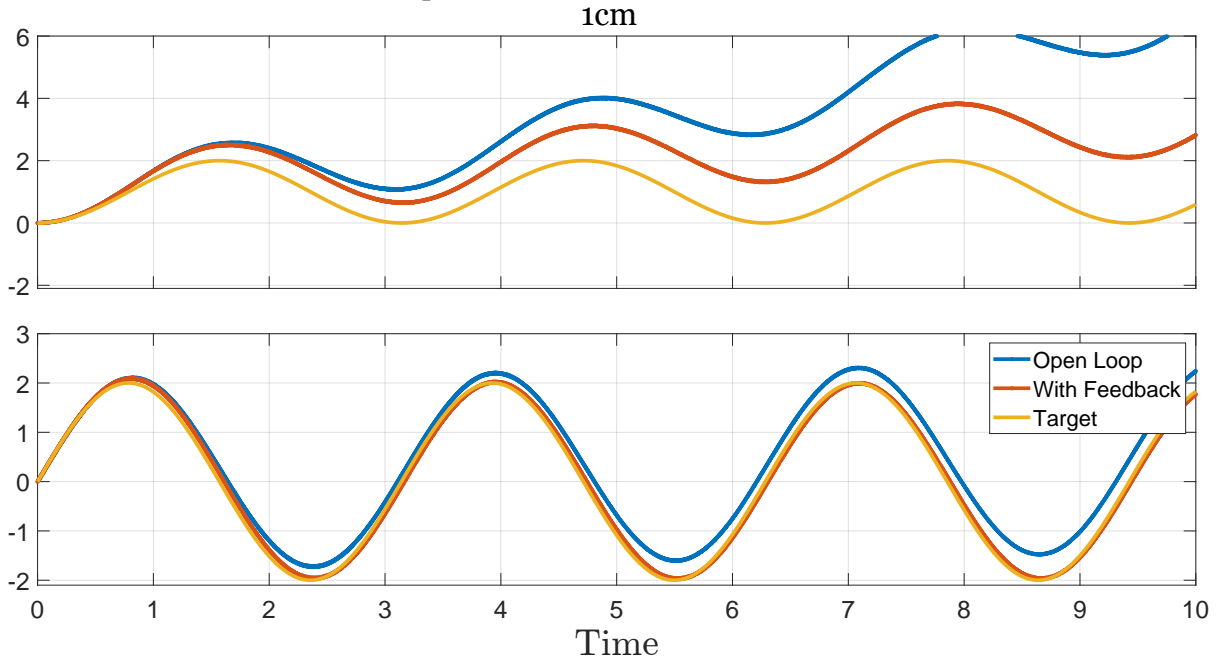

 (b) Comparison of control for our model problem with the controlling and simulating network with and without feedback. Both runs used networks with 50 neurons and identical parameters. Plots for x_1 and x_2 separately.

Figure 4.4.2: Top: Schematic to the addition of feedback in the in the control network. Additions are highlighted in red. Bottom: Resulting improvement of error with the feedback loop added.

Schematically, this can be seen in fig. 4.4.2a. From this we subtract the network output to construct the error signal. While this improves performance, as seen in fig. 4.4.2b, the network output is still unusable due to the error. Thus, efficient tracking is only possible using the analytically calculated matrices \mathbf{W}^f and \mathbf{W}^s and therefore disqualifies this approach as we aim to use the learned matrices.

Additionally, it was not possible to find training rules that would allow the training of the matrices used in the control network, posing further problems for our goal of using learning rules for the entire scheme.

4.4.2 Merging two Networks

Unfortunately, the use of feedback did not help to achieve acceptable results. It is therefore necessary to make a trade-off between biologic plausibility and control scheme performance. The alternative option being a combined network, incorporating both control and simulation at the same time.

As highlighted before, the governing force behind the control was not the network but rather only the definition of c . The network itself is primarily based around producing the necessary spikes and rates to return the corresponding control input u . Therefore, we construct a single network that handles both the control as well as the dynamic system itself. We define c as

$$c = \dot{x} - Ax \quad (4.17)$$

as before in the control network. In the current state, no control matrix is incorporated in the network which means that the network assumes $B = I$ which will be addressed later.

Working as an Open-Loop Controller

To begin, we set a sine wave as our target. As can be seen in fig. 4.4.3, the aforementioned control using c appears to deliver good results using the optimal weights. Both state trajectories almost perfectly overlap the target. As seen before, similar to section 4.4.1, dynamics quickly diverge due to the imperfections in the learned matrices making it impossible for the open loop to properly control the system, leading to an almost complete loss of the target trajectory. Yet the output shows better tracking than the separate networks. The error shown in fig. 4.4.3 is almost purely due to inaccuracies in W^s . If the control is rerun but instead the optimal W^s are used with the learned W^f , greatly improved results can be obtained.

In fig. 4.4.4 the results show that if the ideal W^s is used, control accuracy is greatly improved. Small errors still accumulate over time. These are from the remaining error in W^f that is caused by small errors from training but also because W^f adapts to the potential errors in W^s during training. The opposite configuration yields even worse results, proving the principal error contribution stems from W^s .

As before, the main problem is that due to the open loop design, very precise system information is necessary. With training, only a perturbed system $A' = A + \epsilon$ of the system matrix is learned. Without state feedback, control over A' produces

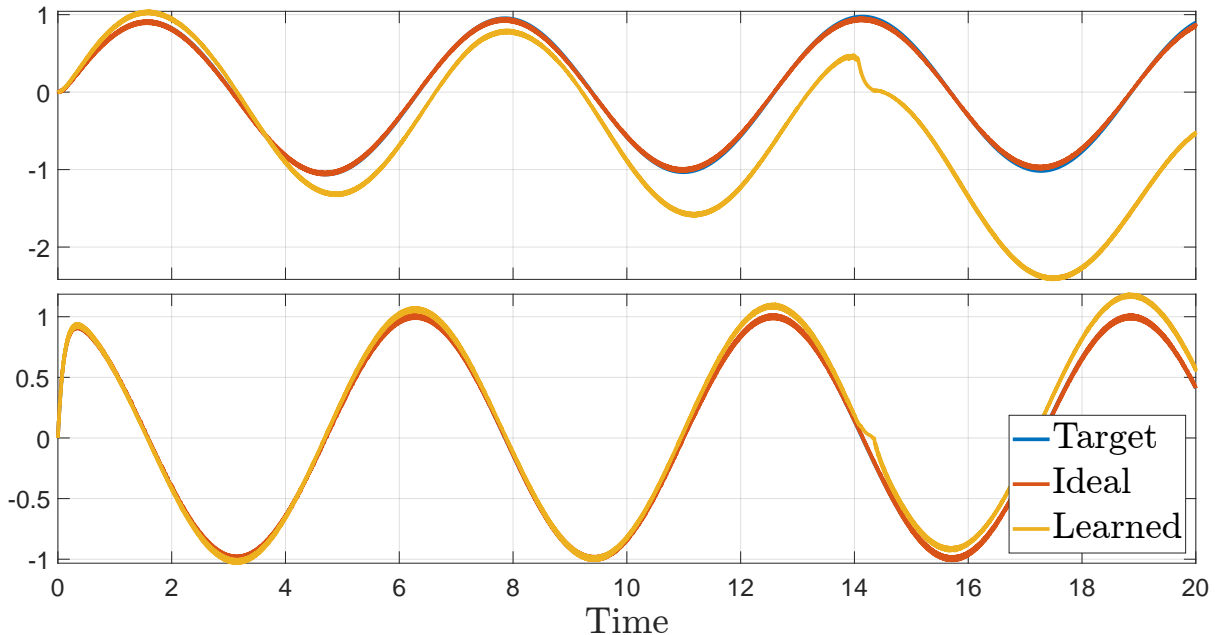


Figure 4.4.3: Control results for the ideal and learned matrices \mathbf{W}^f and \mathbf{W}^s on a sine wave target. Top panel shows the x_1 state and bottom x_2 . Matrices were trained for 1000 epochs using the previously studied optimal parameters.

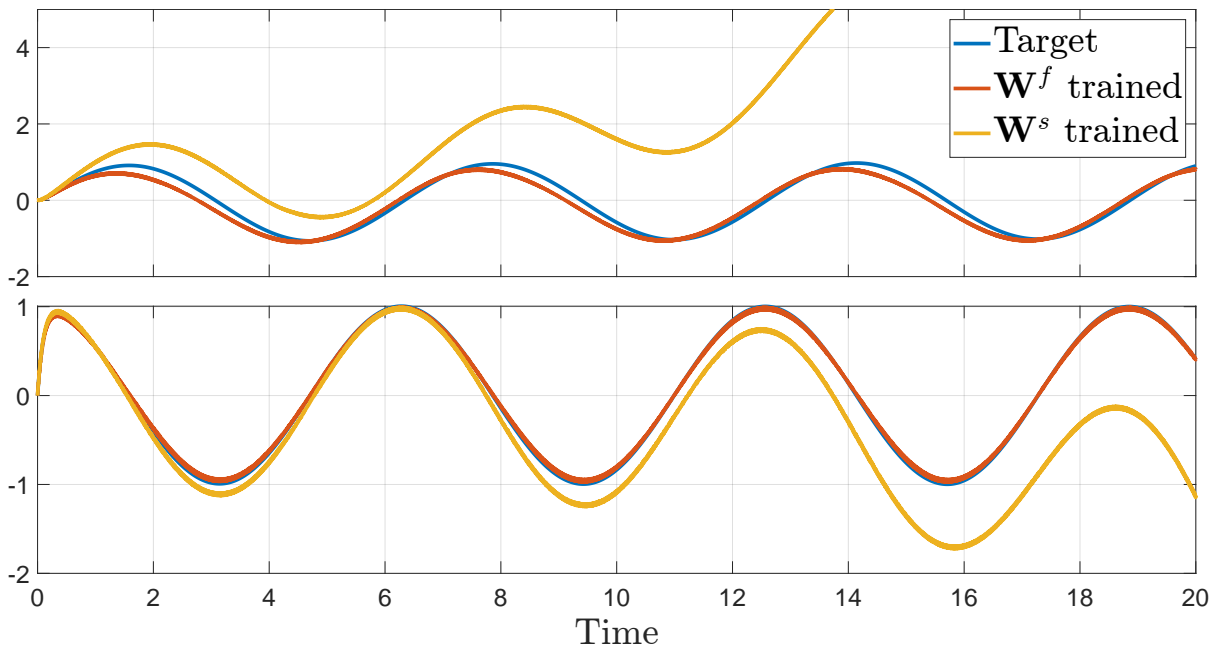


Figure 4.4.4: Control results from fig. 4.4.3 but with only either \mathbf{W}^f or \mathbf{W}^s trained. Top panel shows the x_1 state and bottom x_2 . Matrices were trained for 1000 epochs using the previously studied optimal parameters.

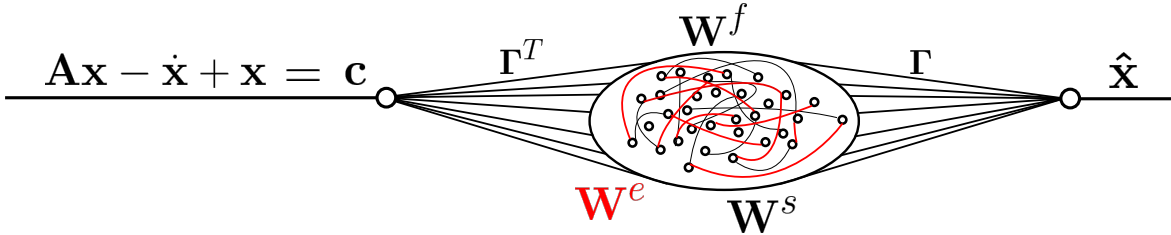


Figure 4.4.5: Add an extra loop to introduce feedback into our control scheme. The outside loop can be integrated into the network similarly to \mathbf{W}^s .

different dynamics which cannot be compensated without state feedback. This limits the applicability of any learned matrices.

Adding Feedback

In order to build a more robust controller, we add feedback to the control scheme as done before. Although this can be done identically by adding the error term directly onto \mathbf{c} , we can change the formulation here due to only one network being present. While we still send the target trajectory to \mathbf{c} , we can move the feedback loop directly into the network. The network output is calculated by $\hat{\mathbf{x}} = \mathbf{\Gamma}\mathbf{r}$. Ignoring the subtraction, this value is then fed back into the network using the same weights using $\mathbf{\Gamma}^T\mathbf{c}$. It is therefore the same as keeping adding another matrix

$$\mathbf{W}^e = -\mathbf{\Gamma}^T\mathbf{\Gamma} \quad (4.18)$$

to the network dynamics. The negative sign accounts for the subtraction we ignored earlier. The adjusted network dynamics are illustrated in fig. 4.4.5. To measure its effectiveness, we run the simulation with the added matrix. In fig. 4.4.6, we can clearly see the network performance is greatly improved. Both trajectories follow their target almost perfectly.

Learning the New Feedback Loop

Instead of introducing another matrix that is multiplied by the neuron firing rates, we can adjust the definition of \mathbf{W}^s to

$$\mathbf{W}^s = \mathbf{\Gamma}^T (\mathbf{A} + (\lambda_d - 1)\mathbf{I}) \mathbf{\Gamma}. \quad (4.19)$$

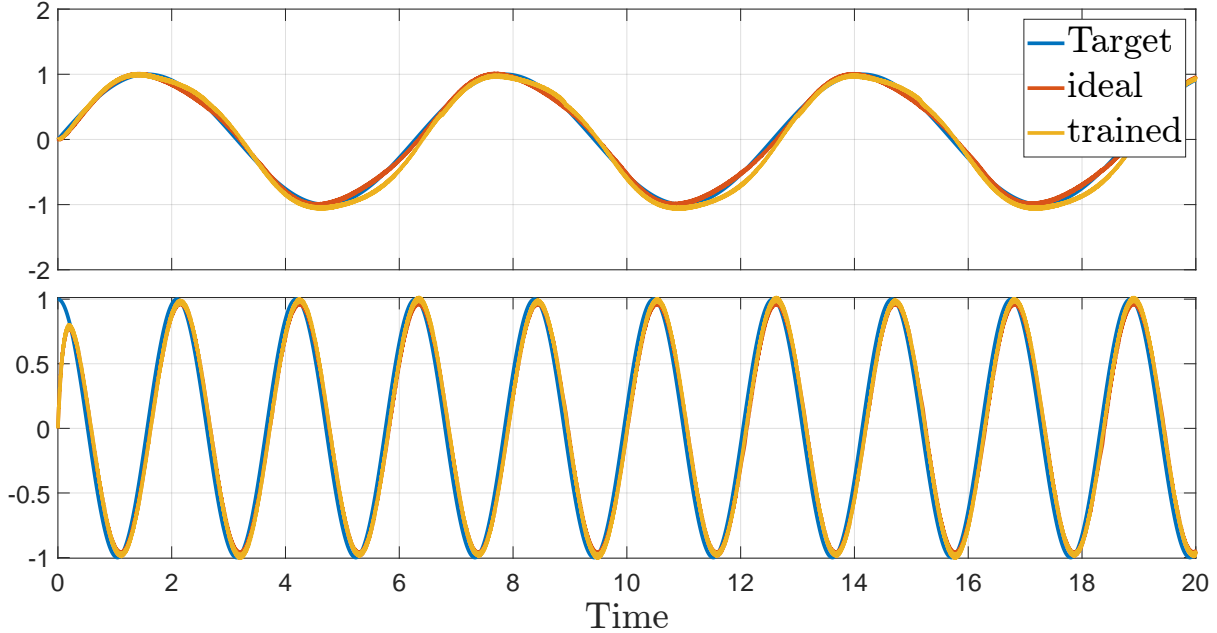


Figure 4.4.6: Control results from fig. 4.4.3 but with the added feedback loop seen in fig. 4.4.5.

This matrix can be further learned by the previous training algorithm by subtracting the identity matrix from \mathbf{A} before training.

We check if the learning of $\mathbf{A} - \mathbf{I}$ gives similar results to the case with the extra loop in fig. 4.4.6. We retrain our model problem using the identical parameter set as before with the identity matrix subtracted.

To measure whether the training was able to reproduce the subtraction we calculate the inner matrix of eq. (4.19) using regression.

$$\mathbf{M}^* = \min_{\mathbf{M}} \|\boldsymbol{\Gamma}^T (\mathbf{M} + \lambda_d \mathbf{I}) \boldsymbol{\Gamma} - \mathbf{W}^s\|_2^2 \quad (4.20)$$

It shows that in this test case the training was able to resolve the subtraction, with relative errors between matrix entries being less than 8%. In fig. 4.4.7 the result of training can be compared to the addition of the extra matrix after training. The final results is sufficiently accurate for almost perfect results. The target is tracked with almost identical performance as in fig. 4.4.6.

Restrictions on \mathbf{B}

All previous results are built on the implicit assumption of $\mathbf{B} = \mathbf{I}$. Although the results are acceptable, this assumption is prohibitively restrictive.

The easiest way to circumvent this restriction would be to have use the pseudo-inverse

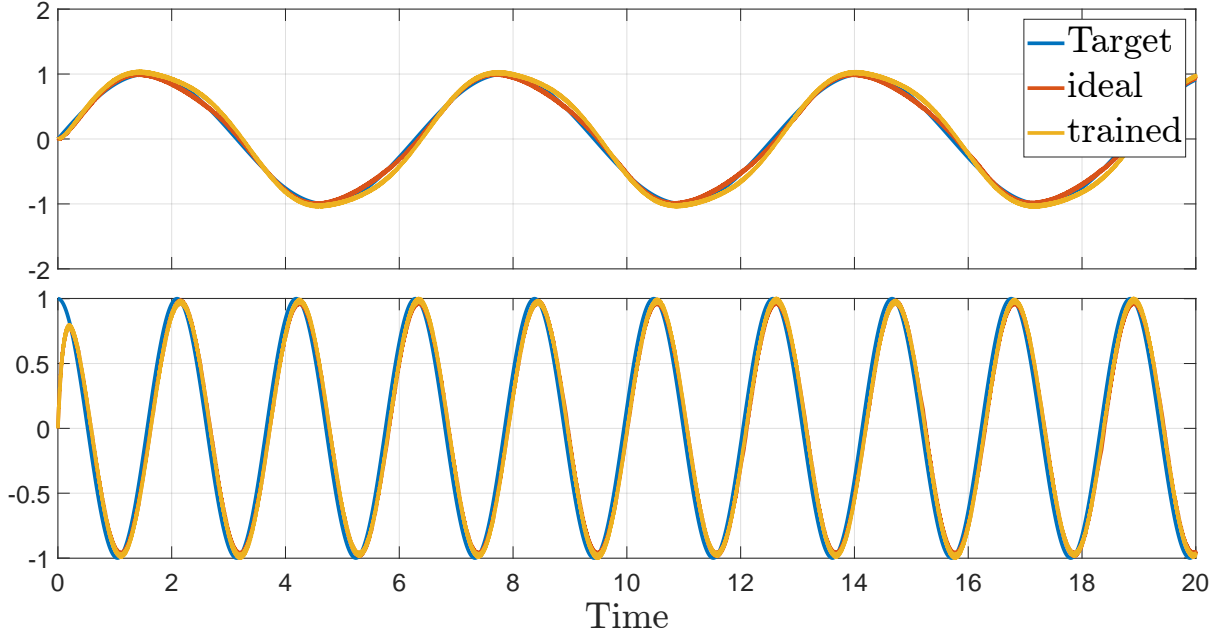


Figure 4.4.7: Control results from fig. 4.4.6 but with the added feedback loop learned and integrated into the network directly.

\mathbf{B}^+ . If \mathbf{B}^+ is available, the computations of network input can be simplified directly to

$$\mathbf{c} = \mathbf{Bu} = \mathbf{BB}^+ (\dot{\mathbf{x}} - \mathbf{Ax}) \quad (4.21)$$

if $\mathbf{c} = \mathbf{Bu}$ is substituted in the derivation of section 3.3 and $\mathbf{u} = \mathbf{B}^+ (\dot{\mathbf{x}} - \mathbf{Ax})$, ignoring the previously added feedback. But \mathbf{B}^+ is often unavailable, moreover, biologically it is unrealistic to assume that the brain does matrix inversion. Instead, we restrict ourselves to matrices \mathbf{B} such that

$$\mathbf{BB}^+ = \mathbf{BB}^T, \quad (4.22)$$

which can be transformed to

$$\begin{aligned} \mathbf{BB}^T &= \mathbf{BB}^+ \\ &= \mathbf{B} (\mathbf{B}^T \mathbf{B})^{-1} \mathbf{B}^T \\ &\rightarrow \mathbf{B}^T \mathbf{B} = \mathbf{I} \end{aligned} \quad (4.23)$$

the condition that the Gram matrix of \mathbf{B} is the identity or the columns of \mathbf{B} form an orthonormal basis. The pseudo-inverse in eq. (4.21) can then be replaced by \mathbf{B}^T .

While this is again a strong limitation, it does increase the applicability of the network.

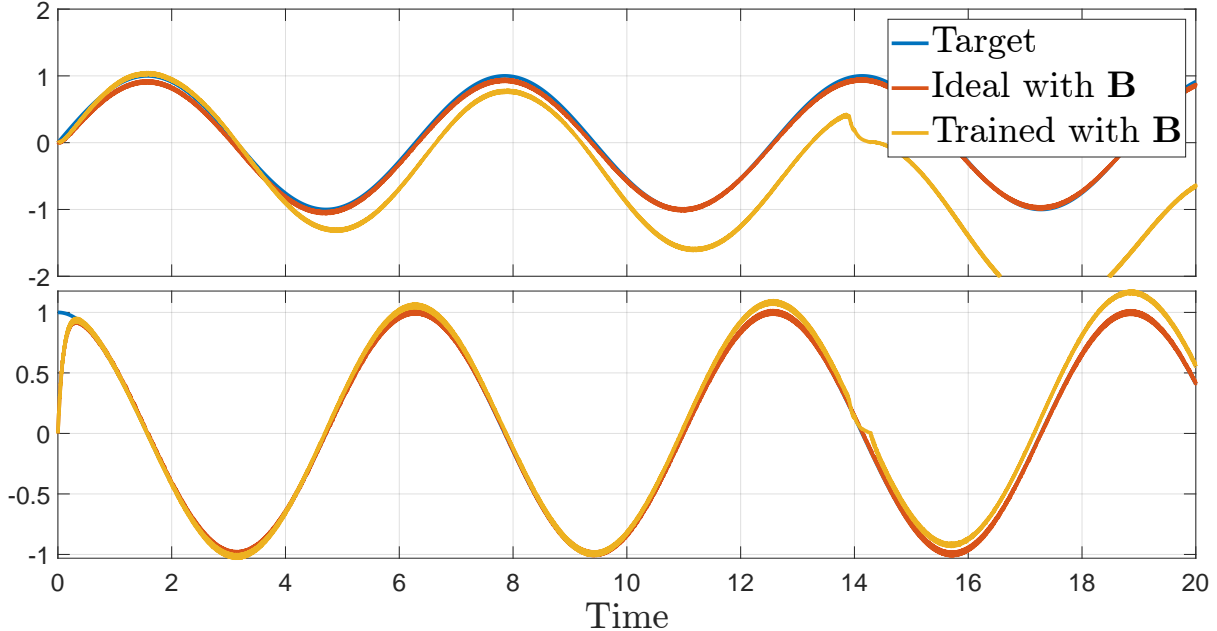


Figure 4.4.8: Control results from fig. 4.4.6 with the input matrix $\mathbf{B} = [0, 1]^T$.

To illustrate this, we rerun the previous simulation with $\mathbf{B} = [0, 1]^T$ in fig. 4.4.8. Unfortunately, the addition of \mathbf{B} ruins the network performance with the trained matrices. Again, this is mainly caused by inaccuracies in \mathbf{W}^s , as the network shows perfect results in fig. 4.4.8 when both \mathbf{W}^s and \mathbf{W}^f (fig. 4.4.8) or just \mathbf{W}^s (not shown) is computed analytically.

The main reason the network performs subpar is the addition of $\mathbf{B}\mathbf{B}^T$ towards the error signal introduced before. As can be seen from fig. 4.4.8, the error is primarily concentrated in the x_1 state which is not directly accessible by neither the error signal nor the network input \mathbf{c} due to

$$\mathbf{B}\mathbf{B}^T = \begin{bmatrix} 0 & 0 \\ 0 & 1 \end{bmatrix} \quad (4.24)$$

removing any potential control over x_1 , causing small inaccuracies to let the network diverge over time.

4.4.3 Limitations

The main limitation of the approaches presented here is the learning accuracy of \mathbf{W}^s . Both presented approaches deliver good results with analytically computed matrix weights. Either of them is usable to control a system if \mathbf{W}^s calculated analytically. Only if either \mathbf{B} or the learning is neglected, both approaches can perform accurately. Ignoring \mathbf{B} hugely limits the applicability of the whole network despite the accurate

results. To the above mentioned limitations all the limitations of previous sections also apply. This concerns especially the application to bigger systems, random initialization of weights before training, or the choice of Γ .

The addition of the error signal is necessary in order to balance the network noise. Due to lack of feedback, it is impossible to be accounted for. Therefore inherent noise in the network is completely unchecked. Noise can alternatively be mitigated by scaling Γ and the subsequent threshold to small scales. In this case, the number of spikes to represent the same signal will be increased, reducing the relative importance of spikes caused by noise. By doing this, the network is basically converted into a classic rate network.

Chapter 5

Conclusions

The development of the spiking neural network controller for controlling a linear system involved three distinct stages. The controller utilized the Efficient balanced coding scheme, incorporating biologically plausible principles. In the initial stage, simulation, the SNN was capable of simulating any given dynamical system using analytically calculated values.

As a second step, a dedicated controller was designed to generate the control signal u . This controller, built on the same SNN architecture, was added in front of the previous stage to generate the necessary control signals. The controller, when combined with the previous stage demonstrated effective control over the system dynamics. However, it's worth noting that the effectiveness of the control stage was contingent on specific conditions related to the control problem, limiting its general applicability.

Moreover, the dynamics of the control stage were predominantly stemming from the definition of the external inputs c rather than the entire network. For control, c served as a forcing term to the network, bridging the necessary input to push the network into following the desired trajectory. The main objective of the control network was the generation of spikes and subsequent output of the control signal u .

The purely open loop design of the control encountered the typical design challenges e.g. in aspects of noise or system error. In a separate similar derivation the emerging explicit error term was insignificant in combatting these issues.

Thirdly, the analytically derived network dynamics of the first stage were learned using

local learning rules. The fast recurrent dynamics were learned by an unsupervised learning rule while the slow dynamics were trained through a supervised student-teacher approach. The learning performance was examined, with parameters fine-tuned to yield a significant improvement in network accuracy for our model problem. Challenges in the learning process were primarily associated with the random initialization of the matrices intended for training, scaling of the learning rate, form of the training input sequences and the initialization of Γ . Higher-dimensional problems, in general, were only applicable in specific cases with manual parameter tuning, yielding mixed results overall.

In the final step, when applying the previously learned matrices with the control scheme, challenges arose due to the open-loop design and inherent perturbations in the learned matrices, resulting in control failures. To address this, an extra feedback loop was introduced into the network, modifying the definition of c to incorporate error feedback. Although error feedback showed overall improvement, the errors remained unacceptably high when working with two networks in series. In a separate exploration, a single network was constructed, combining both approaches. By adopting the control network's definition of c , results were comparable to the two network approach. However, this came with the prohibitive restriction of necessitating $B = I$. Attempts to enable orthonormal input matrices into the network were possible, though limited by the mandatory use of the analytically computed matrices in stage one. The addition of feedback did not give any improved results.

The primary limitation stems from inaccuracies in W^s . Under the premise that a highly accurate W^s could be learned, either method can yield viable results for control. Overall, the network and learning rule choices align with biological plausibility. However, the chosen control scheme as well as the construction of the single network is questionable. It remains unclear whether plausible learning rules for the control network exist. Additionally, the computation of c requiring the target state, its derivative and the system matrix itself bring the entire control aspect in question.

All in all, the goal of creating a controller for arbitrary systems was not fully achieved. Due to limitations in control as well as in learning the use cases for the

presented scheme are highly limited if analytically computed matrices are not utilized. Additionally, the inherent tuning of for different systems makes the approach inviable as a "black box."

Nonetheless, control can be obtained if additional information is available and conditions are met. Under these assumptions, control can be accurate with up to a single spike difference from the target, highlighting the SNN's immense potential.

5.1 Future Work

There are a numerous ways to build upon the work that presented here. These extensions can be grouped into enhancing the capabilities, incorporating more biological plausibility, or topics that warrant further investigation.

Extending capabilities

Learning of Γ

A straightforward step to enhance our network's learning capabilities involves allowing the learning of the Feed-Forward weights Γ , as proposed in [16]. While this has been briefly attempted here, the rigorous integration and testing is lacking.

In first tests, the combination of feed-forward training and the learning of \mathbf{W}^s was unsuccessful and requires further research.

Learning during Control

In most neural networks, training and testing are two distinct phases in the deployment process. Similarly, in our network, training demands a white noise process to enable optimal firing of all neurons. Training with non-zero mean signals, e.g already a desired reference trajectory in a control setting, could enable the network to adapt to a changing environment and significantly enhance its capabilities. Combining feed-forward learning and training non-whitened input using the covariance matrix $\Sigma = \text{cov}(\mathbf{x}, \mathbf{x})$ and recentring the input $\mathbf{x}_c = \mathbf{x} - \langle \mathbf{x} \rangle$ by its mean, as seen in [84] could yield interesting results.

Another intriguing approach to enable continual learning is to further integrate the in section 2.3.1 mentioned methods of EWC. While this has not been researched for

SNNs yet, it could potentially open ways to build networks that can increase in their neuron count or the number of represented states over time. Adding neurons while the network is active and training could give a more adaptable controller, activating "sleeping neurons" if the problem at hand requires more robustness or precision.

Non-linear systems and Control The restriction to linear systems poses limits on the applicability to broader set of problems. To that, methods have already been revised to extend the simulation to non-linear problems [3]. By using sigmoid basis functions dependent on the firing rate instead of linear r itself, non-linearities are introduced. A matrix similar to \mathbf{W}^s is then trained by the student-teacher approach presented here using a slightly adopted learning rule.

Biologic plausibility

Dale's Law

There are some immediate developments available. First of all could be the implementation of Dale's Law.

Following Dale's principle, it is not possible for a neuron to act as an excitatory and inhibitory neuron at the same time. In the network built in this project, this has been ignored for simplicity. In order to adhere to Dale's law, it would be necessary to separate groups of excitatory and inhibitory neurons that interact both with themselves and each other. This would also require an adjustment of the learning rules and can be implemented following the supplementary material of [16].

Synaptic Delays

Another increase of biological plausibility would be the integration of synaptic delays. In this implementation of network architecture, a spike is processed within the same time-step and as such changes the network instantaneously. In [68], the authors show that the addition of delays results in the network ping-ponging, the rapidly alternating firing of spikes. They propose conditionally Poisson firing neurons that allow for synaptic delays while retaining the network accuracy and robustness.

Investigating

Different Noise Types

The previous study on the input sequences for learning could be extended upon with a more rigorous testing and examination of spiking behaviour. Additionally, different noise types could be considered, not limited to white noise. During testing, inputs with less smoothing yielded better results. This was attributed to fast-changing signal inputs causing an increase of error, spiking and subsequent parameter adjustment. This could be explored further using Blue or violet noise.

Spiking Imbalance In addition to investigating the noise, spiking behaviour during learning also merits further exploration. During training, the system matrix \mathbf{A} had significant influence over the spike distribution over neurons. This resulted only a couple of neurons contributing to more than 90% of total spikes at the end of training. It was found that eigenvalue grouping appears to be the main factor in the spike distribution.

It is desirable that spikes during training are as evenly distributed as possible, as the least trained neuron causes the highest error. Therefore this imbalance can lead prolonged training times. However, since the system matrix \mathbf{A} is known, adapting training input to the system could improve spike distribution and, consequently, reduce training time.

5.2 Final Words

All in all, the network demonstrates the capability of controlling a dynamic system. However, the limitations set mostly by the control concept makes the realistic use of this approach impossible. The requirement on the input matrix $\mathbf{B} = \mathbf{I}$ for the presented approach is fundamentally restrictive and therefore demands the use of the exact, instead of the learned, matrices. Meanwhile even when the necessary conditions for control in stage 2 are met, network performance can still be subpar, necessitating further investigation.

Nonetheless the found accuracy as well as the proven robustness by previous authors given by a discrete spiking neural network in the context of biologically plausibility

CHAPTER 5. CONCLUSIONS

was impressive, fulfilling the set out goal in the beginning in accuracy as well as on robustness and noise thanks to the chosen network architecture. If all necessary conditions are met and the additional information is available, the control can produce acceptable performance that might be useful in specific tasks.

Bibliography

- [1] Abdolrasol, Maher G. M., Hussain, S. M. Suhail, Ustun, Taha Selim, Sarker, Mahidur R., Hannan, Mohammad A., Mohamed, Ramizi, Ali, Jamal Abd, Mekhilef, Saad **and** Milad, Abdalrhman. “Artificial Neural Networks Based Optimization Techniques: A Review”. **in:** *Electronics* **10.21** (**3 november 2021**), **page** 2689. ISSN: 2079-9292. DOI: 10 . 3390 / electronics10212689. URL: <https://www.mdpi.com/2079-9292/10/21/2689> (**urlseen** 10/02/2023).
- [2] Adrian, E. D. **and** Zotterman, Yngve. “The impulses produced by sensory nerve-endings: Part II. The response of a Single End-Organ”. **in:** *The Journal of Physiology* **61.2** (**23 april 1926**), **pages** 151–171. ISSN: 00223751. DOI: 10 . 1113/jphysiol.1926.sp002281. URL: <https://onlinelibrary.wiley.com/doi/10.1113/jphysiol.1926.sp002281> (**urlseen** 16/11/2022).
- [3] Alemi, Alireza, Machens, Christian, Denève, Sophie **and** Slotine, Jean-Jacques. “Learning arbitrary dynamics in efficient, balanced spiking networks using local plasticity rules”. **in:** (**2017**). Publisher: arXiv Version Number: 2. DOI: 10 . 48550 / ARXIV . 1705 . 08026. URL: <https://arxiv.org/abs/1705.08026> (**urlseen** 06/12/2023).
- [4] Almomani, Ammar, Alauthman, Mohammad, Alweshah, Mohammed, Dorgham, O. **and** Albala, Firas. “A comparative study on spiking neural network encoding schema: implemented with cloud computing”. **in:** *Cluster Computing* **22.2** (**june 2019**), **pages** 419–433. ISSN: 1386-7857, 1573-7543. DOI: 10 . 1007/s10586-018-02891-0. URL: <http://link.springer.com/10.1007/s10586-018-02891-0> (**urlseen** 15/11/2022).
- [5] Amin, Hesham H. “Automated Adaptive Threshold-Based Feature Extraction and Learning for Spiking Neural Networks”. **in:** *IEEE Access* **9** (**2021**), **pages** 97366–97383. ISSN: 2169-3536. DOI: 10 . 1109/ACCESS . 2021 . 3094262.

- URL: <https://ieeexplore.ieee.org/document/9471863/> (**urlseen 20/08/2023**).
- [6] Andrew, Alex M. "Spiking Neuron Models: Single Neurons, Populations, Plasticity". **in:** *Kybernetes* 32.7 (1 october 2003). ISSN: 0368-492X. DOI: 10.1108/k.2003.06732gae.003. URL: <https://www.emerald.com/insight/content/doi/10.1108/k.2003.06732gae.003/full/html> (**urlseen 15/11/2022**).
 - [7] Azevedo, Frederico A. C., Carvalho, Ludmila R. B., Grinberg, Lea T., Farfel, José Marcelo, Ferretti, Renata E. L., Leite, Renata E. P., Jacob Filho, Wilson, Lent, Roberto **and** Herculano-Houzel, Suzana. "Equal numbers of neuronal and nonneuronal cells make the human brain an isometrically scaled-up primate brain". **in:** *The Journal of Comparative Neurology* 513.5 (10 april 2009), **pages** 532–541. ISSN: 1096-9861. DOI: 10.1002/cne.21974.
 - [8] Bekolay, Trevor, Bergstra, James, Hunsberger, Eric, DeWolf, Travis, Stewart, Terrence C., Rasmussen, Daniel, Choo, Xuan, Voelker, Aaron Russell **and** Eliasmith, Chris. "Nengo: a Python tool for building large-scale functional brain models". **in:** *Frontiers in Neuroinformatics* 7 (2014). ISSN: 1662-5196. DOI: 10.3389/fninf.2013.00048. URL: <http://journal.frontiersin.org/article/10.3389/fninf.2013.00048/abstract> (**urlseen 30/11/2023**).
 - [9] Bengio, Y., Simard, P. **and** Frasconi, P. "Learning long-term dependencies with gradient descent is difficult". **in:** *IEEE Transactions on Neural Networks* 5.2 (march 1994), **pages** 157–166. ISSN: 1045-9227, 1941-0093. DOI: 10.1109/72.279181. URL: <https://ieeexplore.ieee.org/document/279181/> (**urlseen 07/02/2023**).
 - [10] Bing, Zhenshan, Baumann, Ivan, Jiang, Zhuangyi, Huang, Kai, Cai, Caixia **and** Knoll, Alois. "Supervised Learning in SNN via Reward-Modulated Spike-Timing-Dependent Plasticity for a Target Reaching Vehicle". **in:** *Frontiers in Neurorobotics* 13 (3 may 2019), **page** 18. ISSN: 1662-5218. DOI: 10.3389/fnbot.2019.00018. URL: <https://www.frontiersin.org/article/10.3389/fnbot.2019.00018/full> (**urlseen 31/03/2022**).
 - [11] Boerlin, Martin, Machens, Christian K. **and** Denève, Sophie. "Predictive Coding of Dynamical Variables in Balanced Spiking Networks". **in:** *PLOS Computational Biology* 9.11 (14 november 2013). Publisher: Public Library

- of Science, e1003258. ISSN: 1553-7358. DOI: 10.1371/journal.pcbi.1003258. URL: <https://journals.plos.org/ploscompbiol/article?id=10.1371/journal.pcbi.1003258> (**urlseen** 20/09/2022).
- [12] Bohté, Sander M., Kok, Joost N. **and** Poutré, Han La. “SpikeProp: backpropagation for networks of spiking neurons”. **in:** *The European Symposium on Artificial Neural Networks*. 2000. URL: <https://api.semanticscholar.org/CorpusID:14069916>.
- [13] Bouganis, Alexandros **and** Shanahan, Murray. “Training a spiking neural network to control a 4-DoF robotic arm based on Spike Timing-Dependent Plasticity”. **in:** *The 2010 International Joint Conference on Neural Networks (IJCNN)*. 2010 International Joint Conference on Neural Networks (IJCNN). Barcelona, Spain: IEEE, **july 2010**, **pages** 1–8. ISBN: 978-1-4244-6916-1. DOI: 10.1109/IJCNN.2010.5596525. URL: <http://ieeexplore.ieee.org/document/5596525/> (**urlseen** 10/08/2023).
- [14] Bourdoukan, Ralph, Barrett, David, Deneve, Sophie **and** Machens, Christian K. “Learning optimal spike-based representations”. **in:** *Advances in Neural Information Processing Systems*. **byeditor**F. Pereira, C. J. Burges, L. Bottou **and** K. Q. Weinberger. **volume** 25. Curran Associates, Inc., 2012. URL: https://proceedings.neurips.cc/paper_files/paper/2012/file/3a15c7d0bbe60300a39f76f8a5ba6896-Paper.pdf.
- [15] Bourdoukan, Ralph **and** Denève, Sophie. “Enforcing balance allows local supervised learning in spiking recurrent networks”. **in:** *Advances in Neural Information Processing Systems*. **byeditor**C. Cortes, N. Lawrence, D. Lee, M. Sugiyama **and** R. Garnett. **volume** 28. Curran Associates, Inc., 2015. URL: https://proceedings.neurips.cc/paper_files/paper/2015/file/3871bd64012152bfb53fdf04b401193f-Paper.pdf.
- [16] Brendel, Wieland, Bourdoukan, Ralph, Vertechi, Pietro, Machens, Christian K. **and** Denève, Sophie. “Learning to represent signals spike by spike”. **in:** *PLOS Computational Biology* 16.3 (16 march 2020). Publisher: Public Library of Science, e1007692. ISSN: 1553-7358. DOI: 10.1371/journal.pcbi.1007692. URL: <https://journals.plos.org/ploscompbiol/article?id=10.1371/journal.pcbi.1007692> (**urlseen** 20/09/2022).

- [17] Brette, Romain. "Philosophy of the Spike: Rate-Based vs. Spike-Based Theories of the Brain". *in: Frontiers in Systems Neuroscience* 9 (10 november 2015). ISSN: 1662-5137. DOI: 10.3389/fnsys.2015.00151. URL: <http://journal.frontiersin.org/Article/10.3389/fnsys.2015.00151/abstract> (**urlseen** 16/11/2022).
- [18] Bullock, Daniel, Grossberg, Stephen **and** Guenther, Frank H. "A Self-Organizing Neural Model of Motor Equivalent Reaching and Tool Use by a Multijoint Arm". *in: Journal of Cognitive Neuroscience* 5.4 (1 october 1993), **pages** 408–435. ISSN: 0898-929X, 1530-8898. DOI: 10.1162/jocn.1993.5.4.408. URL: <https://direct.mit.edu/jocn/article/5/4/408/3102/A-Self-Organizing-Neural-Model-of-Motor-Equivalent> (**urlseen** 10/08/2023).
- [19] Chen, Yunhua, Mai, Yingchao, Feng, Ren **and** Xiao, Jinsheng. "An adaptive threshold mechanism for accurate and efficient deep spiking convolutional neural networks". *in: Neurocomputing* 469 (16 january 2022), **pages** 189–197. ISSN: 0925-2312. DOI: 10.1016/j.neucom.2021.10.080. URL: <https://www.sciencedirect.com/science/article/pii/S092523122101568X> (**urlseen** 20/08/2023).
- [20] Clarke, D.D. **and** Sokoloff, L. "Circulation and energy metabolism of the brain". *in: Basic Neurochemistry: Molecular, Cellular, and Medical Aspects* (1999), **pages** 637–669.
- [21] Demin, Vyacheslav **and** Nekhaev, Dmitry. "Recurrent Spiking Neural Network Learning Based on a Competitive Maximization of Neuronal Activity". *in: Frontiers in Neuroinformatics* 12 (15 november 2018), **page** 79. ISSN: 1662-5196. DOI: 10.3389/fninf.2018.00079. URL: <https://www.frontiersin.org/article/10.3389/fninf.2018.00079/full> (**urlseen** 20/03/2023).
- [22] Denève, Sophie **and** Machens, Christian K. "Efficient codes and balanced networks". *in: Nature Neuroscience* 19.3 (march 2016), **pages** 375–382. ISSN: 1097-6256, 1546-1726. DOI: 10.1038/nn.4243. URL: <http://www.nature.com/articles/nn.4243> (**urlseen** 18/10/2022).
- [23] DeWolf, Travis, Stewart, Terrence C., Slotine, Jean-Jacques **and** Eliasmith, Chris. "A spiking neural model of adaptive arm control". *in: Proceedings of the Royal Society B: Biological Sciences* 283.1843 (30 november 2016), **page** 20162134. ISSN: 0962-8452, 1471-2954. DOI: 10.1098/rspb.2016.2134.

- URL: <https://royalsocietypublishing.org/doi/10.1098/rspb.2016.2134> (**urlseen** 15/12/2022).
- [24] Diehl, Peter U., Neil, Daniel, Binas, Jonathan, Cook, Matthew, Liu, Shih-Chii **and** Pfeiffer, Michael. “Fast-classifying, high-accuracy spiking deep networks through weight and threshold balancing”. **in:** *2015 International Joint Conference on Neural Networks (IJCNN)*. 2015 International Joint Conference on Neural Networks (IJCNN). Killarney, Ireland: IEEE, **july** 2015, **pages** 1–8. ISBN: 978-1-4799-1960-4. DOI: 10.1109/IJCNN.2015.7280696. URL: <http://ieeexplore.ieee.org/document/7280696/> (**urlseen** 17/11/2022).
- [25] Diehl, Peter U., Zarrella, Guido, Cassidy, Andrew, Pedroni, Bruno U. **and** Neftci, Emre. “Conversion of artificial recurrent neural networks to spiking neural networks for low-power neuromorphic hardware”. **in:** *2016 IEEE International Conference on Rebooting Computing (ICRC)*. 2016 IEEE International Conference on Rebooting Computing (ICRC). San Diego, CA, USA: IEEE, **october** 2016, **pages** 1–8. ISBN: 978-1-5090-1370-8. DOI: 10.1109/ICRC.2016.7738691. URL: <http://ieeexplore.ieee.org/document/7738691/> (**urlseen** 17/11/2022).
- [26] Eliasmith, Chris **and** Anderson, Charles H. *Neural engineering: computational, representation, and dynamics in neurobiological systems*. 1. MIT Press paperback ed. Computational neuroscience. Cambridge, Mass.: MIT Press, 2004. 359 **pagetotals**. ISBN: 978-0-262-55060-4.
- [27] Eshraghian, Jason K., Ward, Max, Neftci, Emre O., Wang, Xinxin, Lenz, Gregor, Dwivedi, Girish, Bennamoun, Mohammed, Jeong, Doo Seok **and** Lu, Wei D. “Training Spiking Neural Networks Using Lessons From Deep Learning”. **in:** *Proceedings of the IEEE* 111.9 (**september** 2023), **pages** 1016–1054. ISSN: 0018-9219, 1558-2256. DOI: 10.1109/JPROC.2023.3308088. URL: <https://ieeexplore.ieee.org/document/10242251/> (**urlseen** 30/11/2023).
- [28] Feldman, Daniel E. “The Spike-Timing Dependence of Plasticity”. **in:** *Neuron* 75.4 (**august** 2012), **pages** 556–571. ISSN: 08966273. DOI: 10.1016/j.neuron.2012.08.001. URL: <https://linkinghub.elsevier.com/retrieve/pii/S0896627312007039> (**urlseen** 21/03/2023).

- [29] Goodfellow, Ian, Bengio, Yoshua **and** Courville, Aaron. *Deep learning*. Adaptive computation and machine learning. Cambridge, Massachusetts: The MIT Press, 2016. 775 **pagetotals**. ISBN: 978-0-262-03561-3.
- [30] Graves, Alex, Eck, Douglas, Beringer, Nicole **and** Schmidhuber, Juergen. “Biologically Plausible Speech Recognition with LSTM Neural Nets”. **in:** *Biologically Inspired Approaches to Advanced Information Technology*. **byeditor**Auke Jan Ijspeert, Masayuki Murata **and** Naoki Wakamiya. redactor David Hutchison, Takeo Kanade, Josef Kittler, Jon M. Kleinberg, Friedemann Mattern, John C. Mitchell, Moni Naor, Oscar Nierstrasz, C. Pandu Rangan, Bernhard Steffen, Madhu Sudan, Demetri Terzopoulos, Dough Tygar, Moshe Y. Vardi **and** Gerhard Weikum. **volume** 3141. Series Title: Lecture Notes in Computer Science. Berlin, Heidelberg: Springer Berlin Heidelberg, 2004, **pages** 127–136. ISBN: 978-3-540-27835-1. DOI: 10.1007/978-3-540-27835-1_10. URL: http://link.springer.com/10.1007/978-3-540-27835-1_10 (**urlseen** 14/12/2022).
- [31] Guo, Wenzhe, Fouda, Mohammed E., Eltawil, Ahmed M. **and** Salama, Khaled Nabil. “Neural Coding in Spiking Neural Networks: A Comparative Study for Robust Neuromorphic Systems”. **in:** *Frontiers in Neuroscience* 15 (4 march 2021), **page** 638474. ISSN: 1662-453X. DOI: 10.3389/fnins.2021.638474. URL: <https://www.frontiersin.org/articles/10.3389/fnins.2021.638474/full> (**urlseen** 20/03/2023).
- [32] Hochreiter, Sepp **and** Schmidhuber, Jürgen. “Long Short-Term Memory”. **in:** *Neural Computation* 9.8 (1 november 1997), **pages** 1735–1780. ISSN: 0899-7667, 1530-888X. DOI: 10.1162/neco.1997.9.8.1735. URL: <https://direct.mit.edu/neco/article/9/8/1735-1780/6109> (**urlseen** 07/02/2023).
- [33] Hodgkin, A. L. **and** Huxley, A. F. “A quantitative description of membrane current and its application to conduction and excitation in nerve”. **in:** *The Journal of Physiology* 117.4 (1952). _eprint: <https://onlinelibrary.wiley.com/doi/pdf/10.1113/jphysiol.1952.sp004764>, **pages** 500–544. ISSN: 1469-7793. DOI: 10.1113/jphysiol.1952.sp004764. URL: <https://onlinelibrary.wiley.com/doi/abs/10.1113/jphysiol.1952.sp004764> (**urlseen** 21/09/2022).

- [34] Hodgkin, A. L. **and** Huxley, A. F. “Currents carried by sodium and potassium ions through the membrane of the giant axon of *Loligo*”. **in:** *The Journal of Physiology* 116.4 (28 **april** 1952), **pages** 449–472. ISSN: 0022-3751, 1469-7793. DOI: 10.1113/jphysiol.1952.sp004717. URL: <https://onlinelibrary.wiley.com/doi/10.1113/jphysiol.1952.sp004717> (**urlseen** 21/03/2023).
- [35] Huang, Fuqiang. “Dynamics and Control in Spiking Neural Networks”. **in:** (15 **december** 2019). Publisher: Washington University in St. Louis. DOI: 10.7936/YA3F-RK28. URL: https://openscholarship.wustl.edu/eng_etds/495 (**urlseen** 14/10/2022).
- [36] Huang, Fuqiang **and** Ching, ShiNung. “Spiking networks as efficient distributed controllers”. **in:** *Biological Cybernetics* 113.1 (**april** 2019), **pages** 179–190. ISSN: 0340-1200, 1432-0770. DOI: 10.1007/s00422-018-0769-7. URL: <http://link.springer.com/10.1007/s00422-018-0769-7> (**urlseen** 23/10/2022).
- [37] Huang, Fuqiang, Riehl, James **and** Ching, ShiNung. “Optimizing the dynamics of spiking networks for decoding and control”. **in:** *2017 American Control Conference (ACC)*. 2017 American Control Conference (ACC). ISSN: 2378-5861. **may** 2017, **pages** 2792–2798. DOI: 10.23919/ACC.2017.7963374.
- [38] Indiveri, Giacomo **and** Sandamirskaya, Yulia. “The Importance of Space and Time for Signal Processing in Neuromorphic Agents: The Challenge of Developing Low-Power, Autonomous Agents That Interact With the Environment”. **in:** *IEEE Signal Processing Magazine* 36.6 (**november** 2019), **pages** 16–28. ISSN: 1053-5888, 1558-0792. DOI: 10.1109/MSP.2019.2928376. URL: <https://ieeexplore.ieee.org/document/8887553/> (**urlseen** 09/12/2022).
- [39] Ioffe, Sergey **and** Szegedy, Christian. *Batch Normalization: Accelerating Deep Network Training by Reducing Internal Covariate Shift*. 2 **march** 2015. arXiv: 1502.03167[cs]. URL: <http://arxiv.org/abs/1502.03167> (**urlseen** 07/02/2023).
- [40] Izhikevich, E.M. “Simple model of spiking neurons”. **in:** *IEEE Transactions on Neural Networks* 14.6 (**november** 2003). Conference Name: IEEE Transactions on Neural Networks, **pages** 1569–1572. ISSN: 1941-0093. DOI: 10.1109/TNN.2003.820440.

BIBLIOGRAPHY

- [41] Jacobs, Nathan S., Allen, Timothy A., Nguyen, Natalie **and** Fortin, Norbert J. “Critical Role of the Hippocampus in Memory for Elapsed Time”. **in:** *Journal of Neuroscience* 33.34 (21 **august** 2013). Publisher: Society for Neuroscience Section: Brief Communications, **pages** 13888–13893. ISSN: 0270-6474, 1529-2401. DOI: 10 . 1523 / JNEUROSCI . 1733 – 13 . 2013. URL: <https://www.jneurosci.org/content/33/34/13888> (**urlseen** 19/08/2023).
- [42] Jaeger, Herbert. “The “echo state” approach to analysing and training recurrent neural networks – with an Erratum note”. **in:** (2010).
- [43] Jin, Yingyezhe **and** Li, Peng. “Performance and robustness of bio-inspired digital liquid state machines: A case study of speech recognition”. **in:** *Neurocomputing* 226 (22 **february** 2017), **pages** 145–160. ISSN: 0925-2312. DOI: 10 . 1016 / j . neucom . 2016 . 11 . 045. URL: <https://www.sciencedirect.com/science/article/pii/S0925231216314606> (**urlseen** 14/12/2022).
- [44] Johnson, Erik C., Jones, Douglas L. **and** Ratnam, Rama. “A minimum-error, energy-constrained neural code is an instantaneous-rate code”. **in:** *Journal of Computational Neuroscience* 40.2 (april 2016), **pages** 193–206. ISSN: 0929-5313, 1573-6873. DOI: 10 . 1007 / s10827 – 016 – 0592 – x. URL: <http://link.springer.com/10.1007/s10827-016-0592-x> (**urlseen** 24/11/2022).
- [45] Johnston, Daniel **and** Wu, Samuel Miao-sin. *Foundations of cellular neurophysiology*. Cambridge, Mass: MIT Press, 1995. 676 **pagetotals**. ISBN: 978-0-262-10053-3.
- [46] Kempter, Richard, Gerstner, Wulfram **and** Hemmen, J. Leo van. “Hebbian learning and spiking neurons”. **in:** *Physical Review E* 59.4 (1 **april** 1999), **pages** 4498–4514. ISSN: 1063-651X, 1095-3787. DOI: 10 . 1103 / PhysRevE . 59 . 4498. URL: <https://link.aps.org/doi/10.1103/PhysRevE.59.4498> (**urlseen** 21/03/2023).
- [47] Kirkpatrick, James, Pascanu, Razvan, Rabinowitz, Neil, Veness, Joel, Desjardins, Guillaume, Rusu, Andrei A., Milan, Kieran, Quan, John, Ramalho, Tiago, Grabska-Barwinska, Agnieszka, Hassabis, Demis, Clopath, Claudia, Kumaran, Dharshan **and** Hadsell, Raia. “Overcoming catastrophic forgetting in neural networks”. **in:** *Proceedings of the National Academy of Sciences* 114.13 (28 **march** 2017), **pages** 3521–3526. ISSN: 0027-

- 8424, 1091-6490. DOI: 10.1073/pnas.1611835114. URL: <https://pnas.org/doi/full/10.1073/pnas.1611835114> (**urlseen** 30/08/2023).
- [48] Lazar, Andreea, Pipa, Gordon **and** Triesch, Jochen. “SORN: a self-organizing recurrent neural network”. **in:** *Frontiers in Computational Neuroscience* 3 (2009). ISSN: 1662-5188. URL: <https://www.frontiersin.org/articles/10.3389/neuro.10.023.2009> (**urlseen** 17/12/2023).
- [49] Lee, Jun Haeng, Delbruck, Tobi **and** Pfeiffer, Michael. “Training Deep Spiking Neural Networks Using Backpropagation”. **in:** *Frontiers in Neuroscience* 10 (8 **november** 2016). ISSN: 1662-453X. DOI: 10.3389/fnins.2016.00508. URL: <http://journal.frontiersin.org/article/10.3389/fnins.2016.00508/full> (**urlseen** 10/02/2023).
- [50] Legenstein, Robert, Pecevski, Dejan **and** Maass, Wolfgang. “A Learning Theory for Reward-Modulated Spike-Timing-Dependent Plasticity with Application to Biofeedback”. **in:** *PLoS Computational Biology* 4.10 (10 **october** 2008). **byeditor**Lyle J. Graham, e1000180. ISSN: 1553-7358. DOI: 10.1371/journal.pcbi.1000180. URL: <https://dx.plos.org/10.1371/journal.pcbi.1000180> (**urlseen** 30/10/2023).
- [51] Li, Xiangang **and** Wu, Xihong. *Constructing Long Short-Term Memory based Deep Recurrent Neural Networks for Large Vocabulary Speech Recognition.* 10 **may** 2015. arXiv: 1410.4281[cs]. URL: <http://arxiv.org/abs/1410.4281> (**urlseen** 07/02/2023).
- [52] Lillicrap, Timothy P., Cownden, Daniel, Tweed, Douglas B. **and** Akerman, Colin J. “Random synaptic feedback weights support error backpropagation for deep learning”. **in:** *Nature Communications* 7.1 (8 **november** 2016), **page** 13276. ISSN: 2041-1723. DOI: 10.1038/ncomms13276. URL: <https://www.nature.com/articles/ncomms13276> (**urlseen** 12/12/2023).
- [53] Liu, Yuxiang **and** Pan, Wei. “Spiking Neural-Networks-Based Data-Driven Control”. **in:** *Electronics* 12.2 (7 **january** 2023), **page** 310. ISSN: 2079-9292. DOI: 10.3390/electronics12020310. URL: <https://www.mdpi.com/2079-9292/12/2/310> (**urlseen** 06/09/2023).
- [54] Maass, Wolfgang. “Liquid State Machines: Motivation, Theory, and Applications”. **in:** Cooper, S Barry **and** Sorbi, Andrea. *Computability in Context*. IMPERIAL COLLEGE PRESS, **february** 2011, **pages** 275–296. ISBN:

- 978-1-84816-277-8. DOI: 10.1142/9781848162778_0008. URL: http://www.worldscientific.com/doi/abs/10.1142/9781848162778_0008 (**urlseen** 31/10/2022).
- [55] Maass, Wolfgang. "Networks of spiking neurons: The third generation of neural network models". in: *Neural Networks* 10.9 (december 1997), pages 1659–1671. ISSN: 08936080. DOI: 10.1016/S0893-6080(97)00011-7. URL: <https://linkinghub.elsevier.com/retrieve/pii/S0893608097000117> (**urlseen** 09/12/2022).
- [56] Maass, Wolfgang, Joshi, Prashant **and** Sontag, Eduardo D. "Computational Aspects of Feedback in Neural Circuits". in: *PLoS Computational Biology* 3.1 (19 january 2007). byeditor Rolf Kotter, e165. ISSN: 1553-7358. DOI: 10.1371/journal.pcbi.0020165. URL: <https://dx.plos.org/10.1371/journal.pcbi.0020165> (**urlseen** 07/11/2022).
- [57] Maass, Wolfgang **and** Markram, Henry. "On the computational power of circuits of spiking neurons". in: *Journal of Computer and System Sciences* 69.4 (december 2004), pages 593–616. ISSN: 00220000. DOI: 10.1016/j.jcss.2004.04.001. URL: <https://linkinghub.elsevier.com/retrieve/pii/S0022000004000406> (**urlseen** 07/11/2022).
- [58] Mayer, Hermann, Gomez, Faustino, Wierstra, Daan, Nagy, Istvan, Knoll, Alois **and** Schmidhuber, Jurgen. "A System for Robotic Heart Surgery that Learns to Tie Knots Using Recurrent Neural Networks". in: *2006 IEEE/RSJ International Conference on Intelligent Robots and Systems*. 2006 IEEE/RSJ International Conference on Intelligent Robots and Systems. Beijing, China: IEEE, october 2006, pages 543–548. ISBN: 978-1-4244-0258-8. DOI: 10.1109/IROS.2006.282190. URL: <http://ieeexplore.ieee.org/document/4059310/> (**urlseen** 07/02/2023).
- [59] McKennoch, S., Dingding Liu **and** Bushnell, L.G. "Fast Modifications of the SpikeProp Algorithm". in: *The 2006 IEEE International Joint Conference on Neural Network Proceedings*. The 2006 IEEE International Joint Conference on Neural Network Proceedings. Vancouver, BC, Canada: IEEE, 2006, pages 3970–3977. ISBN: 978-0-7803-9490-2. DOI: 10.1109/IJCNN.2006.246918. URL: <http://ieeexplore.ieee.org/document/1716646/> (**urlseen** 21/08/2023).

- [60] Nair, Vinod **and** Hinton, Geoffrey E. “Rectified Linear Units Improve Restricted Boltzmann Machines”. **in:** (2010).
- [61] Neftci, Emre O., Mostafa, Hesham **and** Zenke, Friedemann. “Surrogate Gradient Learning in Spiking Neural Networks”. **in:** (2019). Publisher: arXiv Version Number: 2. DOI: 10.48550/ARXIV.1901.09948. URL: <https://arxiv.org/abs/1901.09948> (**urlseen** 21/08/2023).
- [62] Nicola, Wilten **and** Clopath, Claudia. “Supervised learning in spiking neural networks with FORCE training”. **in:** *Nature Communications* 8.1 (20 december 2017), **page** 2208. ISSN: 2041-1723. DOI: 10.1038/s41467-017-01827-3. URL: <https://www.nature.com/articles/s41467-017-01827-3> (**urlseen** 14/12/2023).
- [63] Nielsen, Michael A. “Neural Networks and Deep Learning”. **in:** (2015). Publisher: Determination Press. URL: <http://neuralnetworksanddeeplearning.com> (**urlseen** 10/02/2023).
- [64] Pascanu, Razvan, Mikolov, Tomas **and** Bengio, Yoshua. *On the difficulty of training Recurrent Neural Networks*. 15 february 2013. arXiv: 1211.5063[cs]. URL: <http://arxiv.org/abs/1211.5063> (**urlseen** 07/02/2023).
- [65] Patel, Jigneshkumar **and** Goyal, Ramesh. “Applications of Artificial Neural Networks in Medical Science”. **in:** *Current Clinical Pharmacology* 2.3 (1 september 2007), **pages** 217–226. ISSN: 15748847. DOI: 10.2174/157488407781668811. URL: <http://www.eurekaselect.com/openurl/content.php?genre=article&issn=1574-8847&volume=2&issue=3&spage=217> (**urlseen** 02/12/2022).
- [66] Pfeiffer, Michael **and** Pfeil, Thomas. “Deep Learning With Spiking Neurons: Opportunities and Challenges”. **in:** *Frontiers in Neuroscience* 12 (2018). ISSN: 1662-453X. URL: <https://www.frontiersin.org/articles/10.3389/fnins.2018.00774> (**urlseen** 15/12/2022).
- [67] Putney, Joy, Conn, Rachel **and** Sponberg, Simon. “Precise timing is ubiquitous, consistent, and coordinated across a comprehensive, spike-resolved flight motor program”. **in:** *Proceedings of the National Academy of Sciences* 116.52 (26 december 2019). Publisher: Proceedings of the National Academy of Sciences, **pages** 26951–26960. DOI: 10.1073/pnas.1907513116. URL: <https://www.pnas.org/doi/10.1073/pnas.1907513116> (**urlseen** 14/12/2022).

- [68] Rullán Buxó, Camille E. **and** Pillow, Jonathan W. “Poisson balanced spiking networks”. in: *PLOS Computational Biology* 16.11 (20 november 2020). **byeditor**Daniele Marinazzo, e1008261. ISSN: 1553-7358. DOI: 10 . 1371 / journal . pcbi . 1008261. URL: <https://dx.plos.org/10.1371/journal.pcbi.1008261> (**urlseen** 18/12/2023).
- [69] Sak, Haşim, Senior, Andrew **and** Beaufays, Françoise. *Long Short-Term Memory Based Recurrent Neural Network Architectures for Large Vocabulary Speech Recognition*. 5 february 2014. arXiv: 1402.1128[cs, stat]. URL: <http://arxiv.org/abs/1402.1128> (**urlseen** 07/02/2023).
- [70] Shrestha, Sumit Bam **and** Song, Qing. “Adaptive learning rate of SpikeProp based on weight convergence analysis”. in: *Neural Networks* 63 (march 2015), **pages** 185–198. ISSN: 08936080. DOI: 10 . 1016 / j . neunet . 2014 . 12 . 001. URL: <https://linkinghub.elsevier.com/retrieve/pii/S0893608014002676> (**urlseen** 21/08/2023).
- [71] Soures, Nicholas **and** Kudithipudi, Dhireesha. “Deep Liquid State Machines With Neural Plasticity for Video Activity Recognition”. in: *Frontiers in Neuroscience* 13 (2019). ISSN: 1662-453X. URL: <https://www.frontiersin.org/articles/10.3389/fnins.2019.00686> (**urlseen** 10/08/2023).
- [72] Stagsted, Rasmus, Vitale, Antonio, Binz, Jonas, Renner, Alpha, Bonde Larsen, Leon **and** Sandamirskaya, Yulia. “Towards neuromorphic control: A spiking neural network based PID controller for UAV”. in: *Robotics: Science and Systems XVI*. Robotics: Science and Systems 2020. Robotics: Science **and** Systems Foundation, 12 july 2020. ISBN: 978-0-9923747-6-1. DOI: 10 . 15607 / RSS . 2020 . XVI . 074. URL: <http://www.roboticsproceedings.org/rss16/p074.pdf> (**urlseen** 10/08/2023).
- [73] Stimberg, Marcel, Brette, Romain **and** Goodman, Dan Fm. “Brian 2, an intuitive and efficient neural simulator”. in: *eLife* 8 (20 august 2019), e47314. ISSN: 2050-084X. DOI: 10 . 7554 / eLife . 47314. URL: <https://elifesciences.org/articles/47314> (**urlseen** 30/11/2023).
- [74] Sun, Hongze, Cai, Wuque, Yang, Baoxin, Cui, Yan, Xia, Yang, Yao, Dezhong **and** Guo, Daqing. *A Synapse-Threshold Synergistic Learning Approach for Spiking*

- Neural Networks*. 3 **april** 2023. arXiv: 2206.06129 [cs, q-bio]. URL: <http://arxiv.org/abs/2206.06129> (**urlseen** 20/08/2023).
- [75] Sun, Shiliang, Cao, Zehui, Zhu, Han **and** Zhao, Jing. *A Survey of Optimization Methods from a Machine Learning Perspective*. 23 **october** 2019. arXiv: 1906.06821 [cs, math, stat]. URL: <http://arxiv.org/abs/1906.06821> (**urlseen** 10/02/2023).
- [76] Tanaka, Gouhei, Yamane, Toshiyuki, Héroux, Jean Benoit, Nakane, Ryosho, Kanazawa, Naoki, Takeda, Seiji, Numata, Hidetoshi, Nakano, Daiju **and** Hirose, Akira. “Recent advances in physical reservoir computing: A review”. **in:** *Neural Networks* 115 (**july** 2019), **pages** 100–123. ISSN: 08936080. DOI: 10.1016/j.neunet.2019.03.005. URL: <https://linkinghub.elsevier.com/retrieve/pii/S0893608019300784> (**urlseen** 29/10/2022).
- [77] Tang, Zaiyong **and** Fishwick, Paul A. “Feedforward Neural Nets as Models for Time Series Forecasting”. **in:** *ORSA Journal on Computing* 5.4 (**november** 1993), **pages** 374–385. ISSN: 0899-1499, 2326-3245. DOI: 10.1287/ijoc.5.4.374. URL: <http://pubsonline.informs.org/doi/10.1287/ijoc.5.4.374> (**urlseen** 02/02/2023).
- [78] Tavanaei, Amirhossein **and** Maida, Anthony. “BP-STDP: Approximating backpropagation using spike timing dependent plasticity”. **in:** *Neurocomputing* 330 (**february** 2019), **pages** 39–47. ISSN: 09252312. DOI: 10.1016/j.neucom.2018.11.014. URL: <https://linkinghub.elsevier.com/retrieve/pii/S0925231218313420> (**urlseen** 22/08/2023).
- [79] Thiruvarudchelvan, Vaenthan, Crane, James W. **and** Bossomaier, Terry. “Analysis of SpikeProp convergence with alternative spike response functions”. **in:** *2013 IEEE Symposium on Foundations of Computational Intelligence (FOCI)*. 2013 IEEE Symposium on Foundations of Computational Intelligence (FOCI). Singapore, Singapore: IEEE, **april** 2013, **pages** 98–105. ISBN: 978-1-4673-5901-6. DOI: 10.1109/FOCI.2013.6602461. URL: <http://ieeexplore.ieee.org/document/6602461/> (**urlseen** 21/08/2023).
- [80] Thorpe, Simon, Delorme, Arnaud **and** Van Rullen, Rufin. “Spike-based strategies for rapid processing”. **in:** *Neural Networks* 14.6 (**july** 2001), **pages** 715–725. ISSN: 08936080. DOI: 10.1016/S0893-6080(01)00083-1.

URL: <https://linkinghub.elsevier.com/retrieve/pii/S0893608001000831> (**urlseen** 19/08/2023).

- [81] Uncini, Aurelio. “Audio signal processing by neural networks”. **in:** *Neurocomputing* 55.3 (october 2003), **pages** 593–625. ISSN: 09252312. DOI: 10 . 1016 / S0925-2312(03)00395-3. URL: <https://linkinghub.elsevier.com/retrieve/pii/S0925231203003953> (**urlseen** 02/02/2023).
- [82] Vaswani, Ashish, Shazeer, Noam, Parmar, Niki, Uszkoreit, Jakob, Jones, Llion, Gomez, Aidan N., Kaiser, Lukasz **and** Polosukhin, Illia. *Attention Is All You Need*. 5 december 2017. arXiv: 1706 . 03762[cs]. URL: <http://arxiv.org/abs/1706.03762> (**urlseen** 02/12/2022).
- [83] Verstraeten, D., Schrauwen, B., D’Haene, M. **and** Stroobandt, D. “An experimental unification of reservoir computing methods”. **in:** *Neural Networks* 20.3 (april 2007), **pages** 391–403. ISSN: 08936080. DOI: 10 . 1016 / j . neunet . 2007 . 04 . 003. URL: <https://linkinghub.elsevier.com/retrieve/pii/S089360800700038X> (**urlseen** 07/11/2022).
- [84] Vertechi, Pietro, Brendel, Wieland **and** Machens, Christian K. “Unsupervised learning of an efficient short-term memory network”. **in:** *Advances in Neural Information Processing Systems*. **byeditorZ.** Ghahramani, M. Welling, C. Cortes, N. Lawrence **and** K. Q. Weinberger. **volume** 27. Curran Associates, Inc., 2014. URL: https://proceedings.neurips.cc/paper_files/paper/2014/file/333222170ab9edca4785c39f55221fe7-Paper.pdf.
- [85] Vigneron, Alex **and** Martinet, Jean. “A critical survey of STDP in Spiking Neural Networks for Pattern Recognition”. **in:** *2020 International Joint Conference on Neural Networks (IJCNN)*. 2020 International Joint Conference on Neural Networks (IJCNN). Glasgow, United Kingdom: IEEE, july 2020, **pages** 1–9. ISBN: 978-1-72816-926-2. DOI: 10 . 1109 / IJCNN48605 . 2020 . 9207239. URL: <https://ieeexplore.ieee.org/document/9207239/> (**urlseen** 22/08/2023).
- [86] Webb, Andrew, Davies, Sergio **and** Lester, David. “Spiking Neural PID Controllers”. **in:** *Neural Information Processing*. **byeditorBao-Liang Lu, Liqing Zhang **and** James Kwok.** **volume** 7064. Series Title: Lecture Notes in Computer Science. Berlin, Heidelberg: Springer Berlin Heidelberg, 2011,

- pages** 259–267. ISBN: 978-3-642-24964-8. DOI: 10.1007/978-3-642-24965-5_28. URL: http://link.springer.com/10.1007/978-3-642-24965-5_28 (**urlseen** 10/08/2023).
- [87] Williams, R. J. and Zipser, D. “Gradient-Based Learning Algorithms for Recurrent Networks and Their Computational Complexity”. in: *Back-propagation: Theory, Architectures and Applications*. Hillsdale, NJ, USA: Lawrence Erlbaum Associates, 1995, **pages** 433–486.
- [88] Yamazaki, Kashu, Vo-Ho, Viet-Khoa, Bulsara, Darshan and Le, Ngan. “Spiking Neural Networks and Their Applications: A Review”. in: *Brain Sciences* 12.7 (30 june 2022), **page** 863. ISSN: 2076-3425. DOI: 10.3390/brainsci12070863. URL: <https://www.mdpi.com/2076-3425/12/7/863> (**urlseen** 22/08/2023).
- [89] Yang, Mingchuan, Xie, Bingyu, Dou, Yingzhe and Xue, Guanchang. “Cascade Forward Artificial Neural Network based Behavioral Predicting Approach for the Integrated Satellite-terrestrial Networks”. in: *Mobile Networks and Applications* 27.4 (august 2022), **pages** 1569–1577. ISSN: 1383-469X, 1572-8153. DOI: 10.1007/s11036-021-01875-6. URL: <https://link.springer.com/10.1007/s11036-021-01875-6> (**urlseen** 02/02/2023).
- [90] Yi, Zexiang, Lian, Jing, Liu, Qidong, Zhu, Hegui, Liang, Dong and Liu, Jizhao. “Learning rules in spiking neural networks: A survey”. in: *Neurocomputing* 531 (april 2023), **pages** 163–179. ISSN: 09252312. DOI: 10.1016/j.neucom.2023.02.026. URL: <https://linkinghub.elsevier.com/retrieve/pii/S0925231223001662> (**urlseen** 20/03/2023).
- [91] Zenke, Friedemann and Ganguli, Surya. “SuperSpike: Supervised learning in multi-layer spiking neural networks”. in: *Neural Computation* 30.6 (june 2018), **pages** 1514–1541. ISSN: 0899-7667, 1530-888X. DOI: 10.1162/neco_a_01086. arXiv: 1705.11146 [cs, q-bio, stat]. URL: <http://arxiv.org/abs/1705.11146> (**urlseen** 21/08/2023).
- [92] Zenke, Friedemann, Poole, Ben and Ganguli, Surya. “Continual Learning Through Synaptic Intelligence”. in: (2017). Publisher: arXiv Version Number: 3. DOI: 10.48550/ARXIV.1703.04200. URL: <https://arxiv.org/abs/1703.04200> (**urlseen** 30/08/2023).

- [93] Zhang, Yong, Li, Peng, Jin, Yingyezhe **and** Choe, Yoonsuck. “A Digital Liquid State Machine With Biologically Inspired Learning and Its Application to Speech Recognition”. in: *IEEE Transactions on Neural Networks and Learning Systems* 26.11 (november 2015). Conference Name: IEEE Transactions on Neural Networks and Learning Systems, **pages** 2635–2649. ISSN: 2162-2388. DOI: 10.1109/TNNLS.2015.2388544.
- [94] Zheng, Shengjie, Qian, Lang, Li, Pingsheng, He, Chenggang, Qin, Xiaoqin **and** Li, Xiaojian. “An Introductory Review of Spiking Neural Network and Artificial Neural Network: From Biological Intelligence to Artificial Intelligence”. in: *arXiv:2204.07519 [cs]* (9 april 2022). arXiv: 2204.07519. URL: <http://arxiv.org/abs/2204.07519> (**urlseen** 20/09/2022).
- [95] Zhou, Shibo, Chen, Ying, Li, Xiaohua **and** Sanyal, Arindam. “Deep SCNN-Based Real-Time Object Detection for Self-Driving Vehicles Using LiDAR Temporal Data”. in: *IEEE Access* 8 (2020). Conference Name: IEEE Access, **pages** 76903–76912. ISSN: 2169-3536. DOI: 10.1109/ACCESS.2020.2990416.

Appendix - Contents

A Control Network Parameters	108
B Learning Parameters	109

Appendix A

Control Network Parameters

Parameter	Description	Value
N	# Neurons	50
λ_d	Decoder filter	10
λ_V	Voltage leak	5
σ_V	Voltage noise scaling	0.001
μ	Quadratic cost	10^{-6}
ν	Linear cost	0
dt	Timestep	10^{-4}
TE	Simulation time	10
Ω	Instantaneous Decoding weights with normalization per column	$\Omega \in \mathbb{R}^{b \times N} \sim N(0, 1), \ \Omega_i\ = 0.01$
Γ	Rate Decoding weights	$\Gamma = 0 \cdot \Omega$
b	# Columns of \mathbf{B}	

Appendix B

Learning Parameters

Parameter	Description	Value
N	# Neurons	50
λ_d	Decoder filter	10
λ_V	Voltage leak	5
β	Linear cost	0.522
dt	Timestep	10^{-4}
TE	Simulation time	10
K	Error Gain	10
N_{ep}	# Epochs	1000
N_s	Steps per epoch	100000
α^s	\mathbf{W}^s learning rate	0.01
α^f	\mathbf{W}^f learning rate	0.005
Γ	Feed-forward weights Uniform around S^{J-1} columns normalized to $\ \Gamma_i\ = 0.03$	
J	# State variables	
p^s	Drop rate of α^s	0.005
p^f	Drop rate of α^f	0.0005
σ	Std. Dev. for input sequence smoothing	6

